

Aus dem Zentrum für Tumor- und Immunbiologie,
Institut für Translationale Onkologie,
Geschäftsführender Direktor: Prof. Dr. Rolf Müller
des Fachbereichs Medizin der Philipps-Universität Marburg

**TRAIL-dependent apoptosis of human
peritoneal mesothelial cells by activated NK
cells promotes ovarian cancer cell invasion
*in vitro***

Inaugural-Dissertation zur Erlangung des Doktorgrades der
Naturwissenschaften

(Dr. rer. nat.)

dem Fachbereich Medizin der Philipps-Universität Marburg
vorgelegt von

Anna Mary Steitz

aus Usingen

Marburg, 2023

Angenommen vom Fachbereich Medizin der Philipps-Universität Marburg

am: 12.10.2023

Gedruckt mit Genehmigung des Fachbereichs Medizin

Dekanin: Prof. Dr. Denise Hilfiker-Kleiner

Referentin: Dr. Silke Reinartz

Korreferent: Prof. Dr. Elke Pogge von Strandmann

*To women suffering from ovarian cancer
& all patients generously taking part in our study*

Table of contents

Abstract	1
Zusammenfassung	3
1. Introduction	5
1.1 Ovarian carcinoma – Statistics, origin and staging	5
1.2 Diagnosis and therapy of ovarian carcinoma.....	6
1.3 The unique TME of HGSC.....	8
1.4 HGSC metastatic route promoted by a complex intercellular signaling network.....	11
1.5 Pro-tumorigenic role of mesothelial cells in the HGSC TME.....	13
1.6 Pro-tumorigenic role of immune cells and tumor immune escape in HGSC.....	15
1.7 T cell differentiation, subtypes and function.....	19
1.8 NK cell maturation, activation and cytolytic functions	20
1.8.1 Cytolytic granules – Granzyme B/Perforin apoptosis signaling	24
1.8.2 Cytotoxic cytokines.....	25
1.8.3 Death receptor ligands	27
1.9 Aim	28
2. Materials and Methods	32
2.1 Materials.....	32
2.1.1 Consumables and equipment.....	32
2.1.2 Chemicals and reagents.....	34
2.1.3 Antibodies.....	36
2.1.4 Recombinant Proteins	38
2.1.5 Kits and MACS microbeads.....	39
2.1.6 Standard buffers and solutions.....	39
2.1.7 Software and internet sites.....	40
2.1.8 Oligonucleotides and design for qPCR.....	41
2.1.9 Culture media	42
2.1.10 Patient samples and characteristics	43
2.1.11 Cell lines.....	43
2.2 Cell biological methods.....	44
2.2.1 Samples derived from HGSC patients, patients with benign gynecological diseases and healthy donors	44
2.2.1.1 Malignant ascites: isolation of peritoneal cell types.....	44

2.2.1.2	Omentum tissue: Isolation and cultivation of HPMC	46
2.2.1.3	Benign peritoneal lavage: Isolation of control group HPMC	47
2.2.1.4	LRS chambers: Isolation of healthy donor lymphocytes.....	47
2.2.2	Cultivation of primary HGSC patient-derived cell types.....	48
2.2.2.1	Primary tumor cell lines.....	48
2.2.2.2	Over night resting step of ex vivo tumor cells.....	49
2.2.2.3	HPMC	49
2.2.3	Cultivation of the K562 cell line	49
2.2.4	Cultivation of the Jurkat cell line	50
2.2.5	Collection of T cell conditioned media (CM)	50
2.2.6	Co-culture experiments	50
2.2.6.1	TAL treatments and co-cultures between T and NK cells	50
2.2.6.2	Co-culture between HPMC or ex vivo tumor cells with TAL or purified T/NK cells.....	51
2.2.7	Identifying involved apoptosis signaling pathway	51
2.2.7.1	Analyzing the involvement of TRAIL signaling pathway	51
2.2.7.2	Analyzing the participation of Fas/FasL-mediated killing.....	51
2.2.7.3	Determining the role of the activating receptor NKG2D	52
2.2.7.4	Analyzing the contribution of NK cell-derived cytokines.....	52
2.2.7.5	Agonistic antibodies CD40 and CD27.....	52
2.2.8	Flow cytometric and fluorescent microscopic readout of co-culture experiments.....	52
2.2.8.1	NK and T cell degranulation analysis	52
2.2.8.2	Detection of apoptotic HPMC and tumor cells.....	53
2.2.8.3	Caspase 3/7 staining of apoptotic HPMC.....	54
2.2.9	Analysis of cell surface receptor expression.....	54
2.2.9.1	Purity and phenotype of isolated cell fractions	54
2.2.9.2	Analysis of receptor expression on lymphocytes	55
2.2.9.3	Analysis of receptor expression on HPMC.....	55
2.2.10	Trans-mesothelial tumor cell invasion	55
2.3	Molecular biology and biochemical methods	57
2.3.1	Affinity proteomic (Olink) analysis of T cell secretomes	57
2.3.2	Analysis of T cell-expressed cytokines on RNA-level.....	58
2.3.2.1	RNA-isolation	58
2.3.2.2	DNase digestion.....	59

2.3.2.3	cDNA synthesis via reverse transcription.....	59
2.3.2.4	Quantitative polymerase chain reaction	59
2.3.3	RNA sequencing of HGSC patient-derived cells	60
2.3.4	Immunohistochemistry	60
2.3.5	Statistics and Bioinformatics.....	61
3.	Results.....	62
3.1	TAL induce apoptosis in HGSC-derived mesothelial cells.....	62
3.2	Identification of the NK cells as effector population within the TAL promoting mesothelial apoptosis	63
3.3	GrB/Perforin apoptosis signaling is blocked by ascites fluid.....	66
3.4	Fas/FasL apoptosis signaling does not play a role in the HGSC TME	67
3.5	HPMC apoptosis induction is independent of the cytotoxic cytokines TNF α and IFN γ	69
3.6	Identification of TRAIL apoptosis signaling conducted by T cell-activated NK cells introducing HPMC clearance in the HGSC TME	70
3.7	T-NK cell crosstalk: soluble mediators secreted by T cells promote TRAIL-dependent cytotoxicity of NK cells against HPMC	73
3.8	Identification of the T cell-secreted cytokines inducing NK cell activation	75
3.9	T cell-secreted cytokines activate TRAIL-mediated NK cell cytotoxic potential.....	78
3.10	HGSC-derived HPMC are susceptible to TRAIL-mediated killing, which is associated with high expression levels of TRAIL death receptors	81
3.11	HGSC tumor cells are resistant against TRAIL-mediated killing by TAL	84
3.12	The HGSC TME sensitizes HPMC to TRAIL-mediated killing by NK cells	85
3.13	HPMC – NK cell crosstalk: Additional mechanisms rendering NK cell activation	86
3.14	Apoptosis of the protective mesothelial barrier promotes HGSC tumor cell invasion.....	89
3.15	In the clinical context: Immunohistological identification of apoptotic mesothelial cells <i>in vivo</i>	92
4.	Discussion.....	95
4.1	HPMC lose their protective function in the HGSC TME	95

4.2	Mechanisms of HPMC vulnerability introduced by lymphocyte-mediated apoptosis	97
4.2.1	Ineffective NK cell cytotoxicity in the TME: Fas/FasL and cytokine-independent HPMC killing	97
4.2.2	Inhibitory effects of ascites on NK cell cytotoxicity	99
4.2.3	Effective NK cell cytotoxicity in the TME: TRAIL-dependent HPMC killing	99
4.3	Mechanisms of HPMC-NK cell crosstalk in the ovarian cancer TME	100
4.4	HPMC themselves recruit and possibly activate leukocytes <i>in vivo</i> .	101
4.5	Pro-tumorigenic effects of ascites – specific NK cell cytotoxicity against HPMC	102
4.6	Mechanisms of T-NK cell crosstalk promoting TRAIL-dependent HPMC killing.....	104
4.7	Limitations of the study and outlook	107
4.8	Conclusion.....	109
References		111
Appendix		127
	Supplementary data	127
	Ethics vote	133
	List of abbreviations, figures and graphs.....	137
	Publications of the author.....	147
	Curriculum Vitae.....	148
	Directory of academic teachers.....	149
	Acknowledgements	150
	Ehrenwörtliche Erklärung	152

Abstract

Transcoelomic dissemination of tumor cells via the malignant peritoneal fluid (ascites) occurs at an early stage of high-grade serous ovarian carcinoma, enabling extensive tumor spreading within the peritoneum. A high quantity of malignant ascites arises during ovarian cancer progression, which is an important characteristic of the unique tumor microenvironment. The ascites is rich in soluble factors and different cell types, including immune cells, promoting the metastatic spread, in particular to the omentum as a first site of tumor implantation. To date, the exact mechanism of peritoneal invasion is still largely unknown. The omentum and further peritoneal organs are covered by a mesothelial layer, physiologically functioning as a protective shield, which is believed to prevent tumor invasion. Different mechanisms leading to a disruption of the protective mesothelium, favoring metastatic outspread, have been discussed. Interestingly, increased mesothelial cell apoptosis introduced during pathological processes, including inflammation and malignancy, have been reported. Strikingly, we are the first to pinpoint the induction of mesothelial cell apoptosis to tumor-associated lymphocytes present within the ovarian cancer tumor microenvironment. Thus, we determined NK cells as the main effectors promoting mesothelial clearance *in vitro*. Soluble factors secreted by activated T cells stimulate the NK cells' cytotoxic potential. Here we discovered TRAIL-dependent killing of omentum-derived mesothelial cells as central mode of NK cell cytotoxicity, as demonstrated by applying a neutralizing anti-TRAIL antibody. Further evidence evolved from enhanced TRAIL expression on NK cells upon stimulation with T cell-secreted mediators, while the corresponding activating death cell receptors, DR4 and DR5, are expressed on mesothelial cells. By contrast, a significant contribution of Fas/FasL signaling or cytotoxic cytokines, including TNF α and IFN γ , could be ruled out. Even though mesothelial apoptosis could generally be induced by granzyme B/perforin, immunosuppressive ascites completely blocked this pathway, which is therefore not important in our system. Affinity proteomic-based analysis (Olink) of T cell-soluble factors comparing the secretomes of untreated and activated T cells revealed mediators inducing NK cell activation and TRAIL up-regulation. Intriguingly, we detected a previously unknown secretome-based crosstalk between ascites-derived T and NK cells mediating TRAIL upregulation

on NK cells mainly by T cell-secreted TNF α , demonstrated by gain and loss of function experiments. A more subordinate role was assigned to further T cell-secreted cytokines linked to NK cell activation and TRAIL signaling, including IL-2, IL-21 and IFN γ , possibly cooperating with TNF α to activate the NK cell cytotoxic potential. In the following, we addressed whether TRAIL-dependent killing mediated by NK cells in the tumor milieu was selectively directed against mesothelial cells. By analyzing the potential of NK cells in killing high-grade serous ovarian carcinoma cells, we found that the primary tumor cells were resistant towards TRAIL-mediated killing, which was associated with decreased expression levels of the death receptors. To further investigate why especially mesothelial cells derived from the malignant tumor microenvironment were prone to TRAIL-dependent killing, mesothelial cells obtained from a benign background were compared and found to be less sensitive to apoptosis induction by NK cells, which was further TRAIL-independent. This could be reasoned by the lower expression of DR4 and indicates that the mesothelial cells might be educated by ascites-derived soluble factors to TRAIL sensitivity, thereby supporting tumor implantation.

A causal link between TRAIL-mediated disruption of the mesothelial barrier by NK cells and enhanced ovarian cancer cell invasion could be proven *in vitro* by a trans-mesothelial invasion assay. Finally, these findings could be clinically accredited by immunohistological analysis of patient samples showing a loss of the mesothelium in the close proximity of early metastatic lesions, while free-floating apoptotic mesothelial cells were present in the ascites.

In conclusion, these novel findings indicate that NK cells, activated primarily by T cell-derived TNF α , play an essential role in promoting transcoelomic dissemination by selectively destroying the protective mesothelial barrier in a TRAIL-dependent manner.

Zusammenfassung

Die transcoelomische Dissemination von Tumorzellen über die maligne peritoneale Flüssigkeit (Aszites) erfolgt schon in einem frühen Stadium des hochgradig serösen Ovarialkarzinoms. Während des Fortschreitens der Erkrankung entwickeln sich große Mengen Aszites, welche eine typische Charakteristik der Tumormikroumgebung darstellt. Im Aszites sind lösliche Faktoren und verschiedene Zellarten, unter anderem Immunzellen, enthalten, welche die Metastasierung prioritär in das Omentum fördern. Der exakte Mechanismus der peritonealen Invasion des hochgradig serösen Ovarialkarzinoms ist bis heute weitestgehend unerforscht. Das Omentum, sowie weitere Organe des Peritoneums, sind von einer Mesothelzellschicht bedeckt, welche eine protektive Barriere darstellt und somit Tumorinvasion verhindern soll. Es werden verschiedene Mechanismen diskutiert, wie die Tumorzellen die protektive Schutzschicht des Peritoneums überwinden und invadieren. Eine verstärkte Apoptoseinduktion in Mesothelzellen wurde unter Inflammation und Malignität beobachtet. Wir konnten als erstes zeigen, dass Apoptose in Mesothelzellen durch Tumor-assoziierte Lymphozyten in der Tumormikroumgebung des Ovarialkarzinoms induziert wird. Hierbei identifizierten wir NK-Zellen als Haupteffektorpopulation, welche die mesotheliale Barriere *in vitro* beseitigen können. Für eine effiziente Stimulation der NK-Zell-Zytotoxizität waren lösliche Mediatoren, die von aktivierten T-Zellen sekretiert wurden, essentiell. Durch die Verwendung eines neutralisierenden anti-TRAIL Antikörpers konnten wir eine TRAIL-vermittelte Apoptoseinduktion in Mesothelzellen aus dem Omentum als zentralen Mechanismus der NK-Zell-Zytotoxizität identifizieren. Darüber hinaus wurde die TRAIL Expression auf der NK-Zellmembran durch die Stimulation mit T-Zell-sekretierten Mediatoren hochreguliert, während die korrespondierenden TRAIL-Rezeptoren, DR4 und DR5, auf den Mesothelzellen ebenfalls deutlich exprimiert sind. Im Gegensatz dazu konnte kein signifikanter Einfluss des Fas/FasL Signalweges festgestellt werden. Auch eine direkte Beteiligung zytotoxischer Zytokine wie TNF α und IFN γ konnten vernachlässigt werden. Obwohl Granzym B/Perforin Apoptose in Mesothelzellen induzieren, wurde dies durch die immunsuppressive Aszites komplett blockiert, weshalb dieser Signalweg in unserem System keine wichtige

Rolle zu spielen scheint. Um die verantwortlichen T-Zell-sekretierten Mediatoren zu identifizieren, wurde eine auf Affinitätsproteomik-basierende Analyse (Olink) der unstimulierten und stimulierten T-Zell-Sekretome durchgeführt. Interessanterweise identifizierten wir hierbei ein zuvor unbekanntes Sekretombasiertes Netzwerk zwischen Aszites-assoziierten T- und NK-Zellen, wobei vor allem T-Zell-sekretiertes TNF α zur verstärkten TRAIL-Expression auf NK-Zellen führt. Dies konnte mittels „Gain-of-Function“ und „Loss-of-Function“ Versuche demonstriert werden. Eine eher untergeordnete Rolle wurde weiteren T-Zell-sekretierten Zytokinen – IL-2, IL-21 und IFN γ – zugesprochen, die ebenfalls mit NK-Zell-Aktivierung und TRAIL-Signalwegen assoziiert sind. Eventuell kooperieren diese Zytokine mit TNF α , um das zytotoxische Potential von NK-Zellen zu aktivieren. Wir konnten zeigen, dass primäre Tumorzellen resistent gegen TRAIL-vermittelte Apoptose waren, was mit einer verminderten Expression der TRAIL-Rezeptoren assoziiert war. Gleichermaßen wurde aus vergleichenden Analysen mit Mesothelzellen aus Patientinnen mit benignen gynäkologischen Erkrankungen ersichtlich, dass diese generell weniger anfällig gegenüber NK-Zell-induzierter Apoptose und darüber hinaus resistent gegenüber TRAIL waren. Grund hierfür könnte sein, dass DR4 auf diesen Mesothelzellen geringer exprimiert ist. Eventuell könnten Aszites-assoziierte Faktoren im Tumormilieu dafür verantwortlich sein, die Mesothelzellen gegenüber TRAIL zu sensibilisieren und dadurch indirekt die Tumorumplantation fördern. Ein kausaler Zusammenhang zwischen der TRAIL-vermittelten Zerstörung des Mesothels durch NK-Zellen und verstärkter Tumorzellinvasion konnte *in vitro* durch transmesotheliale Invasionsversuche bestätigt werden. Zuletzt lassen diese Beobachtungen zusammen mit immunhistologischen Färbungen von Patientenproben eine klinische Relevanz vermuten. In Gewebeschnitten konnte ein Verlust des Mesothels in unmittelbarer Nähe früher Metastasen, sowie apoptotische Mesothelzellen im Aszites nachgewiesen werden. Zusammenfassend konnten wir zeigen, dass NK-Zellen, nach Aktivierung durch T-Zellen, vor allem über die Sekretion von TNF α , eine wichtige Rolle in dem Metastasierungsprozess des hochgradig serösen Ovarialkarzinoms spielen, indem sie in der Tumormikroumgebung selektiv die protektive Mesothelzellschicht über einen TRAIL-vermittelten Mechanismus zerstören und somit die Tumorum Invasion begünstigen.

1. Introduction

1.1 Ovarian carcinoma – Statistics, origin and staging

In 2020 approximately 313,959 new cases of ovarian carcinoma and 207,252 new deaths worldwide were registered (Sung et al. 2021). According to these statistics, ovarian carcinoma is the third most common cancer among the gynecological malignancies worldwide, with an age-standardized incidence rate of 6.6/100 000 women (cervical: 13.3, uterine: 8.7) (Sung et al. 2021). Since ovarian carcinoma is usually not diagnosed until late stages, it is described as the most lethal of all gynecological malignancies with a poor prognosis. The 5-year overall survival rate at advanced stages is only 17% (Huang et al. 2022). Ovarian carcinoma normally occurs in postmenopausal women diagnosed at a median age range of 50-79 (reviewed in Momenimovahed et al. 2019).

The International Federation of Gynaecology and Obstetrics (FIGO) adjusted the staging classification in 2014 to integrate ovarian, fallopian tube and peritoneal cancer in one system (Berek et al. 2021). The reason for this is that other than initially expected, 80% of high-grade serous classified carcinomas of the ovaries or peritoneum (HGSC) could also have evolved from the fimbriae (Berek et al. 2021; Callahan et al. 2007).

Type I, low grade carcinomas, are nowadays believed to originate from a form of endosalpingiosis, such as cortical inclusions of mullerian epithelium, endometriosis and cystadenomas (Berek et al. 2021). These tumors, including low-grade endometrioid, clear cell, borderline and low-grade serous are genetically stable. Type II, high-grade serous carcinomas, high-grade endometrioid and carcinosarcomas evolve from the distant fallopian tube and are associated with TP53 mutations in approximately all cases (Berek et al. 2021). The main sites of metastatic lesions include the omentum, as well as pelvic and abdominal viscera within the peritoneum. Metastasis outside the peritoneum are uncommon (Berek et al. 2021).

Histologically ovarian cancer is classified into serous, mucinous, endometrioid, clear cell, brenner, undifferentiated, mixed epithelial or peritoneal carcinoma with epithelial origin in 90% of cases (Berek et al. 2021; reviewed in Momenimovahed et al. 2019). The tumors are further subclassified by histological grading

describing their differentiation status. Most prevalent are serous carcinomas, which are either described as high- or low-grade dependent on their biology (Berek et al. 2021).

FIGO staging is executed from surgical findings concerning spread, histology and malignant ascites formation: Tumors are classified as stage I if the tumor is restricted to one (IA) or both (IB) ovaries or fallopian tubes, as well as additional surgical spill (IC1), capsule rupture prior to surgery/tumor on the surface of the ovaries or fallopian tube (IC2) or if malignant cells are found in the ascites or peritoneal rinsing fluid (IC3). Stage II tumors exhibit peritoneal cancer or pelvic extensions either on uterus, ovaries and fallopian tubes (IIA) or further intraperitoneal regions (IIB). The classification of stage III tumors further includes cytologically or histologically confirmed metastasis to retroperitoneal lymph nodes (IIIA1) and regions outside the pelvis (IIIA2), with metastasis up to 2 cm in size (IIIB) or greater than 2 cm (IIIC). In stage IV tumors, distant metastasis are found with cytologically positive pleural effusion (IVA) and parenchymal or extra-abdominal metastasis (IVB) (Berek et al. 2021).

About 20% of ovarian, fallopian tube or peritoneal cancer cases are due to hereditary factors. Most important here is the BRCA1/2 gene mutation in 15% of women with high grade non-mucinous ovarian carcinomas, posing the highest genetic risk factor. The risk of developing ovarian, tubal or peritoneal cancer for women with germline mutations in BRCA 1 is approximately 20-50% and 10-20% for mutations in BRCA2. In this case, the median age of diagnosis lies within the 40s (Berek et al. 2021).

Throughout this work, we have focused on high grade serous ovarian carcinoma (including the fallopian tube and peritoneal origin as described above), since this type represents the most frequent ovarian malignancy (Berek et al. 2021).

1.2 Diagnosis and therapy of ovarian carcinoma

Up to this date, there are still no screening techniques effectively reducing the mortality caused by ovarian, tubal or peritoneal carcinomas. At the time of diagnosis, most ovarian cancers are of stage III or IV with unspecific symptoms, including abdominal pain, menstrual irregularities, dyspepsia or digestive problems. As the disease progresses, large volumes of malignant ascites can

form, leading to additional respiratory symptoms. During diagnosis, the presenting patient's age, expression of tumor markers, ascites formation, ultrasound and computer tomography (CT) findings, as well as mono- or bilaterality are considered (Berek et al. 2021). Depending on the cancer stage at the time of the operation, laparotomy with abdominal hysterectomy, bilateral salpingo-oophorectomy, omentectomy and further cytoreductions are performed. Adjacent to primary cytoreduction, chemotherapy applying a platinum-based combination of Carboplatin or Cisplatin with Paclitaxel or Docetaxel represent the standard therapy. Bevacizumab, an antibody directed against vascular endothelial growth factor A (VEGFA) targeting angiogenesis, has been added to the chemotherapy as standard of care in some countries. A slight increase in progression-free survival has been noted in some clinical trials, while the overall survival remained unaffected (reviewed in Mirza et al. 2020; Ledermann 2017). Almost 80% of patients with advanced tumor stage relapse after responding to first-line therapy. The median time to recurrence is hereby 16 months. Adjacent chemotherapy depends on the time of the progression-free interval and obtained platinum-resistance (Berek et al. 2021). Supporting reports demonstrate a benefit of maintenance chemotherapy with poly adenosine diphosphate (ADP)-ribose polymerase (PARP) inhibitors (i.e. Olaparib) after first-line therapy or platinum-sensitive recurrence significantly increasing patient progression-free survival (Berek et al. 2021; reviewed in Mirza et al. 2020). PARP inhibition leads to increasing amounts of single- and double-stranded DNA breaks, which cannot be repaired, finally leading to cancer cell death (reviewed in Mirza et al. 2020). Furthermore, the beneficial effect of immune checkpoint inhibitors in combination with chemotherapy and PARP inhibitor are being tested (Berek et al. 2021). Immune checkpoints are important as negative feedback mechanisms, regulating T cell receptor signaling during antigen presentation preserving self-tolerance. These pathways play an important role in tumor immune escape and include the T cell surface molecules cytotoxic T-lymphocyte antigen 4 (CTLA-4) and programmed death 1 (PD-1) inhibiting T cell activation upon antigen presentation. Cancer cells often express programmed cell death-ligand 1 (PD-L1) binding to PD-1 on T cells and inhibiting their activation. Since this is associated with a bad prognosis, immunotherapy aims at blocking these inhibitory pathways propagating T cell activation and anti-cancer immunity. Patient response largely

relies on the composition of the tumor microenvironment (TME). Higher tumor T cell infiltration is associated with a better response (reviewed in Siminiak et al. 2022). Nevertheless, there is still no benefit in immunotherapy for ovarian cancer patients and side effects are severe (reviewed in Siminiak et al. 2022). A possible reason for this will be addressed in the following thesis.

1.3 The unique TME of HGSC

The TME of HGSC presents special characteristics, distinguishing it from other cancer types and highlighting its severe outcome. A unique feature includes early onset of transcoelomic dissemination enabled by extensive accumulation of peritoneal fluid, the malignant ascites. This equips for effective metastatic spread within the abdominal peritoneum, mainly the omentum (reviewed in Worzfeld et al. 2017; Lengyel 2010). The ascites congregation is reported to facilitate upon vascular endothelial growth factor (VEGF) signaling increasing capillary permeability and decreased lymphatic drainage of the abdomen due to tumor cells blocking the stomata, as illustrated in figure 1 (reviewed in Ford et al. 2020). Therefore HGSC metastatic spread is independent of angiogenesis and the hematological route (reviewed in Weidle et al. 2016).

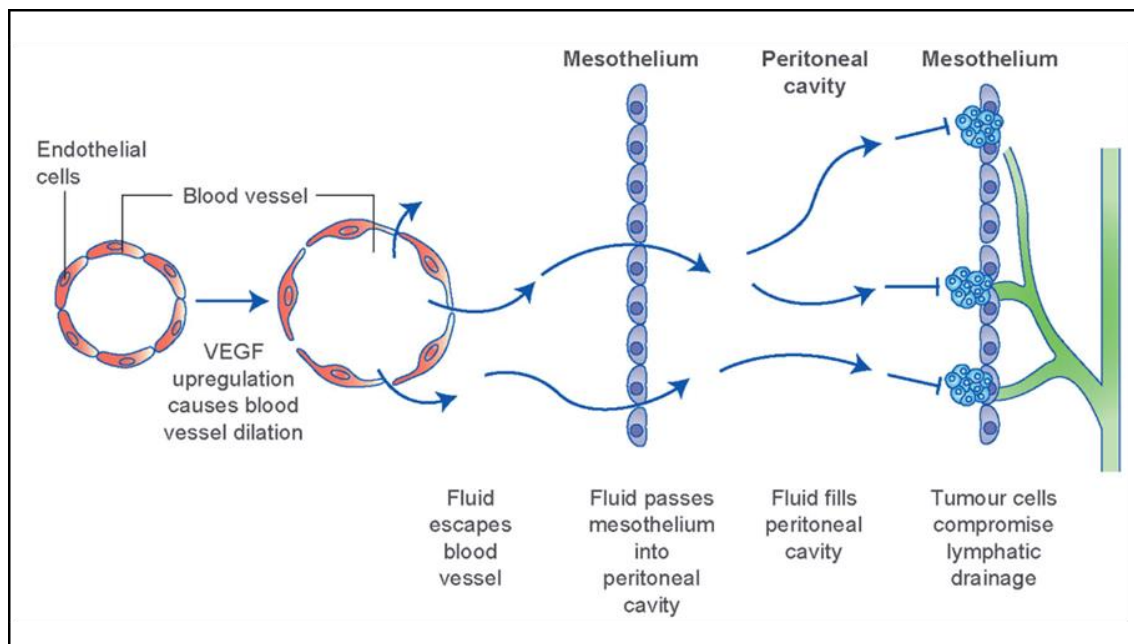


Figure 1. Mechanism of malignant ascites formation during HGSC cancer progression.

VEGF promotes increased vascular permeability, while tumor spheroids block lymphatic drainage facilitating the accumulation of large amounts of peritoneal fluid – ascites. Illustration derived from Ford et al. 2020 (Creative Commons Attribution license:

<http://creativecommons.org/licenses/by/4.0/>).

The malignant ascites forms one part of the unique TME and holds large amounts of soluble factors secreted by the host cells and tumorigenic cancer cells. Previously performed SOMAscan-based proteomic analysis identified 1,305 plasma proteins in total represented in HGSC ascites, of which 356 showed significantly higher levels compared to plasma. Of these proteins, two distinct clusters were found: cluster 1, associated with metastasis-associated processes (i.e. migration, adhesion, extracellular matrix (ECM) remodeling and angiogenesis) linked to a short relapse-free survival (RFS), while cluster 2, associated with immune regulation, linked to increased RFS (Finkernagel et al. 2019). Thus, a complex signaling network between the different cell types within the TME is formed, contributing to a favored metastatic outspread (Worzfeld et al. 2018). As depicted in figure 2, among the host cells immune cells, including tumor-associated macrophages (TAM), T cells, natural killer (NK) cells and B cells can be found, as well as stroma cells, including endothelial cells, human peritoneal mesothelial cells (HPMC), cancer-associated fibroblasts (CAF) and cancer-associated adipocytes (CAA). Tumor cells are present as different-sized spheroids or single cells (reviewed in Kim et al. 2016).

The sites of primary metastasis within the peritoneum and omentum form the second, solid compartment within the TME, as demonstrated in figure 2 (reviewed in Pogge von Strandmann et al. 2017). The omentum is located within the abdomen and it functions to protect the visceral organs while modulating peritoneal homeostasis, including the regulation of inflammation processes, fluid exchange, angiogenesis and it provides stem cells, immune cells and lipids (reviewed in Pogge von Strandmann et al. 2017). It is surrounded by a monolayer of HPMC and mainly constructs fat cells and connective tissue (ECM), as well as lymphocytes (macrophages, B cells, T cells, NK cells, dendritic cells (DC)) and fibroblasts (reviewed in Pogge von Strandmann et al. 2017; Motohara et al. 2019). The specific tropism of HGSC for the omentum demonstrates its important role in providing metastasis-promoting factors (reviewed in Motohara et al. 2019). Contributing to this could be the accumulation of immune cells and capillary networks within milky spots, small functional units described as secondary lymphoid organs (Rangel-Moreno et al. 2009), distributed throughout the

omentum (reviewed in Liu et al. 2016). The milky spots are typically located around glomeruli vessels underneath the mesothelium found to feature stomata at these sites (reviewed in Liu et al. 2016). They function as lymphatic portals, important for peritoneal fluid drainage into the venous system. A strong accumulation of resident lymphocytes can be found at these sites, involved in immune surveillance and leading to a pale appearance explaining the origin of naming these sites ‘Milky Spots’ (reviewed in Sodek et al. 2012). Upon additional damage/change of the mesothelium within the TME, the tumor cells invade and colonize the omentum (reviewed in Liu et al. 2016). Here, the adiposites are re-programmed into CAA and the fibroblasts are re-educated into CAF promoting tumorigenesis (reviewed in Pogge von Strandmann et al. 2017). Moreover, stromal, immune, tumor and mesothelial cells secrete pro-inflammatory cytokines promoting metastatic outspread (reviewed in Liu et al. 2016). The complex signaling network between the different cell types present within both compartments (ascites and metastatic sites at the omentum) driving metastasis will be addressed in more detail in the following (section 1.4).

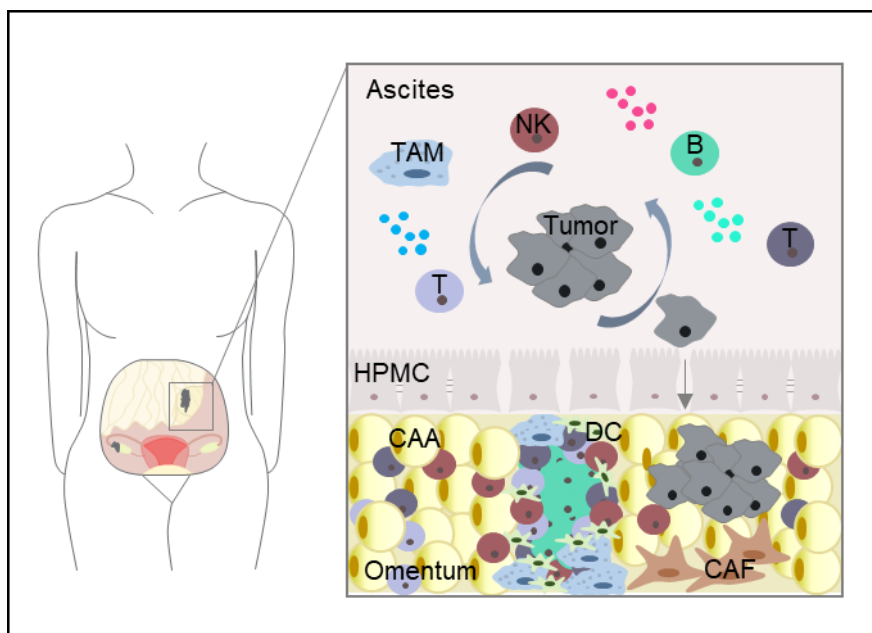


Figure 2. Compartments of the unique HGSC TME. The unique TME of HGSC can be divided into two compartments: (i) The ascites fluid, containing different cell types, including tumor spheroids or single cells, immune cells (TAM, T cells (T), NK cells (NK) and B cells (B)), as well as lower amounts of stroma cells. These cells secrete soluble proteins and exosomes. (ii) The site of primary metastasis, with implantations found in particular at the omentum. The omentum is covered by a HPMC monolayer, masking the ECM and building stomata at sites of underlying

milky spots. The milky spots comprise different immune cells (TAM, T cells, B cells, NK cells, and dendritic cells (DC)). Upon tumor invasion, the adipocytes are turned into CAA and the fibroblasts into CAF. A complex signaling network within and between these compartments promoting tumorigenesis is formed.

1.4 HGSC metastatic route promoted by a complex intercellular signaling network

Ovarian carcinoma metastasis follows the intraperitoneal transcoelomic dissemination by tumor cell release into the peritoneal fluid (reviewed in Sodek et al. 2012). Complex cell-cell communications between cancer cells and host cells provide the pre-requisite for the pre-metastatic niche formation, finally establishing metastatic lesions (reviewed in Ritch and Telleria 2022). As reported in Moss et al. 2009, cleavage of $\alpha 3$ integrin by matrix-metalloproteinase (MMP) 14, expressed by ovarian cancer cells, can induce tumor cell discharge from the primary tumor site (Moss et al. 2009; reviewed in Mei et al. 2023). The anatomical location of the ovaries and fallopian tube – in the abdomen without any physical barrier – is one explanation for the typical HGSC colonization of the peritoneum (reviewed in Mei et al. 2023). The tumor cells are then transported in the circulating malignant ascites, constituting a metastatic surrounding for ovarian carcinoma. Some of the most important signaling pathways forming the TME include ECM remodeling and organization, cell adhesion and regulation of immune response involving the complement system (reviewed in Worzfeld et al. 2017).

During transportation in the ascites, the tumor cells manage to avoid anoikis and immune responses, among others, finally attaching to the mesothelium lining peritoneal organs (reviewed in Mei et al. 2023). CAF present in ascites play a pivotal role in early metastatic steps of ovarian cancer. Upon tumor exfoliation, CAF promote the formation of heterotypic spheroids building the core, while the tumor cells showed high expression levels of integrin $\alpha 5$ (Gao et al. 2019; reviewed in Schoutrop et al. 2022). Further heterotypic spheroids consisting of tumor cells and TAM were found. In an orthotopic murine mouse model, it has been found that TAM within the spheroids secrete EGF leading to an autologous up-regulation of $\alpha M\beta 2$ integrin and ICAM-1 on tumor cells, promoting their interaction. Additionally, via EGF/EGFR signaling, tumor cell proliferation and migration were promoted in a VEGF-mediated manner (Yin et al. 2016; reviewed

in Schoutrop et al. 2022). These spheroids exhibit anchorage-independent survival resisting anoikis, increased adhesion and mesothelial clearance (reviewed in Schoutrop et al. 2022). In accordance with the “seed-and-soil” hypothesis proposed by Stephen Paget (Fidler 2003), the omental surface is similar to the ovarian surface epithelium, enabling tumor cell adaption by functioning as the “soil” (reviewed in Mei et al. 2023). Different involved processes have been described, including the direct binding of tumor cells to HPMC or the underlying ECM, as well as mechanisms of HPMC disruption and ECM remodeling. It has been described that the mesothelium is rendered more adhesive in the context of the TME: The adhesion molecules ICAM-1 and VCAM-1 are up-regulated on mesothelial cells, the tumor cells express CD44 binding to the hyaluronan-rich mesothelial surface, as well as the transmembrane mucin CA125 binding mesothelin on HPMC. Nevertheless, metastatic sites are commonly bereft of the mesothelial barrier, thus the affinity of ECM binding by tumor cells is much larger and mainly mediated via integrins (Niedbala et al. 1985; reviewed in Worzfeld et al. 2017; Sodek et al. 2012). Here, collagen I is the preferential substrate bound by ovarian cancer cells and the main peritoneal ECM component (reviewed in Sodek et al. 2012). In particular, $\alpha 2\beta 1$ integrin is important for the disaggregation of tumor spheroids present in the ascites fluid with subsequent increased adhesion ability to collagen I (Shield et al. 2007; Moser et al. 1996). This was further supported by increased MMP2 and MMP9 expression by tumor spheroids (Shield et al. 2007; reviewed in Ritch and Telleria 2022). It has been reported that upon clearance of the mesothelial barrier and exposure of the collagen-rich matrix, tumor cells preferentially invade the milky spot sites providing a pro-tumorigenic microenvironment, subsequently inducing fibrosis (reviewed in Mei et al. 2023). Interestingly, milky spot adjacent mesothelial cells show an activated cuboidal morphology with reduced integrity exposing the ECM, possibly due to the cytokines secreted by the neighboring lymphocytes (reviewed in Sodek et al. 2012). The pro-inflammatory surrounding of the metastatic site, induced by local immune cells, facilitates cancer progression (reviewed in Sodek et al. 2012). Thus, further mesothelial retraction is promoted by inflammatory cytokines, such as TNF α and IL-1 β , with subsequent increased ECM exposure creating prolonged tumor cell attachment (Stadlmann et al. 2003; reviewed in Sodek et al. 2012). Fibroblasts present within the sub-

mesothelium of the omentum secrete structural proteins building and regulating the ECM, including collagen, fibronectin, elastin and vitronectin. In the TME, these fibroblasts are turned into CAF driven by IL-6 and TGF β (reviewed in Mei et al. 2023). Subsequently, CAF and further host cells secrete different proteins inducing ECM remodeling, enabling tumor invasion and implantation (reviewed in Ritch and Telleria 2022). Reported from own transcriptome data, this role has also been assigned to TAM, showing strong up-regulation of genes involved in ECM remodeling (Finkernagel et al. 2016). The ECM plays a pivotal role in facilitating tumor progression by promoting tumor cell proliferation (ERK, PI3K and Rac signaling), migration and invasion (TGF β and RhoA/Rac signaling, fiber organization/stiffness), survival (modulation of BAX, Bcl-2 and NF- κ B), stemness (STAT3 and Wnt signaling) and by this, finally therapy resistance. Upon deconstruction of the ECM, the omentum is transformed into a stiff and fibrotic tissue (reviewed in Schoutrop et al. 2022). Furthermore, local CAA supply lipids, which the cancer cells use to encounter their energy requirements. Finally, angiogenesis within the metastatic omentum, promoted by CAF-secreted VEGF, enables adequate nutrient supply for tumor implantation (reviewed in Mei et al. 2023). Interestingly, from comparative transcriptomics of omentum-derived and ascites-derived tumor cells, the omental tumor cells showed a significant up-regulation of genes associated with epithelial traits and pro-inflammatory signaling. The transition between epithelial and mesothelial phenotypes possibly plays a role during metastasis and chemoresistance (Sommerfeld et al. 2021; Haslehurst et al. 2012).

Based on these reports from the literature, one can begin to imagine how complex and sufficient the metastatic outspread of HGSC via transcoelomic dissemination is. Therefore, it is important to see the bigger picture and shed light on still unknown mechanisms within the metastatic process.

1.5 Pro-tumorigenic role of mesothelial cells in the HGSC TME

The mesothelial layer represents a protective barrier surrounding the peritoneal organs masking the underlying ECM, which is mainly composed of collagen I and fibronectin, collagen IV and laminin. Mesothelial cells play a key role in peritoneal homeostasis and secrete glycosaminoglycans, mainly hyaluronan, surfactants (i.e. phosphatidylcholine) and proteoglycans apically, providing a gliding surface

for the viscera, preventing organ fusion and impeding cellular attachment or infiltration (reviewed in Ritch and Telleria 2022; Sodek et al. 2012). Therefore, the tumor cells must find a way to overcome the mesothelial covering. It acts as a first line of defense and initiates immune response (reviewed in Ritch and Telleria 2022). Via pattern recognition receptors expressed on the mesothelial cell surface, they can detect pathogens and respond by releasing inflammatory cytokines. Furthermore, upon injury, the entry of inflammatory immune cells into the peritoneal cavity, possibly via milky spots, is regulated by mesothelial cells secreting chemokines and cytokines (MCP-1 and IL-8) and expressing cell surface adhesion molecules (ICAM-1 and VCAM-1). Intriguingly, in response to tissue repair or pathological stimuli, including malignancy, mesothelial cells undergo a form of epithelial-mesenchymal transition (EMT), namely mesothelial-mesenchymal transition (MMT), transforming into myofibroblasts and CAF (Sandoval et al. 2013; reviewed in Sodek et al. 2012; Zheng et al. 2022). This indicates strong mesothelial plasticity (reviewed in Sodek et al. 2012; Zheng et al. 2022). Supporting the reports on mesothelial EMT traits in the presence of ascites (reviewed in Zheng et al. 2022; Ritch and Telleria 2022), own preliminary data revealed the induction of typical EMT characteristics, including the reduction of E-cadherin, increased Slug and ZEB-1 expression, as well as the upregulation of typical fibroblast markers (unpublished data). Furthermore, this reduced the amount of cell-cell contacts measured by zonula occludens-1 (ZO-1) staining (unpublished data). Others have also reported reduced cellular junctions under ascites conditions by oxidative stress, decreasing the integrity of the mesothelial barrier (Mikuła-Pietrasik et al. 2017). Additionally, hepatocyte growth factor (HGF), derived from the tumor cells, facilitated mesothelial senescence with subsequent up-regulation of fibronectin, down-regulation of junctional proteins and secretion of pro-angiogenic factors. Consequently, mesothelial integrity is disrupted and tumor cells can bind to fibronectin, finally promoting invasion (Ksiazek et al. 2009; Pakuła et al. 2019; reviewed in Zheng et al. 2022). This indicates that the mesothelial cells lose their protective function in the context of the TME (reviewed in Sodek et al. 2012). Additionally, HPMC within the TME have been found to produce different cytokines and CCL2, among others, promoting transmesothelial migration/invasion of tumor cells via p38-MAPK signaling (reviewed in Mei et al. 2023). It has been demonstrated that HPMC-

secreted Wnt5a regulates TAM polarization towards an immunosuppressive M2-like status. Subsequent increased chemokine secretion correlates with regulatory T cells and TAM infiltration (reviewed in Mei et al. 2023). Upon myosin- and traction forces exerted by tumor spheroids, they gain access to the ECM normally masked by the mesothelial layer, demonstrating an additional mechanism how the tumor cells overcome this barrier (Iwanicki et al. 2011). Interestingly, during inflammatory processes, such as acute peritonitis or long-term peritoneal dialysis, increased mesothelial apoptosis was registered, which was associated with an increased infiltration of immune cells. A potential involvement of these leukocytes in the apoptosis process was not demonstrated here (Catalan et al. 2003; Chen et al. 2003).

1.6 Pro-tumorigenic role of immune cells and tumor immune escape in HGSC

Immune cells, comprising innate and adaptive counterparts play a crucial role in the HGSC TME and largely contribute to tumor-immune escape, which is supported by different immunological configurations at primary tumor sites, ascites and the metastatic lesions (reviewed in Fucikova et al. 2021). Among the most abundant populations found in the ascites of HGSC patients are lymphocytes (including T cells and NK cells) and TAM (reviewed in Schoutrop et al. 2022).

The presence of tumor-infiltrating lymphocytes (TIL) is associated with an increased 5-year survival rate of HGSC patients. At the same time, this is not the case for the infiltration of stromal regions (reviewed in Fucikova et al. 2021; Schoutrop et al. 2022). Notably, the accumulation and recruitment of CD8+ T effector memory cells in ascites by CXCL9 derived from macrophages is associated with increased relapse-free survival. However, the HGSC TME promotes T cell dysfunction by inhibiting important signaling proteins (Lieber et al. 2018). Furthermore, the tumor cells down-regulate human leukocyte antigen (HLA)-I to escape the cytotoxic T cell attack. T cell exhaustion impairing anti-tumor response characterized by high expression levels of immune checkpoint receptors (ICR), including PD-1, CTLA-4, TIM-3, BTLA and LAG-3, demonstrates a further mechanism of immune evasion (reviewed in Schoutrop et al. 2022; Worzfeld et al. 2017; Worzfeld et al. 2018). Moreover, it has been shown that the

frequency of CD4⁺ T helper cells is increased in ascites compared to the primary tumor site or peritoneal lesions (reviewed in Schoutrop et al. 2022). An increased CD4⁺/CD8⁺ ratio in ascites is associated with poor patient survival (Giuntoli et al. 2009). This demonstrates that the T cell subtype and location of infiltration determine beneficial or detrimental outcomes for the patient (reviewed in Fucikova et al. 2021; Schoutrop et al. 2022). Here, especially regulatory T cells (Treg), correlating with an advanced stage of the disease, suppress an anti-tumor response in the TME (reviewed in Schoutrop et al. 2022). This is achieved by lysis of effector cells, inhibition of antigen-presenting cells (APC), secretion of immunosuppressive cytokines (i.e. IL-10, TGF β 1), as well as depletion of growth factors (reviewed in Fucikova et al. 2021). The unconventional T cell subtypes, $\gamma\delta$ T cells and natural killer T cells (NKT), representative of the interface between adaptive and innate immunity, display elevated levels in ascites. While it has been reported that $\gamma\delta$ T cells can mediate anti- and pro-tumor responses, NKT cells are probably inhibited in the immunosuppressive milieu. The exact role of these T cells remains to be discovered (reviewed in Schoutrop et al. 2022). B cell infiltration has also been associated with improved survival rates. They mainly reside within the stroma, only few have been found within tumor aggregates. Here, cooperative interactions between CD8⁺ T cells and CD20⁺ B cells improve disease outcome (Nielsen et al. 2012; reviewed in Fucikova et al. 2021).

TAM, NK cells, DC, neutrophils and myeloid-derived suppressor cells (MDSC) are examples for innate immune cells found in the TME. The professional antigen-presenting DC link the innate and adaptive immune system by inducing T cell activation. This function is impaired in the TME, by which anti-tumor T cell activation is affected. Inflammatory DC present in the TME produce pro-tumorigenic IL-6 and galectin-1 (Tesone et al. 2016; reviewed in Schoutrop et al. 2022).

TAM represent the most abundant type of myeloid-derived cells within the TME. They display a highly plastic and heterogeneous population of roughly classified pro-inflammatory type 1 (M1) and immunosuppressive type 2 (M2) macrophages with further TAM-specific characteristics (reviewed in Schoutrop et al. 2022; Fucikova et al. 2021). Finkernagel et al. 2016 additionally classified ascites-derived TAM into “bad prognosis” and “good prognosis” TAM based on the

expression levels of CD163 and CD206 cell surface markers (Finkernagel et al. 2016; Worzfeld et al. 2018). High expression levels are associated with a bad clinical outcome and the expression of cytokines and growth factors involved with “monocyte chemotaxis”. Opposing this, low expression levels are linked to increased RFS and the expression of factors assigned to “regulation of T cell chemotaxis” (Reinartz et al. 2014; Worzfeld et al. 2018). Furthermore, Sommerfeld et al. 2021 reported that omental TAM exhibit enhanced proliferative and pro-inflammatory properties compared to ascites TAM. Omentum-derived TAM demonstrated higher expression levels for genes encoding cytokines, growth factors and ECM-associated proteins (Sommerfeld et al. 2021). TAM are highly pro-tumorigenic by promoting tumor cell migration, as demonstrated by own analysis (Steitz et al. 2020), invasion and growth. Upon secretion of CCL6 and CCL23 by omentum tissue-resident TAM, they facilitate tumor cell invasion and finally colonization of the omentum (Krishnan et al. 2020). Via EGFR and VEGFC signaling, TAM facilitating the up-regulation of integrins and ICAM-1, promoting tumor cell adhesion, spheroid formation and implantation (reviewed in Fucikova et al. 2021).

MDSC arise under pathological and inflammatory conditions, in which the differentiation of myeloid progenitor cells and immature myeloid cells is arrested. Therefore, the highly immunosuppressive MDSC correlate with poor survival rates. This results in inhibition of NK and T cell proliferation (reviewed in Schoutrop et al. 2022).

Neutrophils, which can also be found in omental milky spots, promote the pre-metastatic niche formation by forming neutrophil extracellular traps (NET) comprising of chromatin webs, enabling ovarian cancer binding and metastasis. This NETosis of neutrophils was stimulated by tumor cell-secreted factors, including IL-8, G-CSF, GRO α and GRO β , which can also be found in ascites (Lee et al. 2019).

Improved patient survival has been associated with the existence of intratumoral NK cells (Webb et al. 2014). Besides direct cytotoxicity of activated NK cells against tumor cells, they can also engage the adaptive immune system by conventional DC (cDC) recruitment into the TME via release of different

chemoattractants (reviewed in Fucikova et al. 2021). Nevertheless, the NK cell functionality is impaired in the immunosuppressive TME and NK cells are even described as receiving pro-tumorigenic traits (reviewed in Schoutrop et al. 2022). As reported by Levi et al. 2015, tumor-infiltrating NK cells were mainly CD56^{bright}/CD16^{dim}, which expressed increased amounts of VEGF promoting tumor-angiogenesis. Furthermore, it has been described that the NKG2D activating NK cell receptor is down-regulated by macrophage migration inhibitory factor (MIF) present in the TME (Krockenberger et al. 2008). Opposing this, previously performed analysis within our department demonstrated impaired NKG2D function on ascites-derived NK cells, while NKG2D itself was not down-regulated (Vyas et al. 2017). At the same time, the inhibitory checkpoint ligand B7-H6 was up-regulated on the tumor cell surface and the soluble form was present in ascites. This was reported to additionally down-regulate the expression of the activating receptor NKp30 on NK cells, concomitant with reduced IFN γ production (Pesce et al. 2015). Intriguingly, it has recently been reported that NK cells present in the ascites of ovarian cancer patients also express PD-1, leading to their inactivation (Pesce et al. 2016). Subsequently, this could lead to NK cell exhaustion and tumor immune evasion (reviewed in Abel et al. 2018). Besides PD-1, further inhibitory checkpoints are expressed by NK cells, including the T cell Ig and immunoreceptor-based tyrosine inhibitory motif (ITIM) (TIGIT), CD96 (tactile) and TIM-3, among others. Their ligands are up-regulated on tumor cells (reviewed in Sivori et al. 2019). Furthermore, CA125, highly expressed in ascites, induces a strong down-regulation of CD16, concomitant with a slight reduction of the NKG2A receptor on NK cells (Patankar et al. 2005).

Additionally, the recruitment and functionality of immune cells is strongly dependent on the composition of the ECM (reviewed in Pickup et al. 2014; Schoutrop et al. 2022). An unfavorable immune landscape has been linked to high ECM density at the metastatic omentum (Pearce et al. 2018; reviewed in Schoutrop et al. 2022). Interestingly, recent analysis comparing primary tumor lesions and metastatic sites revealed immense differences in ECM structure, infiltrating lymphocyte subtypes and functionality (Gertych et al. 2022; Dötzer et al. 2019; Sommerfeld et al. 2021), possibly promoting tumor progression, which will be further addressed and discussed in this work. A more detailed report on T

and NK cell activation, functions and subtypes can be found in the following sections 1.7 and 1.8.

1.7 T cell differentiation, subtypes and function

The immune response against foreign or pathological influences relies on the interactions and alliances between the innate and adaptive immune system (reviewed in Raskov et al. 2021). As immune cells of the adaptive immune system, T lymphocytes originate from bone marrow progenitor cells, which mature in the thymus. During this process, described as thymopoiesis, T cell receptor (TCR) rearrangement is performed, resulting in CD4⁺/CD8⁺ thymocytes. From subsequent selection CD4⁺ or CD8⁺ thymocytes arise, which migrate into the periphery as naïve T cells (reviewed in Kumar et al. 2018). The TCR is highly diverse, up to 100 million different specificities have been quantified from sequencing analysis (Qi et al. 2014; reviewed in Kumar et al. 2018). T cell differentiation resulting in effector T cells upon activation by APC occurs in three phases, including (i) clonal expansion of activated, pathogen-specific T cells contributing to infection removal, (ii) subsequent T cell apoptosis during the contraction phase and (iii) long-term persistence of memory T cells protecting against a second infection (reviewed in Kumar et al. 2018). These memory T cells can then be found in the previously infected tissue as effector memory cells or located within secondary lymphoid organs as central memory cells (reviewed in Golubovskaya and Wu 2016).

The CD4⁺ T helper cells can differentiate into multiple subsets induced by specific cytokines, including T helper (Th) 1, Th2, Th9, Th17, Th22, Treg and follicular T helper cells (Tfh). Their full differentiation is promoted by different cooperating transcription factors. In turn, the subsets are characterized by specific cytokine profiles, which also determine their functionality as pro- or anti-inflammatory, survival and protection. Generally speaking, Th1 and Th2-derived cytokines are pro-inflammatory and associated with cytotoxicity, Th17 are essential for host defense against foreign pathogens, such as bacteria and fungi, Tfh induce humoral immunity by interacting with B cells and Treg promote immune-suppressive functions (reviewed in Golubovskaya and Wu 2016).

CD8+ cytotoxic T cells can be activated by APC and subsequently differentiate into T stem cell memory cells, T central memory cells, T effector memory cells and T effector cells with increased effector function and decreased memory function and proliferation (reviewed in Golubovskaya and Wu 2016). They express Fas, different integrin family members and secrete IL-2, IL-4 IFN γ and TNF α (Hamann et al. 1997). The transcription factor Eomesodermin (Eomes) is important for CD8+ T cell differentiation. The CD8+ cytotoxic T cells are the main mediators inducing cell death and removing unhealthy cells, while the CD4+ T helper cells enable maintenance of the CD8+ response and prevent exhaustion (reviewed in Golubovskaya and Wu 2016; Luckheeram et al. 2012; Raskov et al. 2021).

1.8 NK cell maturation, activation and cytolytic functions

NK cells are a part of the innate immune response and display 5-20% of circulating lymphocytes in humans. NK cells share similar traits with the innate lymphoid cell (ILC) group since they both produce IFN γ and TNF α upon activation. Additionally, NK cells exert cytolytic functions similar to the CD8+ cytotoxic T cells. NK cells develop and mature in the bone marrow and secondary lymphoid organs and tissues (tonsils, spleen and lymph nodes) in different stages. Upon CD56 (neutral cell adhesion molecule (NCAM)) expression during the final stage, immature NK cells are differentiated into mature NK cells, including the functional stages of CD56^{bright}/CD16^{low} and CD56^{dim}/CD16^{high}. The developmental stages are driven by “gamma chain cytokines”, including IL-2, IL-4, IL-7, IL-9, IL-15 and IL-21, which signal via the type I transmembrane glycoprotein γ_c chain (CD132) and specific cytokine receptors. Most circulating NK cells are CD56^{dim}/CD16^{high}, while the less mature CD56^{bright}/CD16^{low} NK cells are found in secondary lymphoid tissues. The functional differences concern the production of inflammatory cytokines (CD56^{bright}), compared to the cytotoxic functions (CD56^{dim}) (reviewed in Abel et al. 2018).

To obtain their full responsive functionality, NK cells are educated during a process where they interact with self-major histocompatibility complex (MHC)-I rendering them self-tolerant, avoiding autoimmunity. Inhibitory Killer immunoglobulin-like receptors (KIR/CD158), expressed on NK cells, interact with MHC-I molecules (HLA-A, B, C) on target cells. The inhibitory NKG2A (CD159a)

type II transmembrane receptor recognizes HLA-E (reviewed in Abel et al. 2018; Sivori et al. 2019). Their inhibitory signal is transduced via the ITIM present in their cytoplasmic tail. This is important for self-recognition of healthy cells. The LIR-1 type I transmembrane protein represents another HLA-specific inhibitory receptor, able to bind HLA-A, B, C and G, and the cytomegalovirus encoded HLA class I homolog UL18 (Vitale et al. 1999; reviewed in Sivori et al. 2019). Additionally, activating KIR have also been identified, which carry a charged amino acid residue in their transmembrane domain, inducing the interaction with the immunoreceptor tyrosine-based activation motifs (ITAM)-bearing molecules KARAP/DAP12. This engagement with receptor-associated adaptor molecules is important for signal transduction since they lack signaling domains in their cytoplasmic tails (reviewed in Abel et al. 2018; Sivori et al. 2019). NKG2C, also belonging to the activating HLA-specific NK cell receptors, bind HLA-E at low affinity (reviewed in Sivori et al. 2019).

Activating NK cell receptors are important for the recognition of stressed, transformed and virus-infected cells. In particular, the natural cytotoxic receptors (NCR), type I transmembrane molecules of the immunoglobulin-like family, represent the major activating receptors, including NKp46 (NCR1/CD335), NKp44 (NCR2/CD336) and NKp30 (NCR3/CD337). NKp46 and NKp30 are expressed on resting NK cells and are up-regulated upon activation. NKp44, on the other hand, is only expressed on CD56^{bright} NK cells but can be up-regulated on other NK cell subtypes upon cytokine-mediated activation. Their association with different adaptor proteins via their charged amino acid present in the cytoplasmic region is important for their cell surface expression and functionality. The extracellular NCR domains interact with specific virus-derived molecules or stress/malignant transformation-induced translocation of intracellular proteins to the cell surface. Additionally, NKp46 and NKp44 can identify extracellular ligands. The NKG2D activating receptor is a type II transmembrane C-type lectin-like receptor, which binds HLA class I structural homologs, including ULBP and MICA/B. These ligands are up-regulated on the outer membrane of stressed, transformed and infected cells. CD16, a Fcγ receptor, interacts with the Fc part of IgG antibodies, which is limited to diseased cells, inducing antibody-dependent cell-mediated cytotoxicity (ADCC).

Exclusively CD56^{dim} NK cells express CD16. Further co-receptors, including 2B4, NTB-A, DNAM-1, CD59 and NKp80 amplify NK cell activation induced by the NCR or NKG2D. Toll-like receptors (TLR) are also found on NK cells, able to induce NK cell activation upon interaction with bacterial- or viral-specific molecules (reviewed in Sivori et al. 2019). The most important NK cell receptors are illustrated in figure 3 (reviewed in Shankar et al. 2020).

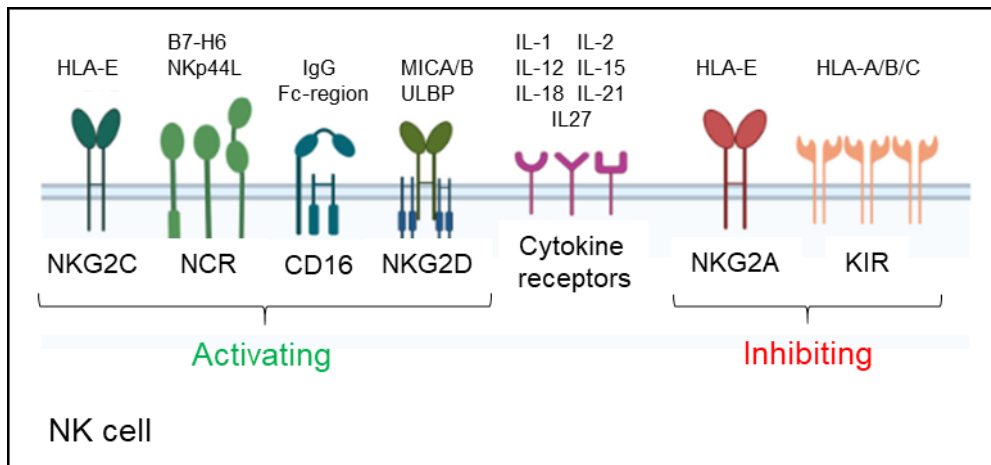


Figure 3. Main activating and inhibiting receptors expressed on NK cells and the corresponding ligands found on target cells. NK cells express different activating (NKG2C, NCR, CD16 and NKG2D) and inhibiting (NKG2A and KIR) receptors, which can interact with ligands expressed on potential target cells. Additionally, cytokine receptors are also found on NK cells. Illustration modified from Shankar et al. 2020 (Creative Commons Attribution license: <http://creativecommons.org/licenses/by/4.0/>).

The function of NK cells is tightly regulated by these activating and inhibitory receptors, described as “altered balance”. Thus, their signaling balance fine-tunes if NK cells kill potential targets and are activated or not (figure 4). As mentioned above, almost all somatic cells present endogenous peptides via MHC-I molecules on their surface, enabling the cells of the immune system to identify the intracellular environment. This further defines the “immunological-self”, which is important for immune tolerance and identification and elimination of “non-self” expressing allogeneic or haploidentical MHC-I. Furthermore, changes in self-MHC-I, characteristic for malignant transformation, can also be detected by NK cells. Self-MHC-I are often down-regulated on tumor cells contributing to the “missing-self” activation of NK cells. Additionally, tumor cells display increased amounts of stress-induced molecules on their surface, which can be bound by activating NK cell receptors, such as NKG2D. This “induced-

self” activation of NK cells finally describes the concept of NK cell cytotoxicity against malignant transformed cells, while MHC-I deficient erythrocytes are spared. The strongest NK cell activation occurs via the “non-self” recognition of transplanted tissue (as illustrated by the scales in figure 4) (reviewed in Abel et al. 2018).

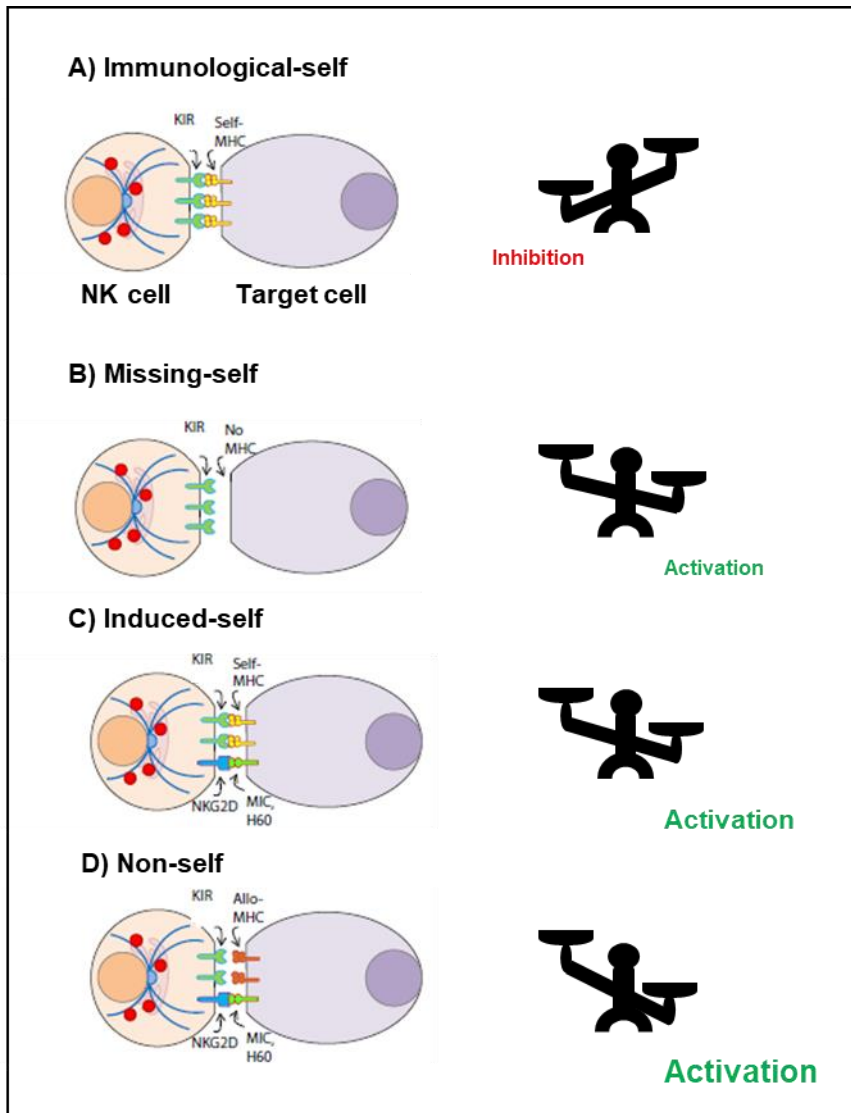


Figure 4. Target cell recognition following the “altered balance” mechanism of NK cell activation. NK cells express activating and inhibitory receptors important for target cell recognition. The major mechanisms of shifting the balance towards an inhibitory or activating signal are depicted here. (A) “Immunological self”: inhibitory KIR on NK cells bind to self-MHC I, leading to NK cell inhibition due to recognition of self-/untransformed cells. (B) “Missing self”: target cell recognition due to decreased MHC I expression, through which the inhibitory NK cell signal is missing. (C) “Induced self”: detection of activating ligands expressed on target cells via activating receptors on NK cells. This can overcome the inhibitory signal and promote NK cell activation. (D) “Non-self”: target cells express allogeneic or haploidentical MHC I (i.e. transplanted

tissue), which cannot be bound by KIR on NK cells, leading to NK cell activation via additional binding of activating ligands. Modified from Abel et al. 2018 (Creative Commons Attribution license: <http://creativecommons.org/licenses/by/4.0/>).

In response to malignancies and pathogens, NK cells mainly produce the Th1-type cytokines IFN γ , TNF α and GM-CSF to facilitate the activation of further immune cells (DC, macrophages, neutrophils and T cells). Via the production of chemotactic cytokines, NK cells recruit effector lymphocytes and myeloid cells to inflamed sites. The production of inflammatory cytokines is highly regulated by transcription factors, such as T-bet (reviewed in Abel et al. 2018). Importantly, NK cells are also sensitized and primed by inflammatory cytokines produced by DC (reviewed in Abel et al. 2018). The mechanisms by which NK cells exert their cytotoxic function include (i) recognition of their target cells, (ii) immunological synapse (IS) formation upon contact and (iii) target cell lysis following different signaling processes (reviewed in Abel et al. 2018), as described in the following (sections 1.8.1-1.8.3) and depicted in figure 5. It is possible that the different mechanisms of induced target cell death work together, triggering target cell lysis very effectively (reviewed in Ramírez-Labrada et al. 2022). IS formation requires the recognition of the target cell by receptor-ligand interactions, as described above. This is followed by the initiation, in which a strong link between the cells is formed via adhesion molecules. Here, particularly LFA-1 integrin, as well as ITIM and ITAM domains, promote actin rearrangement in NK cells. During the subsequent effector stage, the microtubule-organizing center (MTOC) is relocated to the IS and recruits lytic granules, resulting in a strong polarization. These granules fuse with the synaptic membrane, releasing their content into the synaptic cleft, acting as a protective area. Within this cleft, the concentration of the cytotoxic molecules is increased, strongly acting on the target cells, while surrounding cells are protected. Finally, NK cells detach in order to allow cytolytic recycling (reviewed in Ramírez-Labrada et al. 2022).

1.8.1 Cytolytic granules – Granzyme B/Perforin apoptosis signaling

One mechanism of NK cell-mediated killing of target cells is issued via the release of cytotoxic granules holding the serine protease family of different granzymes, as well as the pore-forming proteins perforin and granulysin. Five different granzymes have been found in humans, including granzyme A, B, K, M and H.

They are synthesized as pro-enzymes, which become active upon proteolytical cleavement. The granzymes are located in the endoplasmatic reticulum, followed by the golgi apparatus, where they are finally directed into the secretory granules. Here, the cysteine proteases cathepsin C or H enzymatically activate the granzymes by removing the inhibitory dipeptide. The low pH within the granules (pH 5.5) reduces the enzymatic activity. Their maximal activity can be found at neutral pH upon release from the granules. Different NK cell subsets may contain and release different granzyme-types (reviewed in Ramírez-Labrada et al. 2022). In the presence of calcium, the glycoprotein perforin inserts itself into the lipid bilayer membrane of the target cells, where it polymerizes and forms pores, enabling granzyme passage into the cell (reviewed in Ramírez-Labrada et al. 2022). Among the different granzymes, granzyme B (GrB) has the strongest cytotoxic potential. GrB initiates apoptosis signaling by cleaving and thereby activating intracellular caspase-3 and -7. Additionally, the mitochondria are involved by cleaving Bid leading to the active truncated t-Bid and degrading Mcl-1 releasing Bim. Subsequently, mitochondria outer membrane permeability is initiated, releasing cytochrome c and further pro-apoptotic factors, including SMAC/Diablo. Finally, the apoptosome is formed, which fully activates caspase-3 and -7, important for apoptosis induction. Moreover, GrB induces DNA fragmentation and cleaves further proteins involved in key cellular processes to promote cell death (reviewed in Ramírez-Labrada et al. 2022).

1.8.2 Cytotoxic cytokines

Activated NK cells release the cytotoxic cytokines TNF α and IFN γ contributing to target cell lysis (reviewed in Sedger and McDermott 2014; Jorgovanovic et al. 2020). In order to prosecute TNF α -mediated signaling, the specific receptors, TNF-R1 or TNF-R2, trimerize to enable TNF α binding. The receptor trimers undergo conformational change executed by the pre-ligand assembly domain (PLAD), located within the N-terminal cysteine-rich domain (CRD), important for TNF α binding and signaling. Depending on the receptor bound by TNF α (TNF-R1 or TNF-R2), cell death or cell survival signaling is induced (reviewed in Sedger and McDermott 2014). Apoptosis signaling is executed via TNF-R1 upon release of the intracellular TNF-R inhibitor, silencer of death domain (SODD) protein. This is achieved by PLAD-stabilized TNF-R and recruitment of the TNF-R-associated

death domain protein (TRADD), Fas-associated protein with death domain (FADD) and the TNF-R-associated factor (TRAF)-1, forming the death-inducing signaling complex (DISC). Subsequently, the initiator pro-caspase-8 is recruited and proteolytically cleaved, releasing the active caspase-8. Consequently, caspase-8 enzymatically processes further pro-caspases, including pro-caspase-3, -6 and -7, as well as further cytosolic substrates. The involvement of the mitochondria in the apoptotic process is achieved by caspase-8-induced cleaving of BID. Particularly caspase-3 is essential for cellular apoptosis since it activates the caspase-activated DNase (CAD), which degrades genomic DNA. Caspase-8 protease activity is regulated and inhibited by the caspase-8 inhibitory protein (cFLIP). It interacts with pro-caspase-8 via its death-effector domain (DED) to prevent extensive pro-caspase activation. The inhibitor of apoptosis proteins (IAP) are also an important apoptosis regulator (reviewed in Sedger and McDermott 2014). Controversially, non-death signaling pathways can also be activated by TNF α , including NF κ B, via recruitment of TRADD and TRAF2. NF κ B can promote a positive-feedback loop by transcriptionally inducing the expression of TNF and its receptors, amplifying this signaling pathway. It is further involved in inflammation, since it trans-activates pro-inflammatory cytokines and chemokines. These diverse functions of TNF α demonstrate its' additional ability to induce the production of further cytokines and synergize with interferons (reviewed in Sedger and McDermott 2014).

In the case of IFN γ -induced apoptosis signaling, the JAK/STAT signaling pathway is fundamentally important (reviewed in Kotredes and Gamero 2013; Jorgovanovic et al. 2020). IFN γ binds to its receptor constituted of the two subunits IFNGR1 and IFNGR2. An intracellular association of JAK1 and JAK2 and their activation upon IFN γ binding is important for subsequent signaling. Consequently, the STAT1 transcription factor is activated by phosphorylation and dimerization. In the following, this STAT1 homodimer translocates into the nucleus and anneals to the IFN γ -activated site (GAS) DNA sequence. Upon interaction with co-activator proteins STAT1 full transcriptional capacity is enabled. The transcription of multiple genes, namely Interferon signature genes (ISG), is induced, including caspase-3, -7 and Interferon regulatory factor-1 (IRF-1). These contribute to the apoptotic process i.e. in cancer cells. Negative

regulation of the IFN γ signaling is induced by SHP phosphatases (Shp2), suppressor of cytokine signaling (SOCS) protein family and protein inhibitor of activated STATs (PIAS). IFN γ binding to its receptor can also induce the non-canonical PI3K/AKT signaling pathway (reviewed in Jorgovanovic et al. 2020). A possible crosstalk between both pathways has been described (Gao et al. 2018). Next to the direct effect on cancer cell viability, IFN γ can also function indirectly by interacting with other stroma cells present within the TME (reviewed in Jorgovanovic et al. 2020).

1.8.3 Death receptor ligands

Besides the above-mentioned mechanisms of NK cell cytotoxicity, apoptosis can also be induced by engagement of NK cell-expressed death ligands with death receptors found on target cells. Among the death ligands on the NK cells, TNF α , FasL and TRAIL can be found. Here, only FasL and TRAIL have direct cytotoxic potential upon engagement. They belong to the TNF family and are type II transmembrane proteins. Upon proteolytic cleavement, they are released as a soluble form. Intriguingly, only soluble TRAIL and TNF α retain their functionality, while soluble FasL is inactive. FasL interacts with Fas, inducing receptor clustering and triggering apoptosis signaling. FasL interaction with DcR3 inhibits target cell death. TRAIL can interact with five receptors, of which three are decoy receptors, inhibiting apoptosis signaling (DcR1/TRAIL-R3; DcR2/TRAIL-R4; Osteoprotegerin (OPG)) and two activating death receptors, DR4 and DR5. TNF α can be processed by the TNF α -converting enzyme (TACE) (reviewed in Ramírez-Labrada et al. 2022; Horiuchi et al. 2010).

The death receptors, described as type I transmembrane proteins, contain a cysteine-rich extracellular domain and a conserved cytoplasmic death domain (DD). As a consequence of ligation, the DD induces receptor trimerization and the recruitment of FADD. DED within FADD initiates DISC formation by recruiting procaspase-8, FLIP and RIP-1. Autocatalytic cleavement of procaspase-8 molecules in close proximity into caspase-8, which is now catalytically active, is initiated. Caspase-8 then activates downstream caspase-3 and -7. The mitochondrial apoptotic pathway can also be involved, as described in section 1.8.1 (reviewed in Ramírez-Labrada et al. 2022).

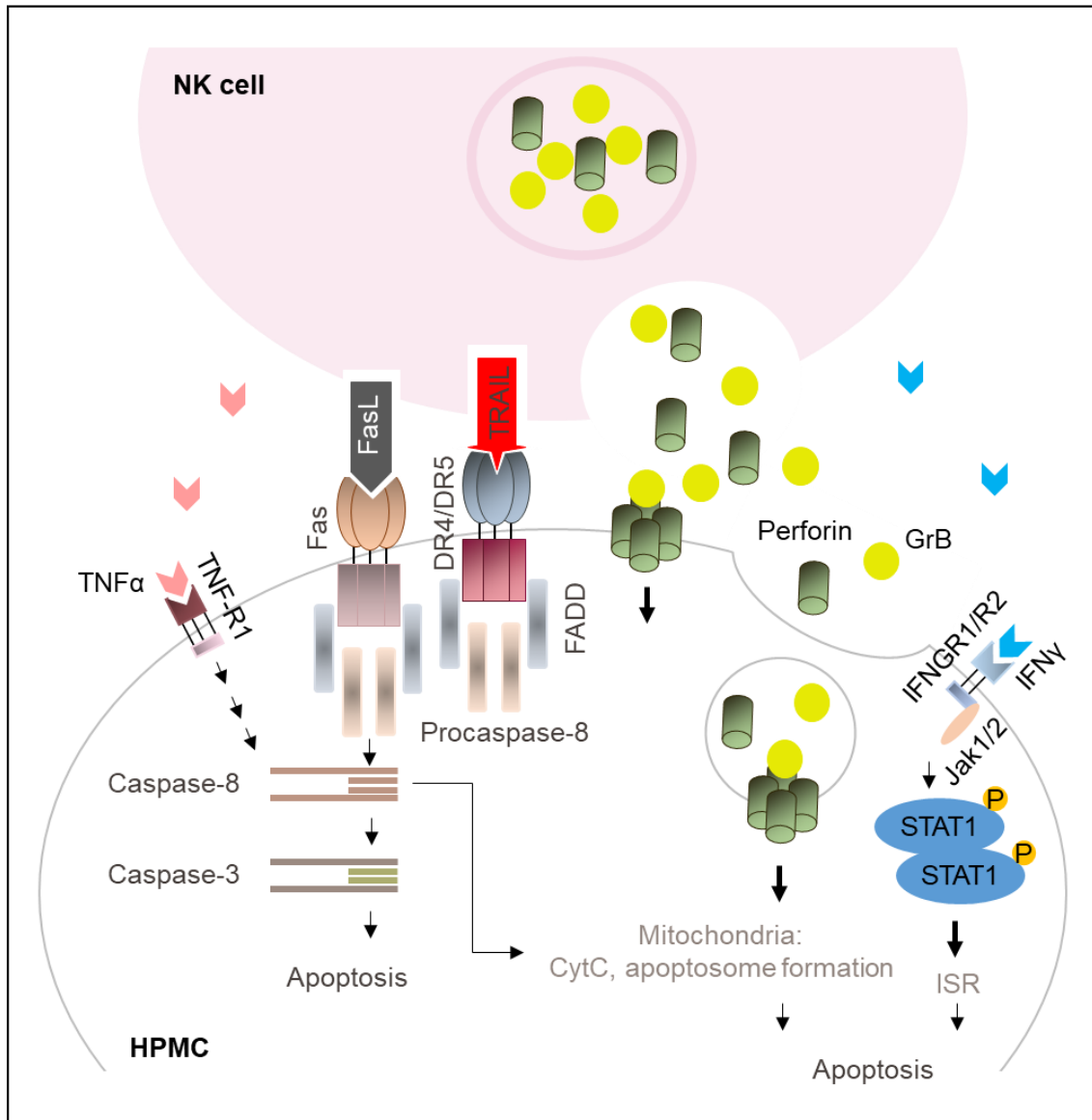


Figure 5. Schematic illustration of apoptosis signaling pathways executed by NK cells. The release of cytolytic granules, containing GrB/Perforin, triggers apoptosis signaling via involvement of the mitochondrial signaling pathway. NK cells can additionally release the cytotoxic cytokines TNF α and IFN γ , triggering distinct signaling pathways, as indicated. Signaling via receptor-ligand interactions, including Fas/FasL and DR4 or DR5 and TRAIL are also possible, triggering apoptosis by a direct activation of caspases.

1.9 Aim

The initial aim of the underlying thesis was to determine the influence of the highly represented TAL within the TME on the mesothelial integrity and the subsequent impact on HGSC progression and metastatic outspread. As previously reported in the literature, HPMC apoptosis can be induced under pathological conditions. Since this role has so far not been accredited to lymphocytes, we determined (i)

the potential of TAL-subsets to induce HPMC apoptosis, (ii) the maintenance of HPMC killing in the presence of immunosuppressive ascites, (iii) mode and selectivity of HPMC killing, (iv) subsequent tumor cell invasion and (v) a possible *in vivo* clinical relevance. As illustrated in the flow chart (figure 6), we approached this by isolating different cell populations from HGSC patient ascites (tumor cells and TAL subsets) and omentum (HPMC). *Ex vivo* tumor cells and HPMC derived from lavage of patients with benign gynecological diseases, served as controls for the specificity of cell death induction. Co-culture experiments between TAL/TAL-subsets and HPMC, control (Ctrl) HPMC or *ex vivo* tumor cells were performed to analyze the cytotoxic effects of TAL and their selectivity by annexin V and caspase-3/-7 staining. Furthermore, the susceptibility of these cell types towards TAL-mediated apoptosis was addressed. To determine the mode of killing, the different apoptosis signalling pathways, including GrB/Perforin, Fas/FasL, cytotoxic cytokines and TRAIL, were analysed by applying neutralizing antibodies, recombinant human (rh-) cytokines and proteins. Additionally, the responsible TAL population was defined and inter-cellular communications between T and NK cells were determined by collecting the T cell secretome. As readout, the induction of mesothelial and tumor cell apoptosis, as well as T and NK cell degranulation in response to HPMC, was flow cytometrically and fluorescence microscopically analyzed. The expression of cell surface ligands and receptor counterparts was measured by flow cytometry to further decipher specific signaling. Olink analysis of T cell-secreted cytokines with the potential to activate NK cells, and qPCR, detecting mRNA expression levels of IL-21 and TNF α , were performed. Finally, transmesothelial invasion assays were established to shed light on the poorly understood HGSC metastatic process and demonstrate the significance of TAL on tumor invasion, resulting from the destruction of the mesothelial barrier. Additionally, RNA sequencing data, previously generated by the research group (Sommerfeld et al. 2021), were analyzed comparing *ex vivo* tumor cells, HPMC, Ctrl HPMC and TAT to determine cellular interactions. We assigned clinical relevance to our findings by analyzing omental and ascites specimens of HGSC patients for the presence of apoptotic mesothelial cells.

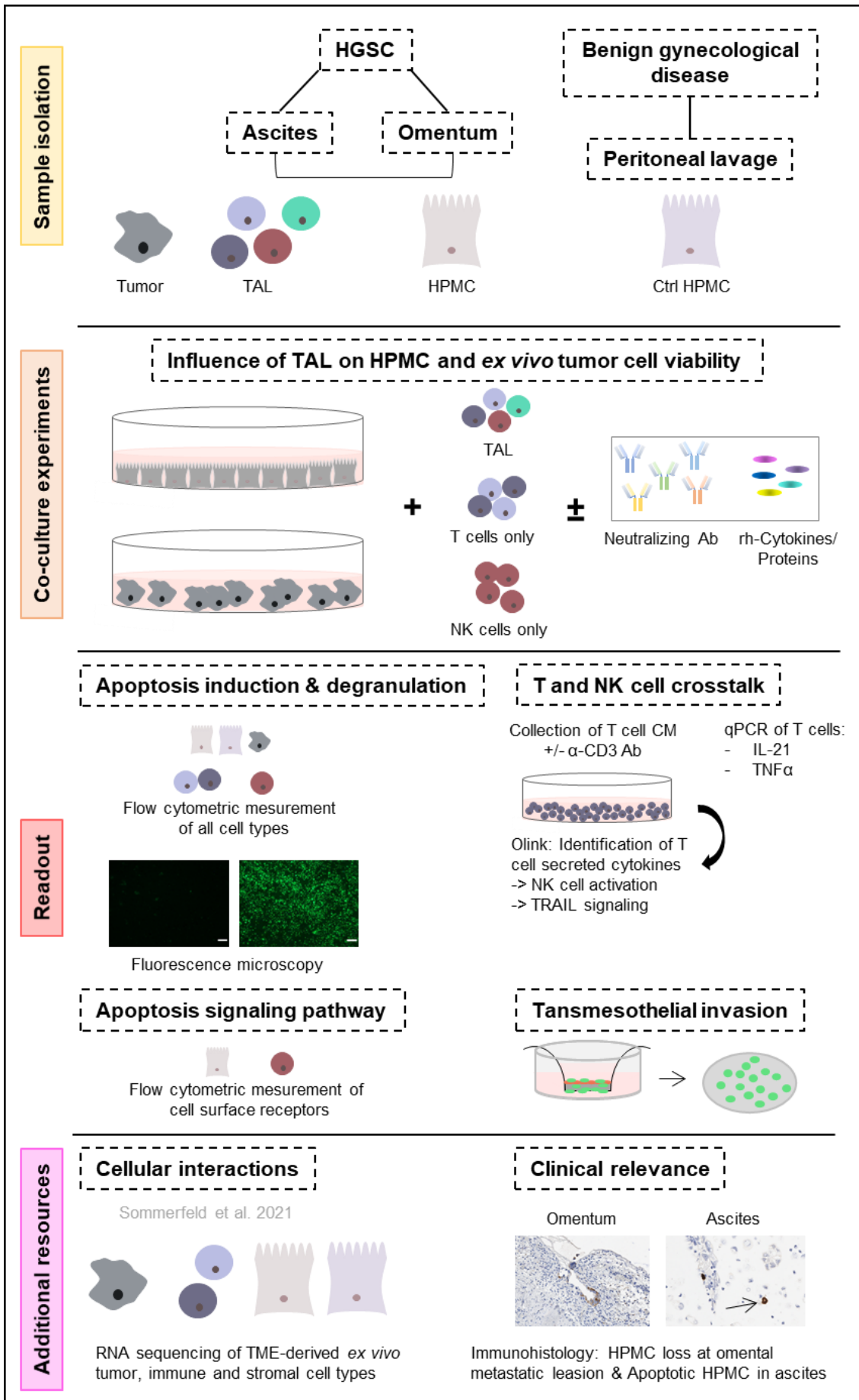


Figure 6. Flow chart illustrating the experimental procedure to determine the role of TAL and mesothelial cells on HGSC tumor progression. For the experimental procedure, tumor, stromal and immune cell types were isolated from HGSC patient-derived ascites and omentum, as well as Ctrl HPMC from the peritoneal lavage of patients with benign gynecological diseases. Co-culture experiments were performed between the different cell types under varying conditions to determine the functions of TAL and TAL subpopulations in the TME. Specific analyses were performed as a read out of the co-culture experiments. Additionally, cellular interactions were further analyzed from previously generated RNA sequencing data (Sommerfeld et al. 2021), comparing different TME-derived cell types. Clinical relevance was determined by Immunohistological analyses of metastasized omentum tissue and matching ascites samples.

2. Materials and Methods

2.1 Materials

2.1.1 Consumables and equipment

Plastic ware and other general consumables applied during cell cultivation and functional analysis, as well as non-sterile procedures were purchased from different companies, including BD Biosciences, BD Falcon, Corning, Eppendorf, Greiner Bio-One, Miltenyi Biotec, Nerbe Plus and Sarstedt. Further equipment applied throughout this PhD thesis is listed in table 1.

Table 1. List of equipment applied conducting experiments

Equipment		Firm
Cell counting chamber	Neubauer	NeoLab, Heidelberg
Centrifuge	Biofuge fresco	Heraeus Instruments, Hanau
	Biofuge pico	Heraeus Instruments, Hanau
	Multifuge 1	Heraeus Instruments, Hanau
	Multifuge 3	Heraeus Instruments, Hanau
	Fresco 17	Heraeus Instruments, Hanau
CO ₂ incubator	Heracell 240i	Thermo Scientific, Hamburg
Flow Cytometer (Fluorescence activated cell sorting (FACS))	FACS Canto II	Becton/Dickinson, Heidelberg
Fridge	Fridge (4 °C)	Liebherr Premium, Bieberach
Freezer	Freezer (-20 °C)	Liebherr Premium, Bieberach

	HERAfreeze HFUT SERIES (-80 °C)	Thermo Scientific, Hamburg
Heating block	ThermoStat plus	Eppendorf, Hamburg
Incubator		Binder, Tuttlingen
Laboratory deduction		Wesemann, Leipzig
Liquid nitrogen tank	Cryo biological storage system	Thermolyne/Thermo Fischer Scientific, Hamburg
Magnetic stirr	Variomjag	Thermo Fischer Scientific, Hamburg
Magnet for magnetic-activated cell sorting (MACS) cell isolation	MACS magnet	Miltenyi biotec, Bergisch Gladbach
Microscope	Leica DMI3000 B	Leica Microsystems, Wetzlar
	Axiovert 40 CFL	Zeiss, Jena
Microwave	Privileg 7533P	Quelle, Fürth
Pipets	Pipetboy	Eppendorf, Hamburg
	Multipette®	Eppendorf, Hamburg
qPCR System	Mx3000P	Agilent, Santa Clara (USA)
	PCR workstation	PeqLab, Erlangen
Q-Tips		
Roller	Roller 6 digital	IKA, Staufen
Spectrometer	Nanodrop 1000 V3.7	PeqLab, Erlangen
Sterile bench	MSC ADVANTAGE	Thermo Scientific, Hamburg
Thermo cycler	Stratagene Mx3000P	Agilent Technologies Böblingen
Vortex	MS2 Minishaker	IKA, Staufen
Water bath	Type 1083	GFL, Burgwedel

Water system	MilliQ	Millipore, Eschborn
Weighing machine	ABT 220-4M	Kern, Balingen

2.1.2 Chemicals and reagents

The chemicals and reagents applied for the experiments conducted throughout this work are listed in table 2.

Table 2. List of chemicals and reagents applied for experimental procedures

Reagents	Firm
3,3',5-Triiodo-L-thyronine	Sigma-Aldrich, Steinheim
AB-Serum	Sigma-Aldrich, Steinheim
Acetic acid	Carl Roth, Karlsruhe
Acrylamid stock solution	Carl Roth GmbH, Karlsruhe
Agarose (Ultra Quality)	Carl Roth, Karlsruhe
Albumin bowine fraction	SERVA, Heidelberg
All-trans-retinoic acid	Sigma-Aldrich, Steinheim
Bromphenol blue	Thermo Fischer Scientific, Hamburg
BSA (Albumin Bovine Fraction, Cohn Modified)	Sigma-Aldrich, Steinheim
β -Mercaptoethanol	Sigma-Aldrich, Steinheim
CellEvent™ Caspase 3/7 Green Detection Reagent	Invitrogen/Thermo Fischer Scientific, Karlsruhe
Celltracker green	Invitrogen/Thermo Fischer Scientific, Karlsruhe
Celltracker orange	Invitrogen/Thermo Fischer Scientific, Karlsruhe
Choleratoxin	Sigma-Aldrich, Steinheim
Chloroform	Merck, Darmstadt
Collagen I (rat tail)	Ibidi, Gräfelfing
Dimethyl Sulphoxide (DMSO) Hybri-Max®	Sigma-Aldrich, Steinheim
DMEM/Hams F12	Merck (Biochrom), Darmstadt

DMEM/Hams F12 + 2mM stab. Glutamin	Merck (Biochrome), Darmstadt
DMSO	Sigma-Aldrich, Steinheim
Dulbecco`s Modified Eagele`s Medium F12	Sigma-Aldrich, Steinheim
Ethylenediaminetetraacetic acid (EDTA)	Carl Roth, Karlsruhe
Ethanol	Carl Roth, Karlsruhe
FACS Clean Solution	BD Biosciences, Heidelberg
FACS Flow Solution	BD Biosciences, Heidelberg
FACS Rinse Solution	BD Biosciences, Heidelberg
FCS (Fetal Calf Serum)	Merck (Biochrome), Darmstadt
Ficoll (Lymphocyte separation media)	CAPRICORN Scientific, Ebsdorfergrund
Glutaraldehyde	Sigma-Aldrich, Steinheim
HCl (Salzsäure) 1M	Merck, Darmstadt
HEPES	Sigma-Aldrich, Steinheim
Hydrocortison	Sigma-Aldrich, Steinheim
IMDM (+ L-Glutamine, 25 mM HEPES)	Gibco by Life Technologies™ (Thermo Fischer Scientific), Hamburg
Insulin	Sigma-Aldrich, Steinheim
Ionomycin	Sigma-Aldrich, Steinheim
Isopropanol	Merck, Darmstadt
KHCO ₃ (Kaliumhydrogencarbonat)	Merck, Darmstadt
Linoleic acid	Cayman Chemical Company, Hamburg
Luminata Forte	Merck, Darmstadt
M199 Media	Gibco by Life Technologies™ (Thermo Fischer Scientific), Hamburg
M199 (1X) Earle's Salts + L-Glutamine	Gibco by Life Technologies™ (Thermo Fischer Scientific), Hamburg
Methanol	Sigma-Aldrich, Steinheim
Monensin (Golgi-Stop)	BD Bioscience, Heidelberg
Natriumchloride (NaCl)	Carl Roth, Karlsruhe
Natrium-Pyruvat (100mM)	Sigma-Aldrich, Steinheim
NP40	Applichem, Darmstadt

O-phosphoryl ethanolamine	Sigma-Aldrich, Steinheim
PBS (DPBS (1X) Dulbecco's Phosphate Buffered Saline)	GibcoR by life technologies™, (Thermo Fischer Scientific), Hamburg
PBS tablets	GibcoR by life technologies™, (Thermo Fischer Scientific), Hamburg
Penicillin/Streptomycin (1000U Pen, 10mg Strep. Pro 1ml in physiol. NaCl)	Sigma-Aldrich, Steinheim
PeqGold (peqGOLD TriFast™)	PeqLab, Darmstadt
Phorbil 12-myristate 13-actetate (PMA)	Sigma-Aldrich, Steinheim
Propidiumiodid	Merck (Calbiochem), Darmstadt
RPMI 1640 with Phenol Red (1X) + GlutaMAX™	Gibco by Life Technologies™ (Thermo Fischer Scientific), Hamburg
Selenious acid	Sigma-Aldrich, Steinheim
Sterile Water	Sigma-Aldrich, Steinheim
Superase-Inhibitor	Invitrogen/Thermo Fischer Scientific, Karlsruhe
Sodium hydroxide (NaOH)	Carl Roth, Karlsruhe
Sodium pyruvat	Sigma-Aldrich, Steinheim
Transferrin	Sigma-Aldrich, Steinheim
Trypan Blue	Sigma-Aldrich, Steinheim
TrypLE™ Express	Gibco by Life Technologies™, (Thermo Fischer Scientific), Hamburg
Trypsin-EDTA (0.05% Trypsin, 0.02% EDTA (1X))	Gibco by Life Technologies™, (Thermo Fischer Scientific), Hamburg
Tris hydrochloride (Tris-HCl)	Sigma-Aldrich, Steinheim
Vectashield	Biozol, Eching
Water (sterile)	Sigma-Aldrich, Steinheim

2.1.3 Antibodies

In the following the antibodies applied for flow cytometric phenotyping of TAL, isolation of cell populations via MACS, control of the purity of the isolated cell fractions, expression of cell surface receptors or ligands, neutralization of receptors, ligands and T cell secreted cytokines, T cell activation, as well as Immunohistochemistry are listed (table 3).

Table 3. List of antibodies applied for flow cytometry, MACS, neutralization and T cell activation

Antibody	Firm	Catalog number	Species
Flow cytometric phenotyping, MACS-isolation & purity control			
Iso-FITC	Miltenyi Biotec	130-113-271	Mouse
Iso-PE	BD Bioscience	555574	Mouse
Iso-APC	Miltenyi Biotec	130-113-269	Mouse
Iso-PECy7	Invitrogen	25-4714-42	Mouse
Iso-eFluor 450	Invitrogen	48-4714-80	Mouse
Iso-Fluor 647	BioLegend	400234	Mouse
CD14-FITC	Miltenyi Biotec	130-113-146	Mouse
CD3-APC	BioLegend	300412	Mouse
CD4-PECy7	Southern Biotech	9522-17	Mouse
CD8-APC	Miltenyi Biotec	130-113-154	Mouse
CD19-FITC	Miltenyi Biotec	130-113-168	Mouse
CD56-PE	Miltenyi Biotec	130-113-874	Mouse
CD107a-PE (LAMP-1)	Invitrogen	12-1079-42	Mouse
CD335-eFluor 450 (NKp46)	Invitrogen	48-3359-42	Mouse
EpCAM-PE	Miltenyi Biotec	130-091-253	Mouse
CD45-APC	BioLegend	304011	Mouse
Flow cytometry - expression of cell surface receptors/ligands			
DR4 (TRAIL-R1)	BioLegend	307207	Mouse
DR5 (TRAIL-R2)	BioLegend	307405	Mouse
DcR1 (TRAIL-R3)	Miltenyi Biotec	130-124-904	Mouse
DcR2 (TRAIL-R4)	antibodies.com	A121841	Mouse
MICA/B-Fluor 647	BioLegend	320914	Mouse
NKG2D-FITC	BioLegend	320820	Mouse
TRAIL (CD253)- PE	Invitrogen	12-9927-42	Mouse
FasL-PE	Miltenyi Biotec	130-118-491	Mouse
Fas-APC	Miltenyi Biotec	130-117-813	Mouse
Mouse IgG	Jackson Immuno Research	015-000-002	Mouse

Mouse IgG	BioLegend	400102	Mouse
Human IgG	Jackson Immuno Research	009-000-003	Human
Neutralization			
α -NKG2D	BioLegend	320802	Mouse
α -IL-21	MABTECH	3540-0N-500	Mouse
α -TNF α (Infliximab, Remsima)	Celltrion Healthcare		Chimeric Human/Mouse
α -TRAIL	R&D Systems	MAB375	Mouse
Agonists			
CD40	Bio X Cell InVivoMab	BE0189	Mouse
CD27	Biozol	BYT-ORB746677	Human
T cell activation			
α -CD3 (Okt3)	BioLegend	317302	Mouse
α -CD28	Miltenyi Biotec	130-093-375	Mouse
Immunohistochemistry			
α -Calretinin	DAKO	M 7245	Mouse
α -Cleaved Caspase-3	Cell Signaling	9661	Rabbit
α -Cytokeratin	DAKO	M 0821	Mouse
Alpha-Smooth Muscle Aktin (α -SMA)	Progen	61001	Mouse

2.1.4 Recombinant Proteins

The following recombinant cytokines and proteins were applied for NK cell and HPMC treatment (table 4).

Table 4. List of recombinant cytokines and proteins applied for cellular treatments

rProtein	Firm	Catalog number	Concentration
Cytokines for NK cell treatment			
rh-IL-2	ImmunoTools	11340025	100 μ g/ml

rh-IL-21	PeproTech	200-21-2UG	10 µg/ml
rh-IFN γ	Biomol	51564.100	100 µg/ml
rh-TNF α	PeproTech	300-01A-10UG	20 µg/ml
Protein for HPMC treatment			
rh-TRAIL	Enzo	ALX-201-115	500 µg/ml

2.1.5 Kits and MACS microbeads

The following Kits and MACS microbeads were applied for isolation and purification procedures (table 5).

Table 5. List of kits and microbeads applied for experimental procedures of this thesis

Kits		Firm
Annexin V	FITC Annexin V Apoptosis Detection Kit I	BD Pharmingen
cDNA Synthesis	iScript™ cDNA Synthesis kit	BioRad, München
DNA digestion	TURBO DNA-free kit	Invitrogen/Thermo Fischer Scientific, Karlsruhe
qPCR	ABSolute QPCR SYBER Green Mix	Thermo Fischer Scientific, Hamburg
MicroBeads		Firm
Anti-APC	Anti-APC MicroBeads	Miltenyi Biotec, Bergisch Gladbach
CD14	CD14 MicroBeads Human	Miltenyi Biotec, Bergisch Gladbach

2.1.6 Standard buffers and solutions

Table 6. List of buffers and solutions applied throughout this thesis

Application	Buffers	Composition
Apoptosis staining	1x Annexin V Buffer	10x Annexin V Binding Buffer Aqua Bidest

Cell counting/vital coloring	Trypan blue-solution	0,25 g Trypan Blue Powder Ad 50 ml PBS Dilution 1:10 in PBS 10 µl cell suspension
Flow cytometry	Staining Buffer	Sterile PBS 1% FCS
MACS	MACS Buffer	2 mM EDTA 0.5% BSA In PBS (PH 7,2)

2.1.7 Software and internet sites

Table 7. Software and internet sites applied throughout this thesis

Software		
Software/Internet site	Firm	Application
A plasmid Editor (ApE) v2.0.51	Wayne Davis	Oligonucleotide design for qPCR
BD FACS Diva 8.0	BD Bioscience, San Jose (USA)	Flow cytometry
GraphPad Prism 9	GraphPad Software, La Jolla (USA)	Statistics and figure design
ImageJ	Wayne Rasband	Calculation of pixel scale
Leica Application Suite (LAS) V4.7	Leica Microsystems, Wetzlar	Microscopic pictures
Microsoft Office	Microsoft Corporation, Redmond (USA)	Excel calculations, Graphs designed in PowerPoint and LibreOffice Draw, texts written in Word
NanoDrop 3.1	PeqLab, Erlangen	Spectrophotometric determination of RNA concentration
Python	Python Software Foundation	Analysis of Olink data and creation of box plots

Internet sites		
Ensemble Genome Database	www.ensembl.org	Transcript sequence
UCSC Genome Browser	www.genome.ucsc.edu	<i>In silico</i> PCR
GeneCards	www.genecards.org	Analysis of T cell secreted cytokines

2.1.8 Oligonucleotides and design for qPCR

Oligonucleotides were designed using the program “A plasmid Editor” (ApE) by M. Wayne Davis for Windows. Transcript sequences were discovered in Ensembl genome browser and loaded into ApE. The primers were designed with a GC-content of around 55%, a length of 20 to 25 bp, a qPCR product-length between 150 bp and 300 bp and a melting temperature of about 60°C. Importantly, to avoid DNA amplification, exon-spanning primers were designed. Primers were checked by *in silico* PCR (UCSC Genome Browser). The forward primer for IL-21 (Fw_IL21) was published in Parrish-Novak et al. 2000.

Oligonucleotides were purchased from Sigma-Aldrich and dissolved in nucleotide-free H₂O at a stock concentration of 100 µM. The primers were stored at -20°C. A primer mix of the forward and reverse primer was generated by mixing each primer 1:10 in nucleotide-free H₂O.

A list of the primers applied is depicted in table 8.

Table 8. List of applied oligonucleotides and their sequences

Transcript	Gene	Sequence (5' → 3')
Fw_RPL27	RPL27	AAAGCTGTCATCGTGAAGAAC
Rv_RPL27	RPL27	GCTGTCACTTTGCGGGGGTAG
Fw_IL21	IL-21	TGTGAATGACTTGGTCCCTGAA
Rv_IL21	IL-21	CTGCATTTGTGGAAGGTGGTTTCC
Fw_TNFα	TNFα	GCTCTTCTGCCTGCTGGACTTTG
Rv_TNFα	TNFα	GGTTATCTCTCAGCTCCACGCCA

2.1.9 Culture media

Cell culture media and the components are listed in table 9. These are applied for the cultivation of primary HGSC patient-derived cells and cell lines, as well as conventional cell lines.

Table 9. List of cell culture media and media components

Media	Components	Concentration	Usage
Ovarian Carcinoma Modified Ince media (OCMI)	DMEM-HAMs F12 + M199 FCS Insulin EGF Hydrocortison Choleratoxin HEPES Transferrin Triiodothyronine O-phosphoryl ethanolamine Selenious acid All trans retinoic acid Linoleic acid	1:1 5% 20 µg/ml 10 ng/ml 500 ng/ml 25 ng/ml 10 mM 10 µg/ml 0.2 pg/ml 5 µg/ml 8 ng/ml 25 ng/ml 5 µg/ml	Cultivation of primary patient material isolated from HGSC patients. The media is freshly prepared bi-weekly (Ince et al. 2015)
OCMI-Media/50% ascites pool	OCMI-Media without FCS supplemented with 50% ascites pool (see section 2.2.1.1)	See above	HPMC pre-culture prior to TAL co-culture, rh-TRAIL treatment and invasion assays, over night resting period of primary tumor cells
RPMI-Media	RPMI basal media Human AB serum	5%	2 day culture of TAL, collection

	Sodium-Pyruvate	1%	of T cell supernatants
RPMI-Media for Jurkat cell line cultivation	RPMI basal media FCS Penicillin and Streptomycin Sodium-Pyruvate	10% 1% 1%	Cultivation of Jurkat cell line
IMDM-Media for K562 cell line cultivation	IMDM basal media FCS Penicillin and Streptomycin	10% 1%	Cultivation of K562 cell line
Cell-freezing media	DMSO FCS	10% 90%	Long-term cell storage at -196 °C in liquid nitrogen
PBS (gibco life technologies)	PBS without calcium and magnesium		Cell culture washing steps

2.1.10 Patient samples and characteristics

Samples of patients with diagnosed ovarian carcinoma of HGSC type (n=94), except 6 cases (endometrioid G1, peritoneal G2 and G3, carcinomatosis G3 and ovarian sarcoma) were applied for functional experiments, as well as flow cytometry, Olink secretome analysis, RNA-sequencing, qPCR and immunohistochemistry. As control HPMC, the mesothelial cells of 3 patients with benign gynecological diseases, including Cystadenofibroma, inflammatory and Uterus Myomatosis were applied for functional experiments and flow cytometric analysis. A table (Supplementary table S1) including the patient ID, exact diagnosis with FIGO state, cell type and application can be found in the supplements.

2.1.11 Cell lines

As a positive control for induced NK cell degranulation the K562 myeloid suspension cell line, provided by the research group of Prof. Dr. Elke Pogge von Strandmann, was applied.

The Jurkat T cell leukemia suspension cell line, originally provided by Dr. Miriam Frech, research group of Prof. Dr. Andreas Neubauer, was applied as a positive control for FasL sensitivity.

2.2 Cell biological methods

2.2.1 Samples derived from HGSC patients, patients with benign gynecological diseases and healthy donors

Malignant ascites and omentum tissue samples with metastatic lesions were collected from first line HGSC patients without prior treatment in the course of surgery at the Marburg University Hospital. Control samples of peritoneal lavage for HPMC of patients with benign gynecological diseases were collected during hysterectomy. Written consent was given by each donor taking part in the study confirming to the Declaration of Helsinki. The isolation and purification procedures had been performed by the members of the Reinartz research group. The center for Transfusion Medicine and Hemotherapy at the University Hospital Gießen and Marburg kindly provided the leukocyte-reduction system (LRS) chambers of healthy adult donors for the isolation of peripheral lymphocytes. All these listed sample collections were approved by the local ethics committee (Philipps University Marburg: reference number 205/10) and the ethics votes can be found in the appendix.

2.2.1.1 Malignant ascites: isolation of peritoneal cell types

A protocol for the isolation of peritoneal cells from malignant ascites, including TAM, TAL and tumor cells was established by AG Reinartz (Reinartz et al. 2016; Worzfeld et al. 2018). In order to separate mononuclear cells, as a first step, Lymphocyte Separation Medium 1077 and density gradient centrifugation were applied.

The isolation of tumor spheroids was performed by size exclusion applying 30 µm and 100 µm mesh-sized cell strainers resulting in tumor spheroids of medium (30 µm) and large (>30 µm) size. Magnetic activated cell-sorting (MACS) depleting peritoneal leukocytes via CD45 microbeads following the standard protocol of the supplier (Miltenyi Biotec) was applied to purify small tumor spheroids (<30 µm) and tumor single cells. Dissociation of tumor spheroids applying TrypLE (20 ml/200 µl pellet) resulting in tumor single cells was

performed for a maximum of 10 minutes at room temperature with vortexing steps after 5 minutes for 10 seconds. The purity of the isolated tumor cells was analyzed via flow cytometry measuring the amount of EpCAM+ cells (>80%).

As schematically depicted in figure 7, CD14+ TAMs were depleted via MACS from the remaining peritoneal cells applying CD14 microbeads to receive the total TAL fraction of samples composing less than 3.5% EpCAM+ tumor cells. The TAL were cryopreserved and subject to T and NK cell isolation at a later point. For functional assays, it was necessary to isolate CD3-/CD56+ NK cells. To avoid unspecific NK cell activation, we chose a negative MACS sorting strategy instead of labelling the NK cells directly: The T cells present in the CD14-depleted TAL fraction were labelled with an anti-human CD3-APC antibody (10 μ l/1x10⁷ cells) for 10 minutes at 4°C followed by a washing step and incubation with anti-APC microbeads (20 μ l/1x10⁷ cells) for 15 minutes at 4°C. The cells were loaded onto MS or LS columns and washed 3 times with MACS-Buffer. The CD3+ T cells were eluted from the columns. The CD56+ NK cells were present in the flow through. The isolated fractions' purity was determined via flow cytometry achieving >95% for CD3+ T cells and >80% for CD56+ NK cells. CD19+ B cells represented the main contaminating cell populating within the NK cell fraction.

For some functional experiments, we wanted to analyse the cytotoxic T cell and T helper cell fractions separately, which is why we slightly modified the isolation procedure described above: In the first step the CD3+/CD8+ cytotoxic T cells were purified from the CD14- TAL fraction by labelling with an anti-human CD8-APC antibody (2 μ l/1x10⁷ cells) following the isolation applying anti-APC microbeads. In the second step the flow through was applied to the usual CD3-positive MACS selection described above to purify the CD3+/CD4+ T-Helper cells. The same isolation strategy was applied for peripheral blood mononuclear cells (PBMC) derived from healthy donors.

Besides this, cell-free ascites from serial centrifugation was cryopreserved at -80°C. An ascites pool of n=10 HGSC patients was mixed and applied for co-culture experiments where indicated to reconstitute the *in vivo* situation.

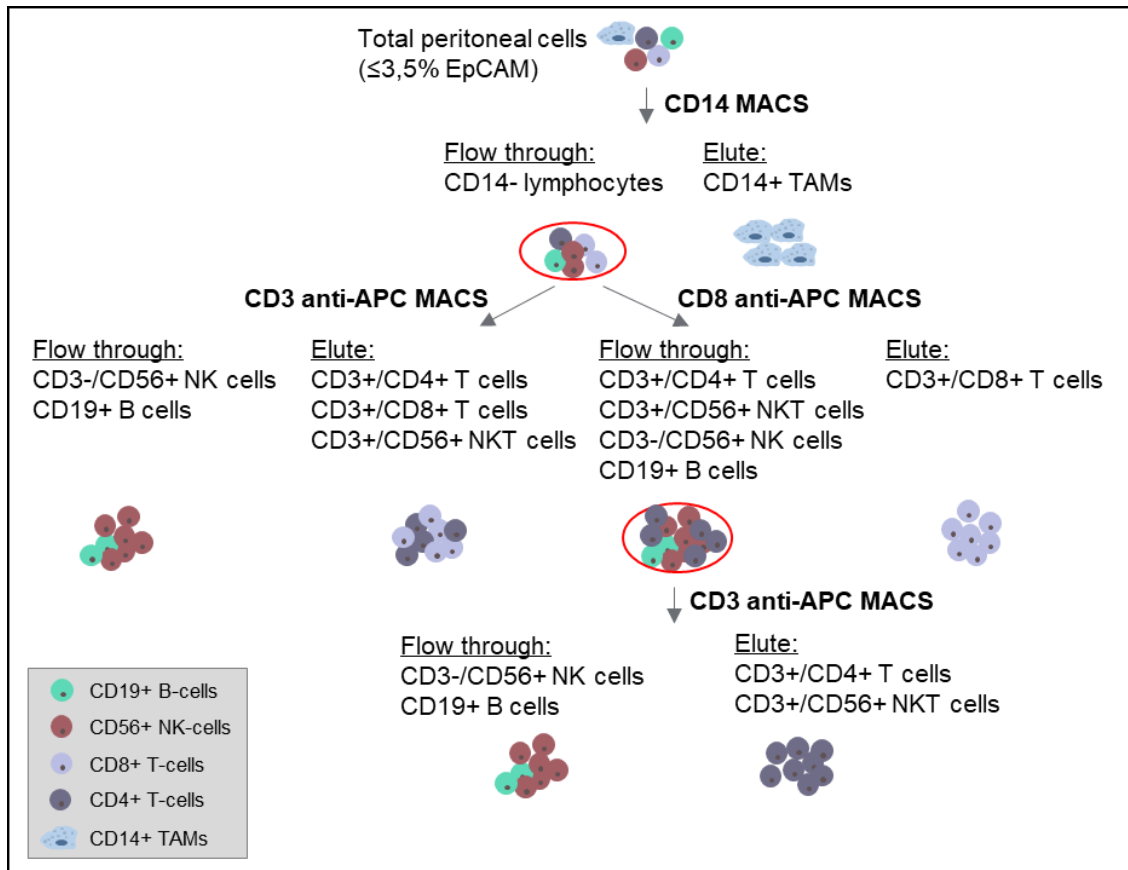


Fig. 7. Isolation strategy of T and NK cells from HGSC patient ascites or healthy donor PBMC. Total peritoneal cells with a maximum of 3.5% EpCAM+ tumor cells were first of all applied for CD14 depletion using the MACS strategy and CD14 microbeads. The CD14- lymphocyte fraction was then either applied for separation of total CD3+ T cells by CD3 anti-APC MACS or individual separation of cytotoxic T cells (CD3+/CD8+) and T-Helper cells (CD3+/CD4+) by CD8 anti-APC MACS (first step) prior to CD3 anti-APC MACS (second step). The flow through contained the CD56+ NK cells with a slight contamination of CD19+ B cells. The same procedure was applied for PBMC derived from healthy donor blood.

2.2.1.2 Omentum tissue: Isolation and cultivation of HPMC

As described in Sommerfeld et al. 2021, HPMCs were isolated from macroscopically tumor-free omentum tissue of HGSC patients. The tissue was minced and trypsinized for 30 minutes in the incubator (37°C, 5% CO₂). The cells were filtered through a 100 µm cell strainer and centrifuged at 300x g for 10 minutes to enrich the HPMC fraction. Next to the direct use (*ex vivo* cells) the HPMCs were initially cultured in RPMI 1640/10% FCS/1% sodium pyruvate/1% Pen-Strep media and the purity was measured by flow cytometry analyzing the presence of contaminating CD45+ lymphocytes and EpCAM+ tumor cells. If the purity was less than 95%, MACS depletion of CD45+ and EpCAM+ cells was

conducted following the manufacturer's protocol. The purity of isolated HPMC was again analyzed via flow cytometry. Further propagation of purified HPMC was performed in OCMI medium (Reinartz et al. 2019).

2.2.1.3 Benign peritoneal lavage: Isolation of control group HPMC

As a HPMC control group, mononuclear cells were purified from lavage of patients with benign gynecological diseases by Ficoll gradient centrifugation and MACS depletion of CD14+ macrophages. The CD14- fraction containing floating HPMC, which was verified by flow cytometry, was cultivated in OCMI medium until confluency was achieved. HPMC purity was determined by cellular staining for mesothelial markers including vimentin and cytokeratin 8, the fibroblast-specific marker FAP and the leukocyte marker CD45.

2.2.1.4 LRS chambers: Isolation of healthy donor lymphocytes

Healthy donor PBMCs were enriched from peripheral blood by ficoll gradient centrifugation. For this, the blood was transferred drop-by-drop from the LRS chamber into a 50 ml falcon containing 10 ml PBS. The blood-PBS-mixture was then transferred drop-wise onto 15 ml ficoll and centrifuged at 1200x g for 20 minutes without centrifugation break. Afterwards, four layers of blood phases appear as depicted in figure 8: Plasma/Platelets – PBMC – Ficoll – Granulocytes – Erythrocytes.

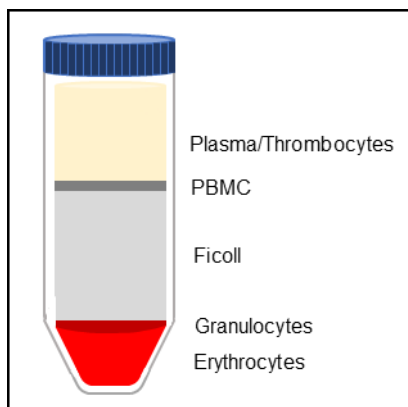


Fig. 8. Layers of blood phases after ficoll gradient centrifugation. The blood was slowly added to the ficoll and centrifuged at 1200x g for 20 minutes. This leads to a separation of all the components: blood plasma/thrombocytes at the top, followed by a ring of PBMCs, remaining ficoll, granulocytes and erythrocytes at the bottom. The PBMCs are of interest and transferred for further preparation steps.

The plasma overlay was discarded and the PBMC fraction was transferred into a new falcon and resuspended in 40 ml PBS. Centrifugation for 10 minutes at 300x g was performed. To remove remaining erythrocytes RBC-lysis was performed by adding 5 ml of RBC-lysis Buffer and incubating at room temperature for 5 minutes. The cells were washed twice in 40 ml PBS. The last centrifugation step was performed at 10x g for 10 minutes to enrich the lymphocytes in the supernatant. Flow cytometric analysis of cell types present was performed by measuring the amount of CD14+, CD3+ and CD56+ cells. Further isolation steps were performed as described for the peritoneal cells in section 2.2.1.1.

2.2.2 Cultivation of primary HGSC patient-derived cell types

2.2.2.1 Primary tumor cell lines

Tumor spheroids originating from HGSC patient ascites OC_37 and OC_58 were applied to establish permanent primary tumor cell cultures (OCMI tumor cells). For this, the description of Ince et al. 2015 was followed, but slightly modified as delineated in Reinartz et al. 2019. The original tumor characteristics remain and the tumor cell propagation is possible long-term without introducing cell culture crisis and by this, genetic alterations, describing the benefits of this culture method.

Cryo-preserved cells were stored long-term in liquid nitrogen (-196°C). Prior to cell thawing, the cryos were decontaminated with methanol to reduce the risk of mycoplasma contamination. The cryos were hand-warmed until almost completely thawed. Cells were then transferred into a 50 ml falcon with direct slow addition of 5 ml ice-cold OCMI cell culture media. Cells were pelleted at 1100 rpm for 10 minutes at room temperature. The supernatant was removed to eliminate remaining DMSO and cell pellets were resuspended in OCMI media supplemented with 5% FCS that had been warmed to 37°C in the water bath. Vital cell counts were established by Neubauer counting chamber mixing 10 µl of the cell suspension 1:10 with trypan-blue (diluted in PBS). The cells were plated onto Primaria™ cell culture plates at a density of around $2 \times 10^4/\text{cm}^2$. During cultivation the cells' morphology and viability were regularly microscopically controlled. The cells were passaged at 90-100% confluency, which accounts for every 2-3 days. The cells were harvested by removing the cell culture media and incubation with trypsin/EDTA for 10 minutes at 37°C and 5% CO₂. Trypsination

was blocked by applying the same amount of OCMI/5% FCS media and transferring the cells into a 50 ml falcon. Determination of cell count and vitality, as well as tumor cell seeding was performed as described above. Importantly, the cells were kept in an incubator with 5% CO₂ at 37°C during cultivation and high passage numbers (maximum 5 passages) were avoided by cryopreserving the cells, enabling the maintainability of their genotype as similar to the original as possible. For cryopreservation, cell pellets were resuspended in ice-cold freezing media (DMSO/10% FCS). Around 2x10⁶ tumor cells were frozen in 1 ml freezing media per cryo. The cryos were stored in a freezing container at -80°C over night to enable a slow reduction of the temperature (-1°C/minute). Afterwards the cryos were transferred into liquid nitrogen. Mycoplasma contamination was excluded prior to experimental use.

2.2.2.2 Over night resting step of *ex vivo* tumor cells

Ex vivo tumor cells were thawed as described above and 5x10⁴ cells per 96-well were plated in OCMI/50% ascites pool media over night. The cells were applied for functional experiments as described in section 2.2.6.2 the next day. They were not further propagated or frozen.

2.2.2.3 HPMC

HPMC were cultivated as described for the primary tumor cell lines (section 2.2.2.1). Importantly, most HGSC patient omentum- and benign peritoneal lavage-derived HPMC could not be cultivated above a total passage number of 5 passages (independent of freezing-thawing cycles). Therefore, the total passage number was not exceeded for the HPMC applied throughout this work. HGSC patient-derived HPMC were cultivated in OCMI/5% FCS media, with adapted media composition where indicated by adding 50% ascites pool instead of FCS or omitting EGF. EGF was removed for invasion assays (section 2.2.10), to guarantee a tight mesothelial monolayer maintaining a cobblestone phenotype and prevent MMT induction by EGF. Benign-derived HPMC were exclusively cultivated in OCMI/5% FCS media.

2.2.3 Cultivation of the K562 cell line

The K562 myeloid suspension cell line was thawed, cultivated and frozen as described in section 2.2.2.1. The only difference was that the cells had been

cultivated in IMDM/10% FCS/1% Pen-Strep media on 75 cm² flasks in suspension and cells were harvested by removing the cell culture media and rinsing the bottom of the flask twice.

2.2.4 Cultivation of the Jurkat cell line

The Jurkat T cell leukemia suspension cell line was cultured in RPMI/10% FCS/1% Sodium Pyruvate/1% Pen-Strep media following the same protocol as for the primary tumor cells in section 2.2.2.1. The suspension cells were again harvested by removing the cell culture media and rinsing the bottom of the cell culture dish twice.

2.2.5 Collection of T cell conditioned media (CM)

T cells were cultivated with or without anti-CD3 antibody stimulation for 2 days in RPMI 1640/5% AB/1% sodium pyruvate. For anti-CD3 antibody stimulation, the wells of a 24-well plate were coated with 0.5 µg/ml anti-CD3 antibody diluted in PBS for 2 hours. Afterwards the wells were washed twice with PBS and once with the cultivation media. 2×10^6 isolated T cells were added per 24-well for cultivation. In selective experiments additional CD28 stimulation was performed by adding 2 µg/ml anti-CD28 antibody directly to the media. After 2 days the supernatant was transferred into Eppendorf reaction tubes and centrifuged at 300x g for 10 minutes to pellet remaining T cells. The supernatant was again centrifuged at 14,000x g for 10 minutes to remove cellular debris. The collected CM was then preserved at -20°C until further use for NK cell stimulation (see section 2.2.6.1) and Olink analysis (see section 2.3.1).

2.2.6 Co-culture experiments

2.2.6.1 TAL treatments and co-cultures between T and NK cells

Depending on the experimental setting, total TAL, purified T cells or T- NK cell mixtures after isolation were cultivated with or without anti-CD3 antibody stimulation in RPMI 1640/5% AB/1% sodium pyruvate or 100% ascites pool for 2 days in the incubator. Again, 2×10^6 lymphocytes were added per well. For the mixture of purified T and NK cells, a ratio of 1:1 was applied. Purified NK cells on the other side were not stimulated with anti-CD3 antibody, but were otherwise cultivated the same way. Moreover, where indicated, NK cells were treated with different combinations of cytokines for 2 days, including 10 ng/ml rh-TNF α , 10

ng/ml rh-IFN γ , 20 ng/ml rh-IL-2 and 10 ng/ml rh-IL-21. Next to co-cultures between T and NK cells with direct cell-cell contacts, the NK cells were also stimulated with T cell CM in a 1:1 dilution in RPMI 1640/5% AB/1% sodium pyruvate. Blocking experiments were conducted applying the CM of anti-CD3 antibody stimulated T cells, which was pre-incubated with 10 μ g/ml neutralizing human anti-IL-21 or anti-TNF α antibody for 1 hour in the incubator prior to their addition to the NK cells.

2.2.6.2 Co-culture between HPMC or *ex vivo* tumor cells with TAL or purified T/NK cells

As demonstrated in figure 10, a HPMC monolayer was grown by plating 4×10^4 HPMCs per 96-well in OCMI/5% FCS or OCMI/50% ascites pool media for two days. Co-culture experiments were conducted by harvesting the stimulated lymphocytes (section 2.2.6.1) applying ice cold EDTA (20 mM in PBS), resuspending them in OCMI/5% FCS media and determining the cell counts. The TAL:HPMC co-culture was performed in a ratio of 10:1 for 6 hours in the incubator. Next to the co-culture of lymphocytes with HPMC, the co-culture with *ex vivo* tumor cells derived from the ascites of HGSC patients was also conducted in the same experimental setting. The *ex vivo* tumor cells were here co-cultured with 100% ascites pool-derived TAL. Afterwards, NK and T cell degranulation, as well as mesothelial and tumor cell apoptosis-induction was measured as described in section 2.2.8.

2.2.7 Identifying involved apoptosis signaling pathway

2.2.7.1 Analyzing the involvement of TRAIL signaling pathway

HPMC responsiveness to TRAIL-mediated killing was analyzed by treatment of HPMC with 100 ng/ml rh-TRAIL for 18 hours in the incubator. Next to this, TRAIL blocking experiments were performed by pre-treating the stimulated lymphocytes with 10 μ g/ml anti-hTRAIL antibody, mouse IgG isotype control and PBS solvent control for 1 hour in the incubator prior to the co-culture with HPMC.

2.2.7.2 Analyzing the participation of Fas/FasL-mediated killing

In order to analyze whether HPMC could be killed by NK cells in a Fas/FasL-dependent manner, soluble sFasL (1-100 ng/ml) was crosslinked with anti-His-Tag antibody (10 μ g/ml) for 1 hour in the incubator. Afterwards the HPMC were

treated with the crosslinked sFasL for 24 hours. As a positive control for Fas/FasL-mediated killing, the Fas-sensitive cell line Jurkat was applied. Fas/FasL-mediated killing of HPMC by NK cells was specifically blocked by pre-incubating TAL with 500 ng/ml anti-FasL antibody or mouse IgG control for 1 hour in the incubator prior to the co-culture with HPMC.

2.2.7.3 Determining the role of the activating receptor NKG2D

TAL were pre-treated with 10 µg/ml anti-NKG2D neutralizing antibody or the appropriate mouse IgG isotype control for 1 hour in the incubator prior to the co-culture with HPMC to determine a possible contribution of the activating NKG2D receptor on specific HPMC killing.

2.2.7.4 Analyzing the contribution of NK cell-derived cytokines

To evaluate a possible direct cytotoxicity of NK cell-secreted cytokines, HPMC were treated with 100 ng/ml rh-TNF α and 25 ng/ml rh-IFN γ for 6 hours in the incubator instead of the co-cultivation with lymphocytes.

2.2.7.5 Agonistic antibodies CD40 and CD27

To determine the impact of CD40 and CD27 signaling on NK cell cytotoxic activation, isolated NK cells were treated with 10 µg/ml agonistic mouse anti-CD40 antibody, human anti-CD27 antibody, as well as corresponding IgG controls for 1 hour in the incubator prior to the co-culture with HPMC.

2.2.8 Flow cytometric and fluorescent microscopic readout of co-culture experiments

To analyze the effect of the co-culture experiments on NK cell or T cell degranulation, as well as HPMC apoptosis induction (figure 9), flow cytometric measurements and fluorescent microscopic analysis of active caspase 3/7 was performed as described in the following.

2.2.8.1 NK and T cell degranulation analysis

The specific degranulation of NK and T cells within the total TAL or purified subsets in response to HPMC co-culture was analysed by adding 5 µl anti-CD107a-PE antibody and 20 nM Monensin (Golgi-Stop) during the 6 hour co-culture between HPMC and the lymphocytes. The anti-CD107a antibody detects lysosomal-associated membrane protein-1 (LAMP-1) on the outer membrane exposed upon degranulation of CD8 $^+$ T cells (Betts et al. 2003) and NK cells

(Alter et al. 2004), as a marker of functional activity. Upon target cell detection, GrB and Perforin, stored among others in intracellular cytolytic granules, are released into the immunological synapse inducing target cell death (Betts et al. 2003; Alter et al. 2004; Peter et al. 1991). Monensin was added to the co-culture experiment in order to avoid PE fluorochrome quenching and subsequent adequate determination, which is linked to the CD107a antibody, after re-internalization and trafficking to the highly acidic environment of endosomal/lysosomal cellular compartments, by neutralizing the pH (Betts et al. 2003; Roederer et al. 1987). As a negative control, unstimulated total TAL, NK and T cells were applied. The co-culture between TAL and K562 cell line under the same conditions as described above (section 2.2.6.2) served as a positive control for NK cell degranulation. TALs or T cells were stimulated with 1 µg/ml Phorbol 12-myristate 13-acetate (PMA) and 15 ng/ml Ionomycin for 6 hours as a positive control for T cell-specific degranulation. The lymphocytes were again harvested by applying EDTA, washed and resuspended in staining buffer for specific labelling of NK (0.5 µl CD335-eFluor 450) and T cell (0.5 µl CD3-APC, 3 µl of 1:10 CD4-PECy7) markers. Antibody staining was performed for 30 minutes at 4°C in the fridge. Specific isotype controls for PE, eFluor 450, APC and PECy7 were also added. Flow cytometric analysis was performed on a FACS Canto II instrument using the Diva and FlowJo™ v10.8 software. The percentage of degranulating CD107a+ cells was determined in NK (CD335+) and T cell (CD3+/CD4+ and CD3+/CD4-) subsets.

2.2.8.2 Detection of apoptotic HPMC and tumor cells

For flow cytometric detection of apoptotic HPMC (figure 10) and *ex vivo* tumor cells, the cells were first of all harvested applying Trypsin/EDTA after the 6 hour lymphocyte co-culture. They were washed and resuspended in staining buffer and labeled with 1 µl anti-CD45-APC antibody for 30 minutes at 4°C to exclude contaminating lymphocytes during the apoptosis analysis. A washing step in Annexin V binding buffer was performed prior to the incubation with 5 µl Annexin V-FITC and 5 µl PI for 15 minutes at room temperature in the dark. 250 µl Annexin V binding buffer was added and the cells were measured immediately. For correct gating HPMC alone were added as a negative control and lymphocytes alone were added to exclude them from the gating. The amount of apoptotic HPMC or

tumor cells within the CD45- population was calculated from the percentage of the total Annexin V+ cells, including the early apoptotic (PI-) and late apoptotic (PI+) cells.

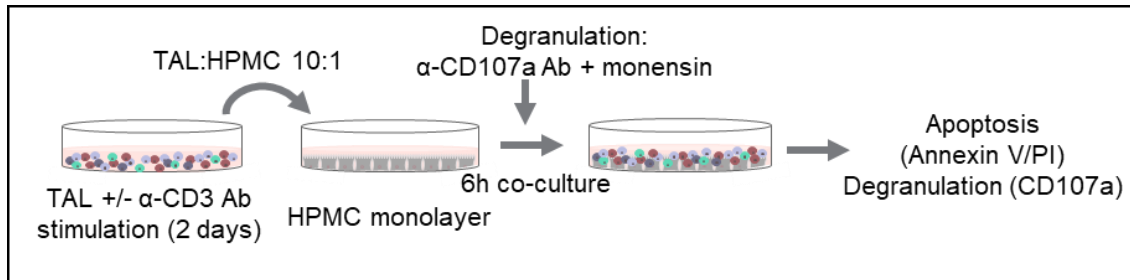


Figure 9. Schematic chart illustrating the experimental procedure of the co-culture experiments. HGSC patient ascites-derived TAL were cultivated with or without anti-CD3 antibody stimulation for two days prior to the co-culture with a monolayer of patient omentum-derived HPMC in a 10:1 ratio for 6 hours. NK/T cell degranulation was determined by directly adding anti-CD107a-PE antibody and monensin to the co-culture. The Lymphocytes were harvested by EDTA and additionally stained for NK and T cell-surface markers, including CD335-eFluor 450 and CD3-APC. HPMC apoptosis induction was analyzed by Annexin V-FITC/PI staining and measurement of the CD45- population.

2.2.8.3 Caspase 3/7 staining of apoptotic HPMC

As a second read out for the induction of HPMC apoptosis by activated TAL, mesothelial cells were plated on 96-well plates coated with a collagen I gel, as used for the invasion assays (section 2.2.10), in order to analyze the caspase-3/7 activation/staining after treatment with rh-TRAIL for 18 hours. 10 μM CellEvent™ Caspase 3/7 Green was added and incubated for 30 minutes at 37°C, 5% CO₂. Without further washing steps, the apoptotic cells were visualized under the fluorescence microscope (Leica DMI3000B).

2.2.9 Analysis of cell surface receptor expression

Specific antibody staining and flow cytometry analysis was performed as described in the following sections 2.2.9.1 - 2.2.9.3. The results were calculated from the percentages of positive cells and geometric mean fluorescence intensities (MFI) subtracting the isotype controls.

2.2.9.1 Purity and phenotype of isolated cell fractions

The isolated (peritoneal) cell fractions` purity and phenotype was analysed by applying the standard protocol for cell surface stainings as described above (section 2.2.8.1), adding an Fc-block by incubating the cells with 50 μl mouse IgG

diluted 1:100 in staining buffer for 15 minutes at 4°C. The following antibodies were applied: 1 µl from 1:10 diluted CD14-FITC, 0.5 µl CD3-APC, 3 µl from 1:10 diluted CD4-PECy7, 0.5 µl CD335-eFluor 450, 1 µl CD45-APC, 1 µl CD56-PE, 1 µl CD19-FITC, 1 µl EpCAM-PE, as well as the corresponding isotype controls.

2.2.9.2 Analysis of receptor expression on lymphocytes

In order to analyze the expression of TRAIL and NKG2D on the surface of NK cells, 5 µl TRAIL-PE and 1 µl NKG2D-FITC together with 0.5 µl CD335-eFluor 450 antibodies were applied following the standard staining procedure. The detection of Fas ligand on the cell surface of lymphocytes was performed by applying 2 µl FasL (CD178)-PE for 10 minutes at 4°C.

2.2.9.3 Analysis of receptor expression on HPMC

The expression of DR4, DR5, DcR1 and DcR2 on HPMC was analyzed by staining with the corresponding antibodies DR4-APC (CD261), DR5-PE (CD262), DcR1-PE (CD263) and DcR2-APC (CD264), applying 1 µl each. The expression of MICA/B on HPMC was performed by staining with 1 µl MICA/B -Fluor 647 following the standard staining protocol. Moreover, the expression of the Fas receptor (CD95) on HPMC was detected applying 2 µl from 1:10 diluted CD95-APC.

2.2.10 Trans-mesothelial tumor cell invasion

In order to decipher the role of TRAIL-mediated killing of HPMC by NK cells on favored trans-mesothelial HGSC tumor cell invasion, a 3D transwell assay system was established, as schematically depicted in figure 10. 24-well transwell inserts with a pore size of 8.0 µm were coated with 10 µl of a 150 µg/ml collagen I gel in OCMI/5 % FCS without EGF media. The gel polymerized in the incubator within 3 hours and was then equilibrated for 1 hour with 100 µl OCMI/5% FCS without EGF media. HPMC derived from a pre-culture in OCMI/50% ascites pool for 3 to 4 days were washed serumfree in OCMI without EGF media and were labelled with 1:1000 diluted cell-tracker orange (CTorange) for 1 hour in the incubator. After washing the cells 3 times with OCMI/5% FCS without EGF media, they were plated onto the collagen I gel with a density of 8×10^4 HPMCs in 300 µl media per transwell insert. On the one hand the HPMC were immediately treated with 100 ng/ml rh-TRAIL for 18 hours prior to tumor cell invasion. On the other

hand the HPMC monolayer was allowed to form over night prior to the addition of TAL derived from a 2 day pre-culture in 100% ascites pool \pm anti-CD3 antibody stimulation in a 10-fold concentration for a 24 hour co-culture. The induction of mesothelial apoptosis was analyzed under the microscope and visualized by performing caspase 3/7 staining (see section 2.2.8.3). The transwell inserts were carefully washed serumfree using OCMI without EGF media for 3 times, finally adding 100 μ l media. Primary tumor cells derived from HGSC patients OC_37 and OC_58 were harvested applying trypsin, washed serumfree in OCMI without EGF media and stained with 1:1000 diluted CTgreen for 30 minutes in the incubator. After the washing steps applying serumfree OCMI without EGF media, the tumor cells were added in a density of 4×10^5 cells per insert in a total volume of 300 μ l media. 600 μ l OCMI/5% FCS without EGF media was added to the bottom well and used as chemoattractant during the 2 hour tumor cell invasion. Remaining, non-invaded tumor cells were removed from the inside of the inserts using q-tips and washing steps with PBS. The invaded tumor cells on the bottom side of the insert's membrane were fixated in methanol, the filters were cut out and fixed onto microscopic slides using vectashield. Microscopic evaluation of invaded tumor cells from 6 visual fields per filter was performed on a Leica DMI3000B microscope. The amount of invaded tumor cells was counted, the mean was determined and the invasion relative to the untreated control with FCS chemoattractant was calculated in Excel.

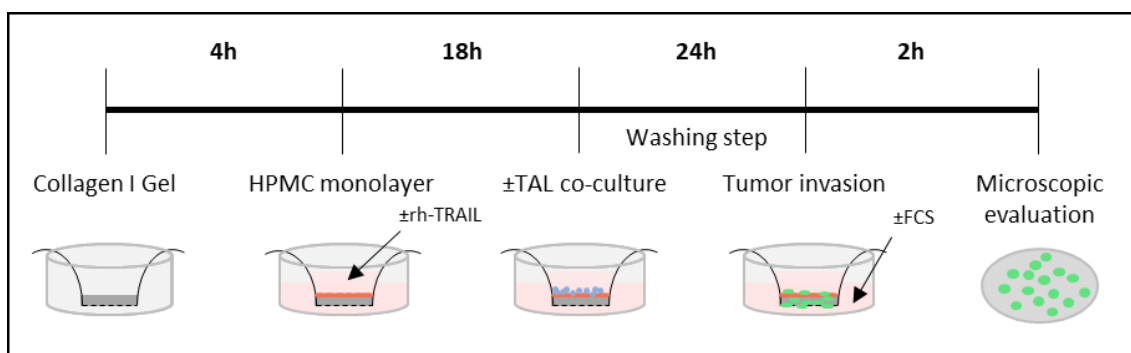


Figure 10. Schematic illustration of *in vitro* 3D trans-mesothelial invasion assays. A monolayer of mesothelial cells was grown on a collagen I gel coated transwell insert. rh-TRAIL was added directly when mesothelial cells were seeded. Untreated mesothelial cells were co-cultured with TAL (\pm anti-CD3 antibody stimulation) for 24 hours. TAL and apoptotic HPMC were removed by washing steps prior to the tumor cell invasion for 2 hours towards an FCS-gradient. Invaded tumor cells were fluorescently microscopically evaluated.

2.3 Molecular biology and biochemical methods

2.3.1 Affinity proteomic (Olink) analysis of T cell secretomes

The CM of unstimulated versus anti-CD3 antibody stimulated T cells derived from the ascites of 5 different HGSC patients were collected as described in section 2.2.5. These CM were then subject to affinity proteomic (Olink) analysis in order to determine differences in the secretion profile upon T cell activation. For this, 80 μ l matched (unstimulated vs. anti-CD3 antibody stimulated) CM-samples, as well as a background media control (RPMI 1640/5% AB-serum/1% sodium-pyruvate), were sent to the translational proteomic core facility at the medical department of the Philipps University Marburg. The CM were previously tested in functional analysis for their ability to activate the NK cells' cytotoxic potential with TRAIL upregulation and specific HPMC killing.

For the Olink analysis the Olink Explore 3072 platform was applied following the standard protocol (v1.5, 2022-12.21). The samples were plated randomized on a 96-well plate and processed in one batch. The Proximity Extension Assay (PEA) technology was used by Olink Explore: two matched antibodies bind simultaneously to the same protein targeting different epitopes. This is the case for every target represented in the Olink panel. These antibodies are covalently labelled with complementary oligonucleotides that hybridize upon simultaneous binding of the antibodies bringing them in close proximity. Short dsDNA sequences result from matching oligonucleotide binding after antibody attachment to their epitope, which are pre-amplified by PCR. These dsDNA sequences contain an assay-specific barcode. In a second PCR, further coding is performed by adding information-providing DNA tags to the barcode enabling the parallel measurement of ~3000 proteins. Subsequent Next-Generation Sequencing (NGS) of the generated libraries was conducted at the Genomics Core Facility of the Department of Medicine (Philipps University Marburg). Protein levels were calculated as Normalized Protein eXpression (NPX, arbitrary unit in log₂ scale provided by Olink). Some mediators were present in more than one panel, including CXCL8, IDO1, IL-6, LMOD1, SCRIB and TNF, for which mean NPX values were applied for subsequent bioinformatic studies. Proteins induced by anti-CD3 antibody stimulation of the T cells were determined by Δ NPX – the differences between the NPX values of matched samples. The median fold

change (FC) values ($2^{\Delta\text{NPX}}$) of n=5 biological replicates were calculated. Finally, false discovery rates (FDR) were calculated following the Benjamini-Hochberg method to nominal p values (unpaired student's t-test of FC values). Mediators secreted by activated T cells promoting NK cell cytotoxicity against HGSC-derived HPMC in a TRAIL-dependent manner were identified by filtering the proteins for "NK cell AND TRAIL" in the genecards.org database. The described analysis was performed by the translational proteomic core facility and Prof. Dr. Rolf Müller.

2.3.2 Analysis of T cell-expressed cytokines on RNA-level

2.3.2.1 RNA-isolation

RNA from unstimulated versus anti-CD3 antibody stimulated T cells was isolated by lysing the cells in TriFast. The T cells were transferred from a 24-well plate (in average 5x 24-wells with 2×10^6 T cells per condition) into Eppendorf reaction tubes and washed once with PBS. 1 ml TriFast was added per tube and the lysates were frozen at -80°C until further processing following the standard protocol.

The TriFast lysates were then thawed, vortexed and kept at room temperature for 5 minutes. 200 μl chloroform/ml TriFast was added and strongly shaken for 15 seconds. The mixture was incubated at room temperature for 3 minutes prior to a 15 minute centrifugation step at 12,000x g, 4°C . After centrifugation, two phases are visual: A sallow aqueous phase at the top and the phenol phase underneath. The upper aqueous phase is transferred into a new Eppendorf reaction tube adding 600 μl isopropanol and mixed by inverting the tubes. In order to visualize the pelleted RNA 60 μg Glyco Blue is added, mixed and incubated for 10 minutes at room temperature. The lysates were then centrifuged and the RNA pellet was washed twice in 1 ml 75% ethanol. The pellet was then left to dry before dissolving the RNA in 15 μl RNase-free water including 1 U/ μl RNase-inhibitor Superase-IN (1:20 from stock). RNA quantification via NanoDrop spectrophotometric measurement and NanoDrop 3.1 software to determine the purity and concentration was performed.

2.3.2.2 DNase digestion

In order to remove remaining DNA from the RNA-lysates, which could influence the qPCR results, DNase digestion using the DNA-free™ DNA Removal kit from Thermo Fischer Scientific was performed following the manufacturer's protocol. 10 µg RNA was applied and the concentration was again measured via NanoDrop spectrophotometer afterwards.

2.3.2.3 cDNA synthesis via reverse transcription

The RNA was reverse transcribed into complementary DNA (cDNA) for qPCR gene expression analysis using the iScript™ cDNA Synthesis kit following the manufacturer's protocol. 250 ng RNA was transcribed including a "minus reverse transcriptase" (-RT) control to ensure primer specificity and exceptional amplification of cDNA. The cDNA was diluted 1:10 in nuclease-free H₂O and kept at -20°C until further use.

2.3.2.4 Quantitative polymerase chain reaction

By applying specific primers (RPL27, IL-21 and TNF α in this case) the cDNA region, the primers bind to, is exponentially amplified during the quantitative polymerase chain reaction (qPCR). The real-time detection of the amplification is possible by applying SYBR Green as fluorescent dye binding to the double stranded DNA to quantify the DNA during the exponential phase of the qPCR. Preparation for the qPCR reaction in qPCR plates: 5 µl absolute qPCR SYBR® Green Mix was mixed with 0.25 µl of primer mix, including the forward and reverse primer in a 1:1 concentration of 10 µM and 4.75 µl template cDNA, resulting in a total volume of 10 µl per well. Each analysis was performed as triplicates determining the mean and standard deviations. Next to the -RT control a H₂O control was added to detect unspecific amplifications and primer dimers. qPCR results were depicted as Cy0 values normalized to the housekeeping gene RPL27. Cy0 calculation was performed to ensure the compatibility between the 3 qPCR machines used in the laboratory. This means that the values are "0 scaled", through which the lowest amplification value is normalized to 0 (Dr. Florian Finkernagel). In this case the assumption of equal reaction efficiency when comparing unknown genes with the standard curve is not necessary (Guescini et al. 2008). qPCRs were performed in the Mx3000P qPCR system applying the following program: activation of hot-start-polymerase (15 min 95°C),

followed by denaturation for 15 seconds at 95°C, annealing for 20 seconds at 60°C and elongation for 15 seconds at 72°C. The denaturation, annealing and elongation steps were repeated in 40 cycles. The melting curve was formed in the end at a temperature range of 72°C to 95°C.

2.3.3 RNA sequencing of HGSC patient-derived cells

As described in Sommerfeld et al. 2021, RNA sequencing of *ex vivo* HGSC omentum-derived HPMC, as well as HGSC ascites-derived tumor cells and tumor-associated T cells was performed and processed. The RNA sequencing data is stored at EBI ArrayExpress (accession numbers: E-MTAB-4162, E-MTAB-10611).

2.3.4 Immunohistochemistry

Matched HGSC patient pairs of paraffin-embedded metastatic omentum tissue samples removed during operation, as well as ascites fluid were subject to immunohistochemical analysis to determine the presence of apoptotic mesothelial cells (n=8 patients). The peritoneal cells present in the ascites fluid were isolated as usual (see section 2.2.1) and frozen. After thawing, cells were fixated in 4% Formalin for 1 hour at room temperature. Afterwards they were washed in 70% EtOH (3x) prior to embedding the cell pellets in 1% agarose gel (80-100 µl/cell pellet). After polymerization of the gels, 4% Formalin was added and incubated for 1 hour in the dark. The gels were then washed in water and kept in 70% EtOH until embedding them in paraffin blocks. Sections were cut from the embedded peritoneal cells and omental tissue for specific antibody staining by the pathology department (UKGM, Marburg, Germany). The respected primary antibodies were retrieved for their heat-induced epitope applying EDTA, following the manufacturer's protocol. Specific staining was carried out on a DAKO autostrainer Link 48. Endogenous peroxidase was blocked prior to the incubation with mouse monoclonal anti-Calretinin antibody (1:100), rabbit polyclonal anti-Cleaved Caspase-3 antibody (1:200), mouse monoclonal anti-Cytokeratin antibody (1:100) and mouse monoclonal anti-Alpha-Smooth Muscle Actin (α -SMA) antibody (1:200) for 45 minutes. Microscopic analyses of the stained sections were performed by the pathology department (Dr. Corinna Keber) afterwards.

2.3.5 Statistics and Bioinformatics

Statistics of comparative data were calculated by paired or unpaired student's t-test (two-sided, unequal variance) using GraphPad Prism. Results were significant where indicated (see figure legends), when the p-value was smaller than 0.05. Analysis of RNA sequencing data, as well as Olink secretome data was assisted by Dr. Florian Finkernagel and Prof. Dr. Rolf Müller. Box plots were created by Prof. Dr. Rolf Müller with python using the Matplotlib boxplot function.

3. Results

3.1 TAL induce apoptosis in HGSC-derived mesothelial cells

In order to evaluate if TAL isolated from ascites could induce apoptosis in omentum-derived HPMC from HGSC patients, a co-culture system was established, as described in section 2.2.6. By conducting these experiments, we observed that TAL obtained from different patients were able to kill HPMC with enhanced apoptosis rates upon prior T cell activation by anti-CD3 antibody stimulation (figure 11A). These results could be confirmed in an autologous system with matched pairs of HPMC and TAL from the same patient, thereby excluding HPMC killing due to a “non-self” attack of the immune cells (figure 11A, blue dots indicating matched autologous pairs). A representative example of the flow cytometric evaluation, comparing the co-culture of HPMC with unstimulated versus anti-CD3 antibody stimulated TAL, is shown as dot blots in figure 11B. To determine which TAL subpopulation induced HPMC apoptosis, the ascites-derived TAL were fractionated into CD3⁺ T cells and CD3⁻/CD56⁺ NK cells prior to the co-culture with HPMC (figure 11C). Hereby we were able to demonstrate that the activated T cells alone could not induce HPMC apoptosis in the absence of NK cells (figure 11C). The unstimulated NK cells alone only had very slight effects on inducing HPMC apoptosis, which was restored back to levels reached by total TAL when activated T cells were added to the NK cell culture in a 1:1 ratio (figure 11C). At the same time, this observation rules out that the inability of TAL subfractions to induce HPMC apoptosis was due to a reduced vitality of the T cells or NK cells after the MACS isolation procedure. Instead, the data suggests a cooperative activity of both immune cell types resulting in the question which mode of killing is active and which cells are the main effectors.

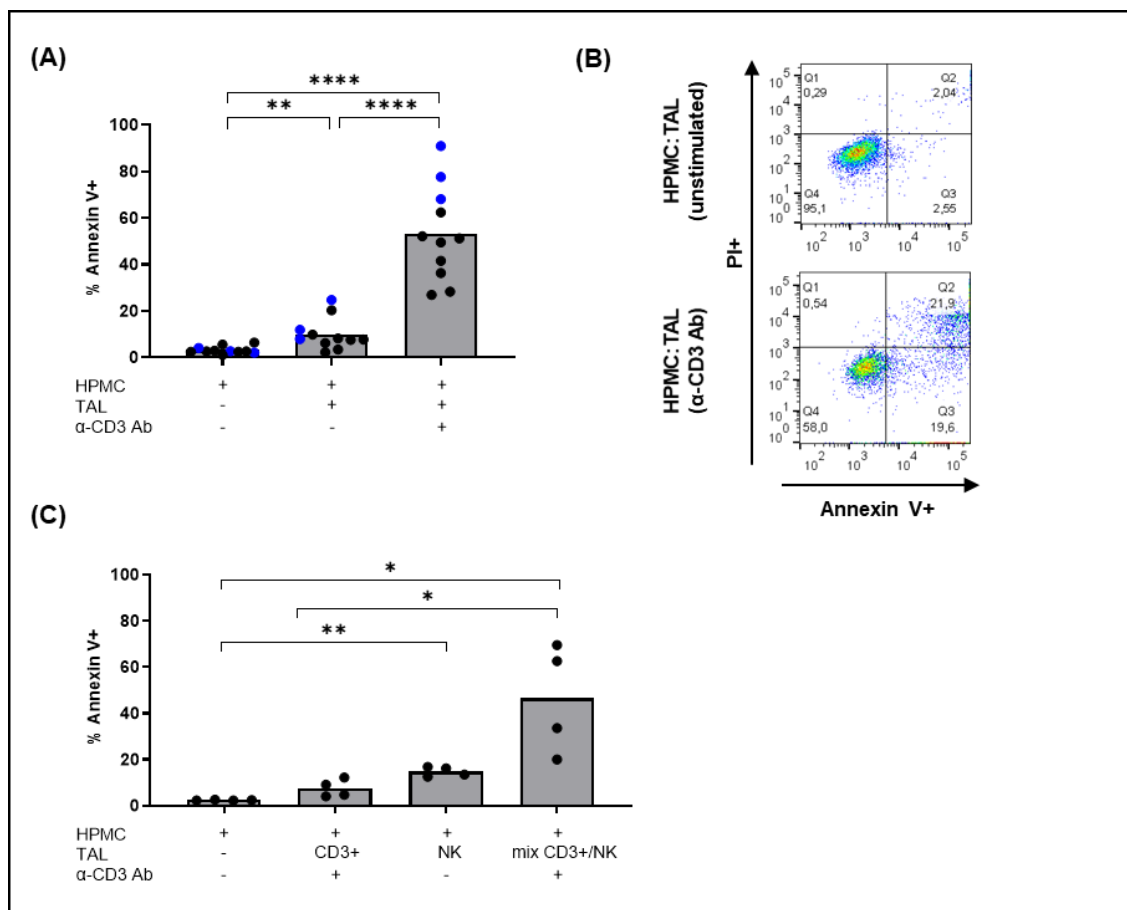


Figure 11. Induction of mesothelial apoptosis upon co-culture with anti-CD3 antibody-activated TAL. (A) The percentage of Annexin V+ HPMC is depicted to determine the amount of apoptotic mesothelial cells after co-cultivation with TAL. Autologous matched patient HPMC – TAL pairs are depicted as blue dots (n=11 total experiments with n=3 autologous pairs). Background HPMC apoptosis was determined from untreated HPMC alone. (B) Representative AnnexinV/PI dot blots of gated HPMC after co-culture with unstimulated versus anti-CD3 antibody stimulated TAL. (C) Percentage of Annexin V+ HPMC after co-culture with TAL sub-fractions (CD3+ T cells and NK cells), as well as 1:1 NK/T cell mixture directly after the MACS isolation procedure (n=4 biological replicates). The mean is indicated by the column height. p-values were calculated by two-sided, paired students' t-test: *= $p < 0.05$, **= $p < 0.01$, ****= $p < 0.0001$.

3.2 Identification of the NK cells as effector population within the TAL promoting mesothelial apoptosis

In the following, we tackled the question of which apoptosis signaling pathway introduced mesothelial apoptosis upon co-culture with TAL. Therefore, we first of all analyzed the GrB/Perforin apoptosis signaling pathway as a possible contributor to HPMC killing. Thus, we determined the induction of NK and T cell degranulation in response to HPMC by flow cytometrically measuring the CD107a expression on the outer membrane. At the same time, we aimed at

deciphering the still unknown effector cell population within the TAL responsible for killing HPMC. As a proof of principle control for these experiments, TAL were co-cultured with the MHC I-deprived K562 myeloid cell line serving as a positive control for NK cell degranulation (Alter et al. 2004) by introducing a “missing-self” activation of NK cells (figure 12A). TAL were treated with PMA, an activator of protein kinase C (PKC), and Ionomycin, a calcium ionophore that also activates PKC, as a positive control for T cell degranulation, introducing T cell activation (Ai et al. 2013; Chatila et al. 1989) (figure 12B). Importantly, we were hereby able to demonstrate that both cell populations within the ascites-derived TAL, NK and T cells, are principally able to degranulate upon sufficient stimulation, as depicted in figure 12A and B. Intriguingly, upon co-cultivation of activated TAL with HPMC, the NK cells strongly degranulated, as determined by the amount of CD335+/CD107a+ cells (figure 12C). At the same time, no CD107a+ T cells (CD3+/CD107a+) could be found, indicating that they did not degranulate in response to the mesothelial cells (figure 12D). In accordance with the previous findings (figure 11C) that the cytotoxic potential of unstimulated NK cells against HPMC was strongly reduced, their degranulation was also lost. However, this could be rescued upon mixture with isolated T cells and anti-CD3 antibody stimulation (figure 12E). Dot plots of the flow cytometric gating determining the degranulating NK (CD335+/CD107a+) and T cells (CD3+/CD107a+) are depicted in figure 12F. The background degranulation, which was slightly higher for anti-CD3 antibody stimulated TAL (around 3%) compared to unstimulated TAL (close to 0%) is shown, as well as the co-culture of HPMC with inactive versus activated TAL. In conclusion, these findings revealed that ascites-associated NK cells gain cytotoxic potential against HPMC, which requires previous activation by T cells. Moreover, cytotoxicity of NK cells targeting HPMC was executed by cellular degranulation representing the GrB/Perforin apoptosis signaling pathway in the underlying experimental setting.

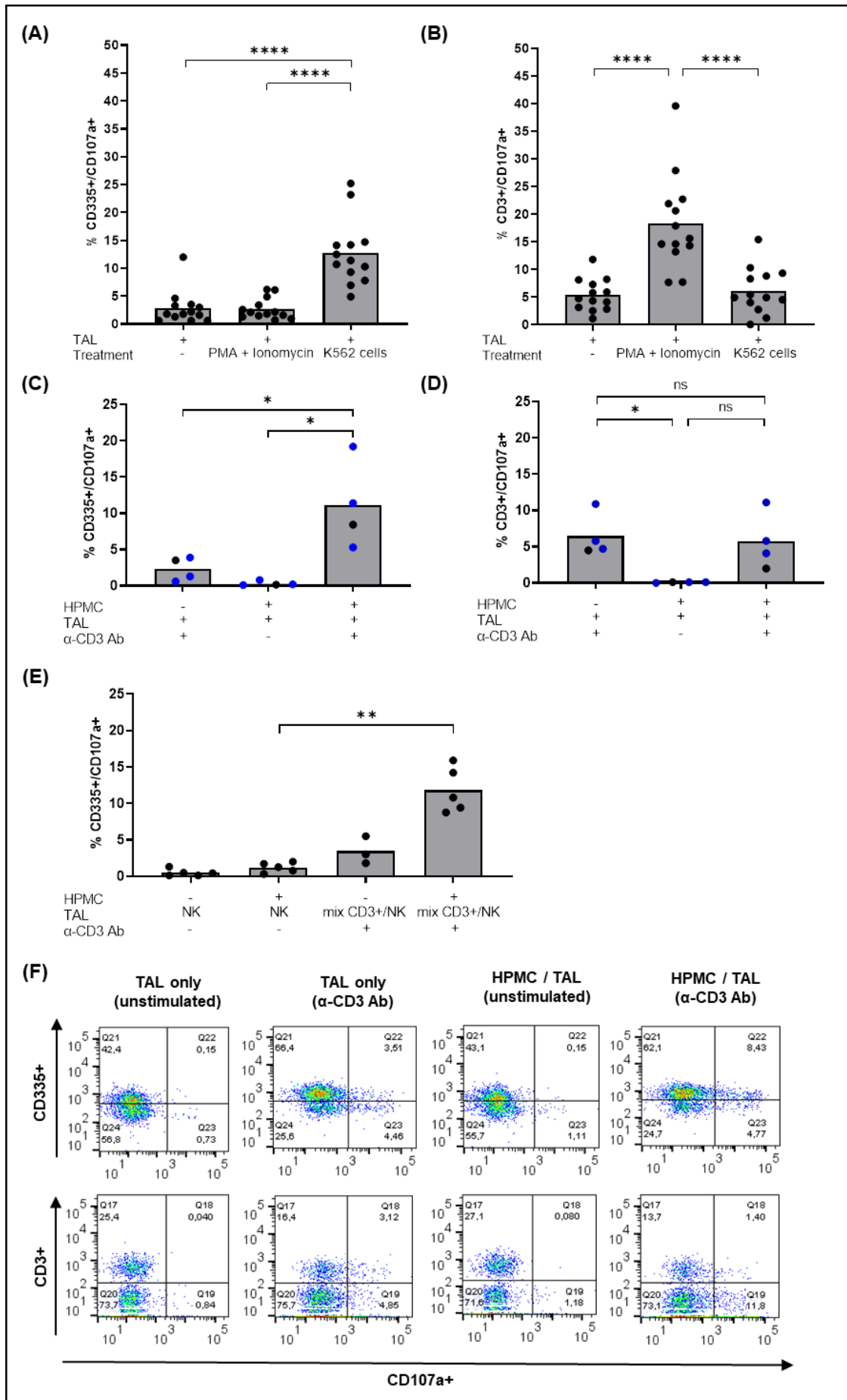


Figure 12. Strong degranulation of NK cells in the presence of HPMC after activation by anti-CD3 antibody stimulated T cells. (A, B) Proof-of-principal analysis of NK and T cell degranulation (n=13 replicates) by flow cytometric measurement after TAL co-culture with K562 cell line (NK cell positive control) or treatment with PMA and Ionomycin (T cell positive control). Cells were gated on CD335+/CD107a+ degranulating NK cells (A) and CD3+/CD107a+ degranulating T cells (B). The background degranulation is depicted for TAL in the absence of further cells or treatments. (C-D) The amount of degranulating NK cells (C) and T cells (D) in response to HPMC is depicted (n=4 biological replicates, blue dots indicate match autologous patient pairs). (E) The percentage of degranulating NK cells is shown after co-culture of HPMC with the isolated NK cell fraction or the 1:1 mixture of NK cells with T cells directly after fractionation (n=5 biological replicates). (F) Representative dot blots depicting the gating of degranulating NK cells and T cells. The column height indicates the mean. p-values were determined by two-sided, paired students' t-test: * $p < 0.05$, ** $p < 0.01$, **** $p < 0.0001$.

3.3 GrB/Perforin apoptosis signaling is blocked by ascites fluid

Seeing as ascites is part of the immunosuppressive TME in HGSC patients (reviewed in Worzfeld et al. 2017), we asked whether the cytolytic potential of activated NK cells against HPMC was sustained under these conditions. Therefore co-culture experiments were conducted as described above (section 2.2.6.2), applying cell-free ascites pool instead of serum for the 2-day cultivation of TAL with or without anti-CD3 antibody stimulation. As indicated in figure 13A, NK cell degranulation was completely blocked in the presence of ascites compared to serum-containing conditions. At the same time, HPMC death induction by TAL, as shown by Annexin V staining, persisted on a similar level regardless of ascites present in the medium (figure 13B). Based on these findings, we proposed that HPMC clearance by activated NK cells could be of clinical relevance since ascites does not suppress the cytolytic activity of NK cells, but a different apoptosis signaling pathway than GrB/Perforin must be active in the malignant context.

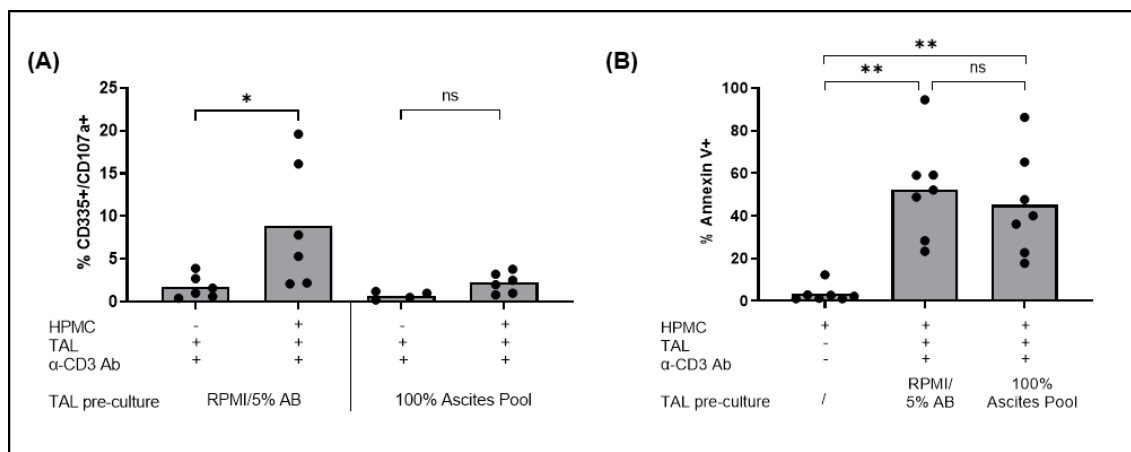


Figure 13. Ascites fluid blocks NK cell degranulation while the induction of mesothelial apoptosis is sustained. (A, B) Comparison of TAL pre-culture in RPMI/5% AB serum/1% sodium pyruvate and 100% ascites pool with anti-CD3 antibody stimulation for 2 days. Afterwards, co-culture with HPMC was performed for 6 hours. (A) NK cell degranulation within the total TAL population in response to HPMC co-culture was flow cytometrically determined and depicted as percentage of CD335+/CD107a+ NK cells (n=6 biological replicates). (B) HPMC apoptosis was determined by Annexin V/PI staining and flow cytometric measurement. The percentage of Annexin V+ HPMC (gated on CD45- cells to exclude apoptotic lymphocytes) is shown (n=7 independent experiments). The column height indicates the mean. p-values were determined by two-sided, paired students' t-test: ns=non-significant with $p > 0.05$, $* = p < 0.05$, $** = p < 0.01$.

3.4 Fas/FasL apoptosis signaling does not play a role in the HGSC TME

Since high expression levels of Fas (CD95) on the HGSC omentum-derived HPMC were sustained in the presence of ascites, we proposed that a Fas/FasL-mediated apoptosis signaling could be of importance in the TME (figure 14A). Multiple concentrations of crosslinked sFasL (1 – 10 – 100 ng/ml) were applied for the treatment of HPMC compared to the Fas-sensitive cell line Jurkat as a control (figure 14B). Of note, HPMC apoptosis could only be induced when applying the highest concentration of sFasL tested (100 ng/ml). In contrast, 10 ng/ml sFasL already induced Jurkat apoptosis at sufficient levels, which were even above the amount of apoptotic HPMC induced by the highest concentration of sFasL. These results indicate that the HPMC were far less responsive than the Jurkat cell line (figure 14B). As a proof-of-concept, an anti-sFasL antibody completely blocked the induction of cellular apoptosis by sFasL in both, HPMC and Fas-sensitive Jurkat cells (figure 14C).

As a prerequisite of Fas/FasL mediated killing of HPMC, it could be shown that CD3- TAL, comprising of mainly NK cells, strongly expressed FasL (CD178), but

this was not further enhanced by anti-CD3 antibody stimulation of TAL (figure 14D). Importantly, in spite of these results, TAL induced HPMC apoptosis independently from the Fas/FasL signaling pathway since adding a blocking anti-FasL antibody to the co-culture did not affect HPMC vitality (figure 14E). The obtained findings revealed that neither GrB/Perforin nor Fas/FasL signaling play an essential role in the TME of ovarian cancer.

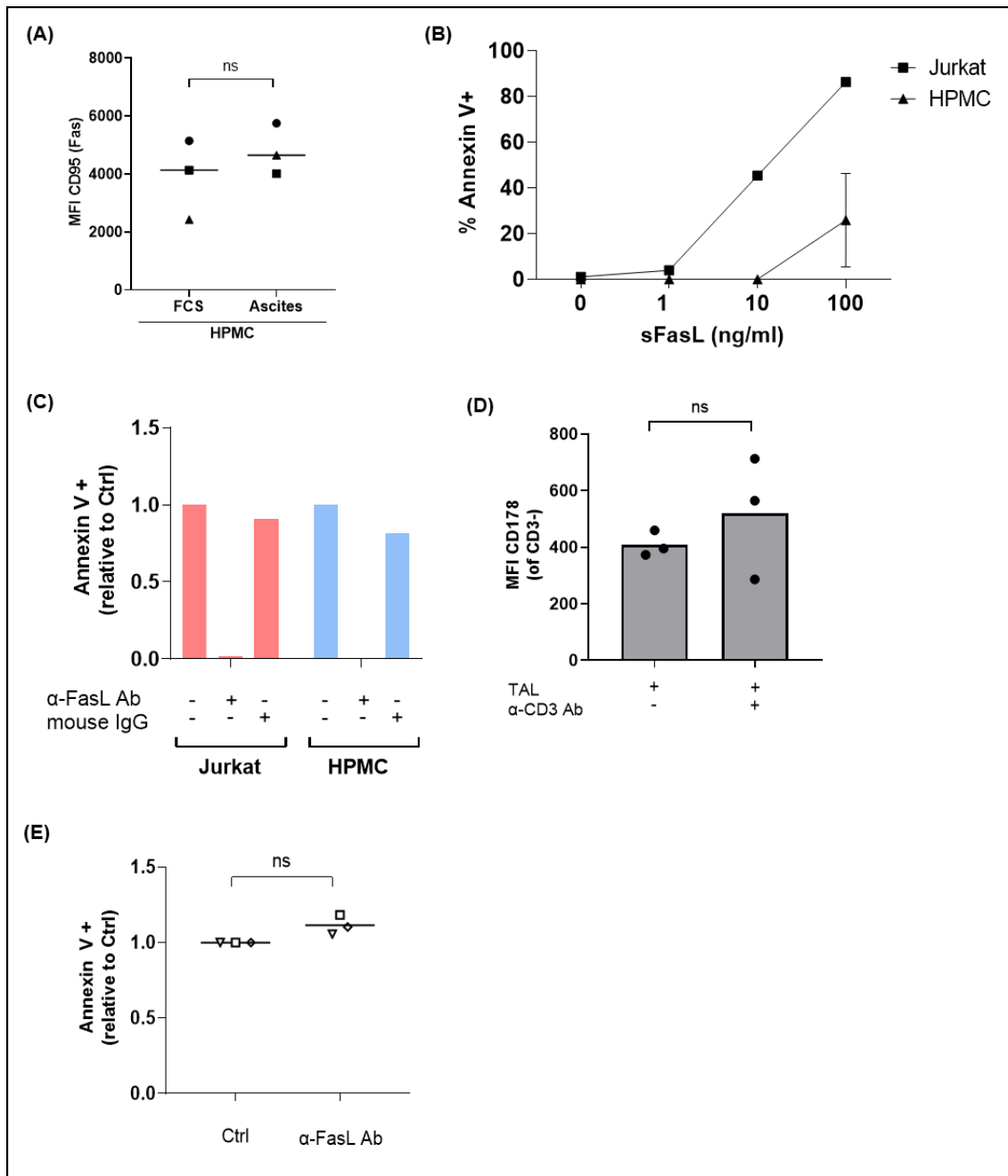


Figure 14. NK cell-mediated killing of HPMC was Fas/FasL independent despite the expression of Fas on HPMC and FasL on NK cells. (A) Determination of Fas (CD95) expression on HPMC pre-cultured in OCMI/5% FCS or OCMI/50% ascites pool for 3 days by flow

cytometry depicting the geometric mean fluorescence intensity (MFI) with subtracted isotype control (n=3 patients). (B) HPMC and Jurkat were treated with increasing concentrations of crosslinked sFasL for 24 h to determine HPMC sensitivity. Apoptosis induction was measured by flow cytometry (% Annexin V+). The baseline apoptosis of untreated cells was subtracted (n=3 HGSC patient HPMC). (C) Proof-of-concept determining the crosslinked sFasL specificity in killing HPMC and Jurkat by incubation with a neutralizing anti-FasL antibody or mouse IgG control. The results are depicted relative to the control without anti-sFasL antibody. (D) FasL (CD178) is expressed on NK cells (CD3-) within unstimulated and anti-CD3 antibody-stimulated TAL. The geometric MFI is depicted with subtracted isotype control (n=3 patients). (E) Co-culture of HPMC with anti-CD3 antibody stimulated TAL (6 hours) pre-treated with the neutralizing anti-FasL antibody or mouse IgG control (Ctrl). Flow cytometric evaluation of Annexin V/PI-stained HPMC depicted relative to the control (Ctrl). Horizontal bars and column heights indicate the mean. p-values were calculated by two-sided, paired t-test: ns=non-significant with $p>0.05$.

3.5 HPMC apoptosis induction is independent of the cytotoxic cytokines TNF α and IFN γ

It has been reported in the literature that NK cells release cytotoxic cytokines, including TNF α and IFN γ , as an additional mechanism introducing target cell death (reviewed in Sedger and McDermott 2014; Jorgovanovic et al. 2020). We therefore sought to analyze the effect of these cytokines on mediating HPMC apoptosis by treating omentum-derived HPMC with IFN γ and TNF α alone or in combination. In order to ensure comparability, the treatment was performed for 6 hours, choosing the same time frame in which NK cell secreted IFN γ and TNF α would have been present during the co-culture (figure 15). Importantly, we did not conduct experiments to detect the secretion of these cytokines by NK cells. As depicted in figure 15, we could not find a direct cytotoxic effect of either of these cytokines on HPMC. In conclusion, the reported release of the cytotoxic cytokines TNF α and IFN γ did not account for NK cell-mediated killing of HPMC.

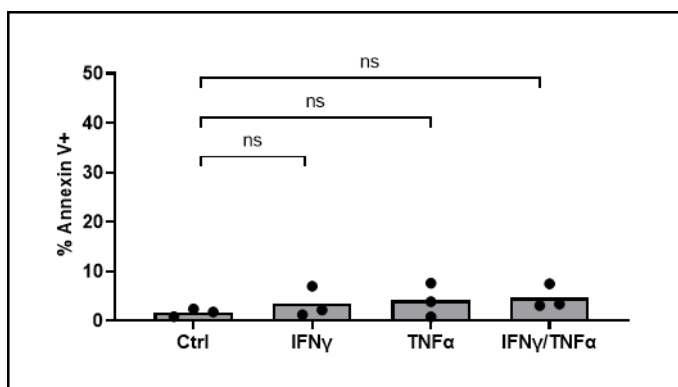


Figure 15. The cytotoxic cytokines TNF α and IFN γ are not able to induce HPMC apoptosis. HPMC were treated with (25 ng/ml) IFN γ and (100 ng/ml) TNF α alone or combined for 6 hours. HPMC apoptosis induction was determined by flow cytometric measurement of Annexin V/PI. Untreated cells served as background controls (Ctrl). The percentage of Annexin V+ HPMC is depicted for n=3 biological replicates. Column heights indicate the mean. p values were calculated by two-sided, paired t-test: ns=non-significant with p>0.05.

3.6 Identification of TRAIL apoptosis signaling conducted by T cell-activated NK cells introducing HPMC clearance in the HGSC TME

Seeing as we were able to rule out the involvement of GrB/Perforin, Fas/FasL and the cytotoxic cytokines TNF α and IFN γ in the induction of mesothelial apoptosis in our system, we next analyzed the role of TRAIL apoptosis signaling. This was addressed by first of all applying a rh-TRAIL protein for the treatment of HPMC and determining the amount of Annexin V+ mesothelial cells via flow cytometry (figure 16A, B). The experiments were conducted applying HPMC derived from a pre-culture in OCMI/5% FCS media (figure 16A) and OCMI/50% ascites pool media (figure 16B). Interestingly, albeit HPMC cultured in serum-containing media were generally prone to TRAIL-mediated killing, the apoptosis rates induced by rh-TRAIL were even enhanced in HPMC derived from cultivation in ascites. As a proof-of-principle, the rh-TRAIL-induced apoptosis was blocked by applying a neutralizing anti-TRAIL antibody in both cases, representing the specificity of the TRAIL-mediated killing by rh-TRAIL protein. As a second readout, HPMC plated on collagen I gel-coated wells were stained for activated caspase-3 and -7 after treatment to microscopically determine the apoptosis signaling introduced by rh-TRAIL (figure 16C). From the light microscopic picture, HPMC apoptosis is visual due to the changed, more fuzzy morphology after incubation with rh-TRAIL. This is confirmed by the fluorescence microscopic pictures showing the green staining of the active caspases within the apoptotic cells. In agreement with the flow cytometric read out, hardly any caspase-stained cells could be found in the untreated HPMC, indicating the lack of apoptosis signaling. This was literally performed to visualize the TRAIL-dependent apoptosis signaling in sporadic experiments, depicting a representative result which was not further quantified.

To investigate a TRAIL-dependent mechanism in HPMC killing by ascites-derived TAL, a neutralizing anti-TRAIL antibody was added to the co-culture between

HPMC and ascites-derived TAL either pre-cultured in the presence of serum (figure 16D) or ascites (figure 16E). As depicted in figure 16D and E, ascites did not suppress mesothelial apoptosis induced by TAL, which is in line with the results depicted in figure 16B. In both cases, applying the anti-TRAIL blocking antibody reduced the amount of apoptotic mesothelial cells significantly. Additionally, the expression of TRAIL on the CD335+ NK cell population present within the total TAL was flow cytometrically determined (geometric MFI gated on CD335+ NK cells). The TRAIL expression was compared between unstimulated TAL and anti-CD3 antibody stimulated TAL pre-cultured in RPMI/5% AB serum or 100% ascites pool. The results revealed a significant up-regulation of TRAIL on NK cells upon T cell activation by anti-CD3 antibody stimulation, again emphasizing the cooperation between T and NK cells. The TRAIL expression on NK cells derived from a TAL pre-culture in 100% ascites pool was slightly reduced compared to RPMI/5% AB serum. However, the difference was not significant, indicating the relevance of NK cell-mediated TRAIL signaling in ascites (figure 16F).

In conclusion, these observations strongly suggest a TRAIL-dependent HPMC killing by T cell-activated NK cells in the HGSC TME, seeing as the TRAIL signaling pathway is sustained in ascites. Moreover, a certain TRAIL-sensitization of HPMC in the presence of ascites seems to take place.

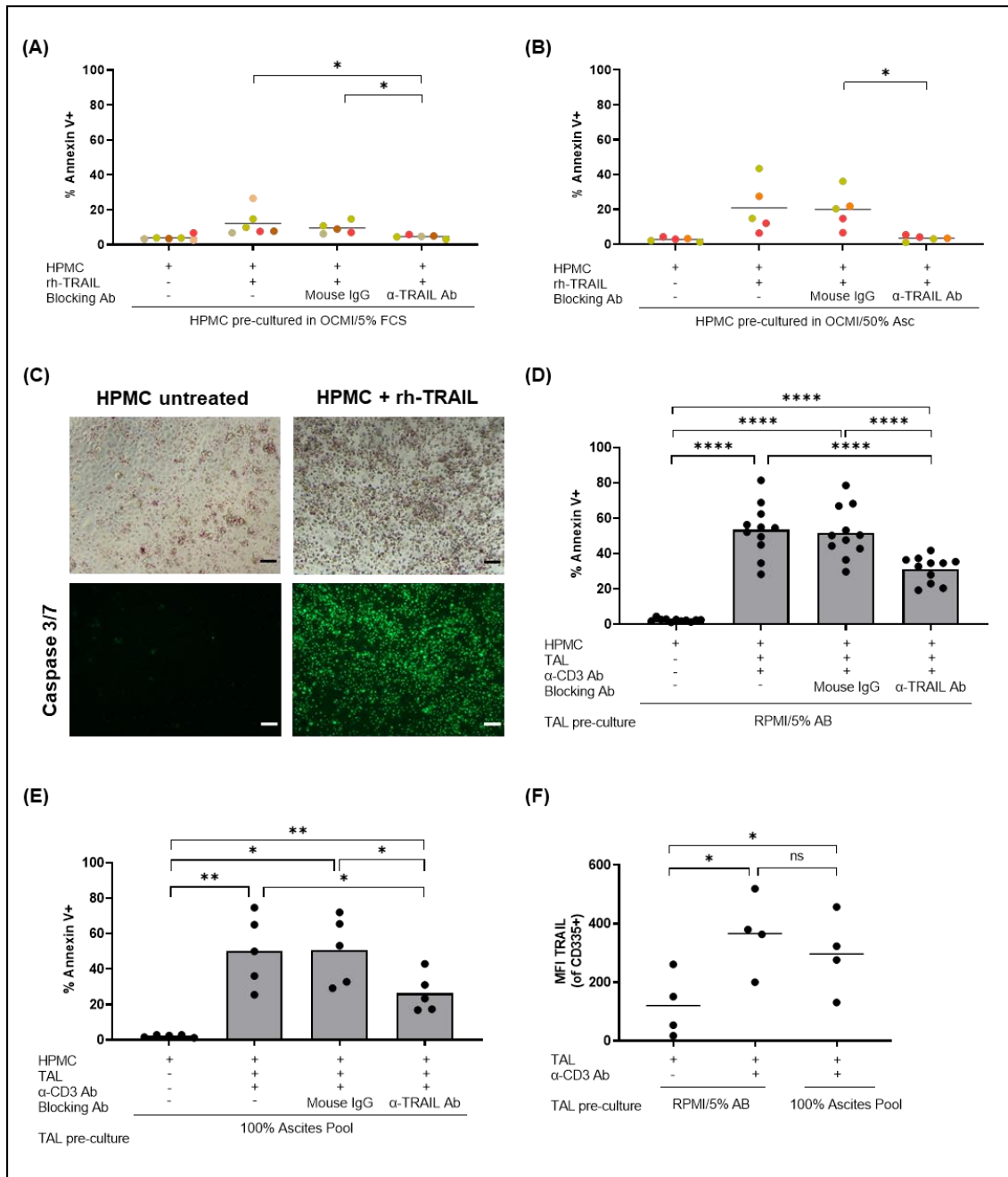


Figure 16. TRAIL-mediated apoptosis of HGSC-derived mesothelial cells. (A, B) Treatment of HPMC with 100 ng/ml rh-TRAIL protein for 18 hours. Induction of mesothelial apoptosis measured via flow cytometry and depicted as Annexin V+ HPMC. The Background of untreated HPMC is shown. A neutralizing anti-TRAIL antibody (10 μ g/ml) or mouse IgG control was applied for rh-TRAIL pre-culture (1h, 37°C). Results were compared between OCMI/5% FCS (n=6 individual experiments) (A) and OCMI/50% ascites pool (Asc) pre-cultured HPMC (n=5 individual experiments) (B). (C) Visualization of apoptotic HPMC, cultured on 150 μ g/ml collagen I gel, after rh-TRAIL treatment under the light microscope and caspase 3/7 staining (10 μ M) detected under the fluorescence microscope. Representative microscopy pictures are depicted. The scale bar indicates 100 μ m size. (D, E) TAL pre-cultured in RPMI/5% AB serum/1% sodium pyruvate were co-cultured with OCMI/5% FCS-derived HPMC (D), TAL pre-cultured in 100% ascites pool were

co-cultured with OCMI/50% ascites pool-derived HPMC (E) for 6 hours. HPMC apoptosis is depicted as percentage of Annexin V+ cells gated on the CD45- population. In both cases, TAL were pre-cultured with 10 µg/ml neutralizing anti-TRAIL antibody for 1 hour. As a control, an unspecific mouse IgG antibody was added. (F) Flow cytometric measurement of TRAIL expression on CD335+ NK cells present within total unstimulated TAL and anti-CD3 antibody-stimulated TAL in RPMI/5% AB or 100% Ascites Pool. Horizontal bars and column heights indicate the mean. p-values were calculated by two-sided, paired t-test: *=p<0.05, **=p<0.01, ****=p<0.0001.

3.7 T-NK cell crosstalk: soluble mediators secreted by T cells promote TRAIL-dependent cytotoxicity of NK cells against HPMC

Since we identified NK cells as the main effector population strongly degranulating in response to HPMC while ascites was absent and anti-CD3 antibody-stimulated T cells did not induce HPMC apoptosis on their own (figure 11C), we believed that the T cells display a more bystander effect. Thus, we addressed the possibility that T cells promote NK cell activation. This led to our inquiry of how the T cells activate the NK cells in the immunosuppressive TME, promoting TRAIL-dependent apoptosis as the main pathway leading to mesothelial cell death. To determine if a direct physical contact between T cells and NK cells was necessary for NK cell activation, we collected conditioned media (CM) of T cells with and without anti-CD3 antibody stimulation. Notably, the results revealed that the secretome of anti-CD3 antibody-stimulated T cells was sufficient in activating the NK cells' cytotoxic potential against HPMC (figure 17A). This indicates that the NK-T cell crosstalk is independent of direct cell-cell contact. Instead, a secretome-based communication seems to be of importance. Next to the CM of total CD3+ T cells, the secretome of T helper cell (CD3+/CD4+) and cytotoxic T cell (CD3+/CD8+) subfractions were also collected to analyze differences in the potential of activating NK cells. The isolation procedure is described in section 2.2.1.1 and depicted in figure 7. The CM of isolated T helper cells and cytotoxic T cells equally promoted the NK cells' cytotoxic potential against HPMC (figure 17A). Based on these findings, we concluded that NK cell activating mediators are secreted by the greater T cell population and not by one subpopulation alone. Therefore, we focused on the T cell secretome of the total CD3+ T cell population in the following. Moreover, the CM of activated T cells was more sufficient in promoting HPMC killing by NK cells compared to the secretome of unstimulated T cells (figure 17B). In line with this observation,

TRAIL expression on NK cells was also significantly up-regulated by the secretome of activated T cells, hinting towards the activation of a TRAIL-dependent NK cell killing mechanism (figure 17C). This could be verified using an anti-TRAIL neutralizing antibody added to the co-culture between T cell CM-stimulated NK cells and HPMC, which significantly decreased the amount of apoptotic/Annexin V+ mesothelial cells (figure 17E). Of note, the NK cell cytotoxic effects after activation by T cell CM were generally lower than the effects of total anti-CD3 antibody stimulated TAL, where the T and NK cells were in direct physical contact. This could be due to dilution effects of the responsible T cell-secreted cytokines in the CM, applied in a 1:1 concentration for NK cell activation. Furthermore, a possible positive feedback loop of NK cell-secreted cytokines upon activation, further stimulating T cells, could be missing here.

Since the T cells had only been activated by anti-CD3 antibody alone and not co-stimulated with anti-CD28 antibody, we wanted to ensure that the CD3 stimulation was already sufficient in rendering the T cells fully functional. As depicted in supplementary figure S1, the CM of anti-CD3/anti-CD28 antibody-stimulated T cells was additionally collected and applied for NK cell activation prior to the co-culture with HPMC. This was directly compared to the NK cell activation by anti-CD3 antibody-stimulated T cell CM alone. The NK cell cytotoxic potential directed against HPMC was flow cytometrically determined by measuring the amount of Annexin V+ HPMC (Supplementary figure S1A) and the up-regulation of TRAIL on NK cells (Supplementary figure S1B). Intriguingly, while the NK cells activated by the CD3/CD28 co-stimulated T cell CM induced HPMC apoptosis at higher levels (Supplementary figure S1A), no increase in TRAIL expression on NK cells upon additional CD28 stimulation of T cells could be observed (Supplementary figure S1B). Generally, CD3 stimulation of T cells alone was sufficient in promoting the secretion of NK cell-activating cytokines. Therefore, anti-CD3 antibody stimulation of T cells alone was performed throughout this work.

In conclusion, we were able to demonstrate that direct physical contact between NK cells and T cells is not necessary, instead, the NK cells can be activated by mediators secreted by anti-CD3 antibody-activated T cells, through which the NK cells gain their full TRAIL-mediated cytotoxic potential against HGSC-derived HPMC.

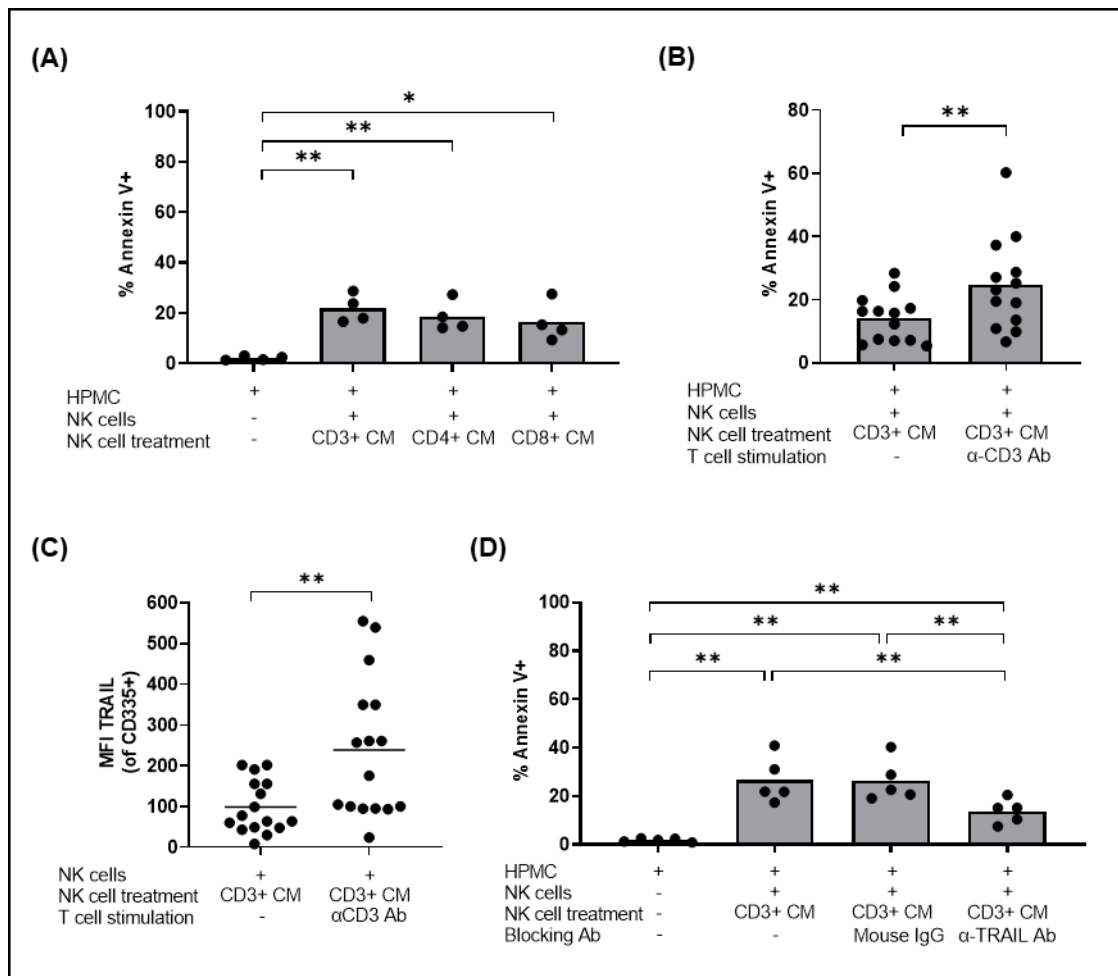


Figure 17. The secretome of anti-CD3 antibody-stimulated T cells promotes TRAIL-mediated NK cell cytotoxic activation directed against HPMC. (A) Percentage of Annexin V+ HPMC (flow cytometry) induced by T cell CM-treated NK cells comparing the CM of total CD3+ T cells and T cell subsets (CD3+/CD4+ or CD3+/CD8+) (n=4 biological replicates). (B) Determination of HPMC apoptosis (% Annexin V+) induction by NK cells treated with the CM of anti-CD3 antibody stimulated versus unstimulated T cells via flow cytometry (n=13 individual experiments). (C) Flow cytometric measurement of TRAIL expression on NK cells treated with the CM of unstimulated versus anti-CD3 antibody stimulated T cells. (E) Incubation of the CM-stimulated NK cells with a neutralizing anti-TRAIL antibody or mouse IgG control prior to the co-culture with HPMC. Flow cytometric analysis of Annexin V+ HPMC. Horizontal bars and column heights indicate the mean. p-values were determined by two-sided, paired student's t-test: *= $p < 0.05$, **= $p < 0.01$.

3.8 Identification of the T cell-secreted cytokines inducing NK cell activation

Seeing as the CM of anti-CD3 antibody-stimulated T cells was sufficient in activating the NK cells, we wanted to identify the important mediators for this purpose. Therefore, affinity proteomics (Olink) and comparative bioinformatics

were applied to analyze the secretome of unstimulated versus activated ascites-derived T cells (n=5 matched pairs). As shown in figure 18A, depicting the fold change of activated relative to untreated T cells, the secretion of 45 proteins linked to NK cell activation and TRAIL signaling was significantly increased upon anti-CD3 antibody stimulation. Among these proteins are members of the TNF ligand superfamily, including TNF α , CD40LG, CD70, FASL, TNFSF8, TNFSF9 and TNFSF10/TRAIL and receptor superfamily, including FAS, TNFRSF10A/TRAILR1, TNFRSF10B/TRAILR2, TNFRSF4 and TNFRSF8, as well as T cell subset specific cytokines such as IL-2, IFN γ , TNF, IL-4, IL-10 and IL17A. Seeing as activated T cells did not promote HPMC apoptosis on their own, the secretion of GrA/GrB, TRAIL and FasL did not play a role in our system and was not further incorporated (figure 11C).

CD40LG and CD70 were also found as activated T cell-secreted proteins, implying a CD40LG/CD40 and CD70/CD27 signaling for the activation of NK cells. This could be excluded, seeing as agonistic anti-CD40 and anti-CD27 antibodies failed to activate the NK cell cytotoxicity against HPMC (figure 18B).

We identified the activated T cell-secreted cytokines IFN γ , IL-2 and TNF α as the most promising to possibly be involved in NK cell activation, expansion and cytotoxic stimulation (figure 18A) (reviewed in Wu et al. 2017; Johnsen et al. 1999; Takeda et al. 2001; Almishri et al. 2016). We could further confirm an increased expression of TNF α on RNA-level by qPCR, as shown in figure 18C. Besides this, we also focused on IL-21, which was not part of the Olink panel but is described to be up-regulated in T cells upon stimulation with the same anti-CD3 antibody (clone Okt3) we used (Sousa et al. 2019). Additionally, we identified IL-21 in public transcriptome datasets at Gene expression Omnibus (GEO) (<http://www.ncbi.nlm.nih.gov/geo>; GSE112899 accession number). We could confirm this up-regulation of IL-21 on mRNA level by qPCR upon anti-CD3 antibody stimulation, as depicted in figure 18C. Here the difference between unstimulated versus stimulated was even higher compared to TNF α (figure 18C). Based on these data, we concentrated on validating the role of T cell-secreted IL-2, IL-21, IFN γ and TNF α on the NK cell cytotoxic function.

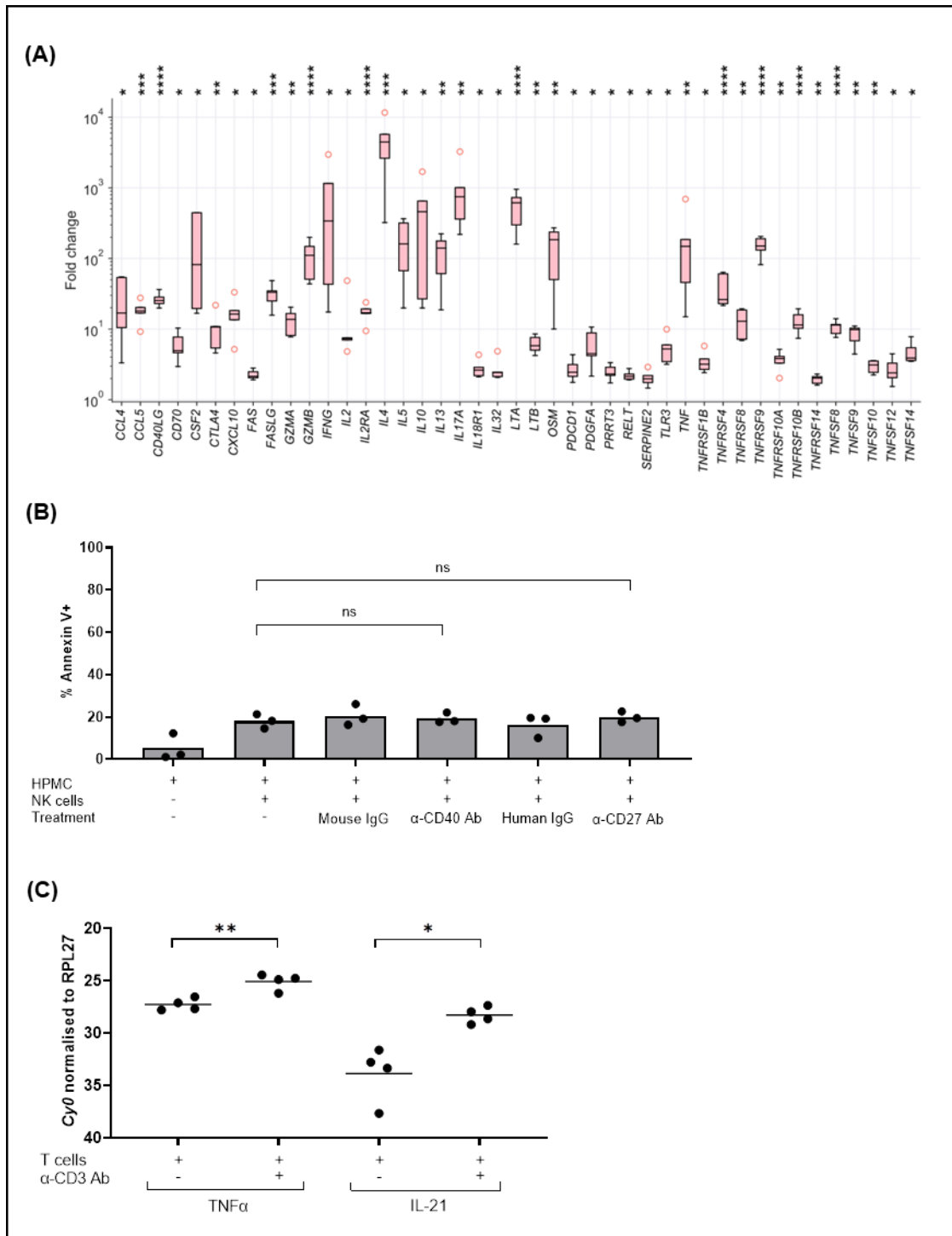


Figure 18. IFN γ , IL-2, TNF α and IL-21 are important cytokines secreted/expressed by anti-CD3 antibody stimulated T cells activating NK cells. (A) The CM of matched pairs of unstimulated and anti-CD3 antibody-stimulated T cells derived from the ascites of HGSC patients were subject to PEA-based affinity proteomics (Olink) conducted by the proteomic core facility. Depicted are cytokines matching the terms “NK cell activation” and “TRAIL” in the GeneCards database (n=45 cytokines). The gene names of the cytokines are indicated. The results are depicted as the fold change of the activated relative to the untreated T cell CM (n=5 matched pairs). Boxplots are shown with the median, the upper and lower quartiles, marked by the box,

the whiskers displaying the range and outliers marked by circles. Statistics were calculated by paired student's t-test: *=FDR<0.05, **=FDR<0.01, ***=FDR<0.001, ****=FDR<0.0001. (B) Ascites-derived NK cells were pre-treated with 10 µg/ml agonistic anti-CD40 and anti-CD27 antibody, as well as corresponding IgG controls (mouse and human) for 1 hour. The amount of apoptotic HPMC is depicted as percentage of Annexin V+ cells gated on the CD45- cell population (n=3 experimental replicates). (C) qPCR analysis of TNFα and IL-21 expression by anti-CD3 antibody stimulated versus unstimulated T cells. Results are shown as *Cy0* normalized to the housekeeping gene RPL27. Horizontal bars indicate the mean. p-values were calculated by two-sided, paired student's t-test: ns=non-significant with p>0.05, *=p<0.05, **=p<0.01, ****=p<0.0001.

3.9 T cell-secreted cytokines activate TRAIL-mediated NK cell cytotoxic potential

According to the literature, IL-2 and IFNγ are important for TRAIL regulation in NK cells (Johnsen et al. 1999; Takeda et al. 2001). Seeing as both were secreted by the activated T cells, we first of all analyzed whether these cytokines also played an important role in our system promoting TRAIL-related NK cell cytotoxicity against HPMC. To address this, NK cells were stimulated with rh-IL-2 alone or in combination with rh-IFNγ. Importantly, rh-IL-2 alone had no effect on NK cell activation measured by the TRAIL expression (figure 19A) and HPMC apoptosis, which was hardly induced by rh-IL-2 treated NK cells (figure 19B). NK cells treated with the combination of rh-IL-2 and rh-IFNγ showed only a slight increase of TRAIL expression concomitant with weak but significant increase of cytotoxicity against HPMC in comparison to the background and untreated/resting NK cells (Figure 19A and B). Seeing as these effects were genuinely low, we concluded that these cytokines do not play a pivotal role in NK cell cytotoxic activation on their own.

In the next step, the role of IL-21 and TNFα secreted by activated T cells on the activation of NK cells was analyzed. Therefore, gain-of-function and loss-of-function experiments were conducted applying rh-IL-21 and rh-TNFα both in combination with rh-IL-2, as well as specific neutralizing antibodies. TRAIL up-regulation on NK cells could not be induced upon treatment with rh-IL-21 combined with rh-IL-2 (figure 19A). However, the induction of mesothelial apoptosis by rh-IL-2/rh-IL-21 treated NK cells was significantly enhanced (figure 19B). This might indicate that another apoptosis signaling pathway was activated

here, which was not further tested due to the explicit relevance of TRAIL signaling in ascites (see section 3.6).

By contrast, TRAIL was significantly up-regulated on NK cells upon treatment with rh-IL-2 and rh-TNF α , as depicted in figure 19A. At the same time, the amount of apoptotic HPMC was also significantly increased (figure 19B). These findings are in line with our previous results, indicating that the TRAIL up-regulation on NK cells and increased HPMC killing go hand in hand. Interestingly, when rh-IL-21 was added to the combination of rh-IL-2 and rh-TNF α for NK cell stimulation, the amount of apoptotic HPMC was even further increased but did not reach statistical significance (figure 19B). This was at least partly dependent on TRAIL due to the slight increase of the TRAIL expression on the treated NK cells (figure 19A). Furthermore, adding a neutralizing anti-TRAIL antibody to the co-culture between HPMC and NK cells stimulated with all three cytokines significantly decreased the amount of apoptotic mesothelial cells (figure 19C). Upon neutralization of T cell-secreted TNF α by applying the anti-TNF α blocking antibody Infliximab during NK cell stimulation, the NK cell cytotoxic potential directed against HPMC was significantly decreased. This was shown by the significantly reduced amount of apoptotic HPMC (figure 19D). In contrast, blocking T cell-secreted IL-21 did not affect NK cell cytotoxic activation and HPMC killing (figure 19D). These results underline the substantial relevance of T cell-derived TNF α as a critical mediator for the activation of NK cells to act out their killing abilities, while IL-21, IL-2 and IFN γ seem to play a more ancillary role. It is conceivable that a network of different T cell-derived cytokines work together to activate the NK cells. Therefore, certain cytokines possibly do not show any effect on their own in our read-out but in unison with other cytokines.

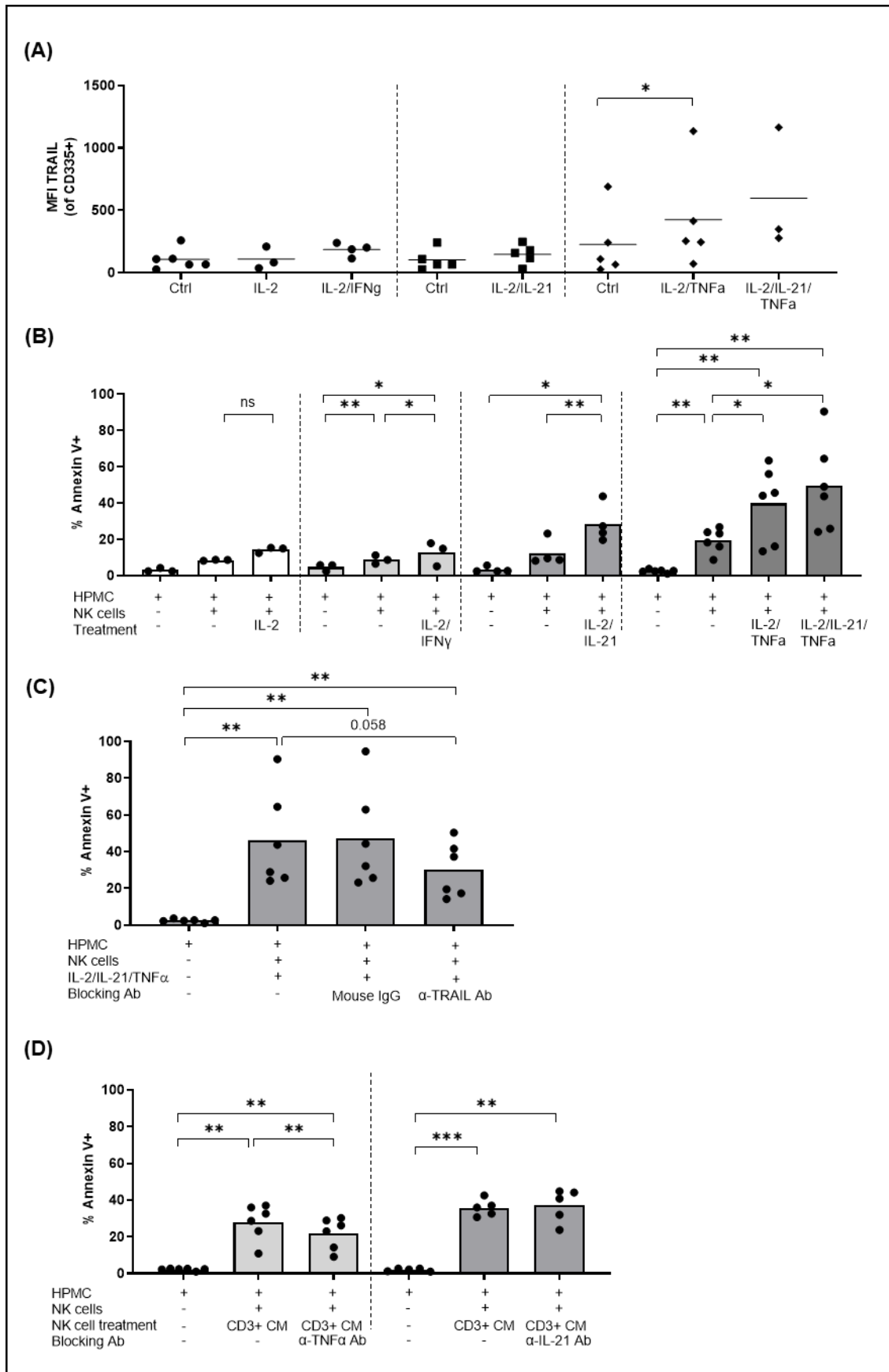


Figure 19. T cell-secreted TNFα is an important effector cytokine activating NK cells in the TME. (A, B, C) Gain-of-function analysis by treating ascites-derived NK cells with different

cytokine combinations for 2 days: rh-IL-2 (200 U/ml) alone, rh-IL-2 + rh-IFN γ (10 ng/ml), rh-IL-2 + rh-IL-21 (10 ng/ml), rh-IL-2 + rh-TNF α (10 ng/ml) and rh-IL-2 + rh-IL-21 + rh-TNF α . TRAIL expression on treated NK cells was analyzed by flow cytometry depicting the geometric MFI (A) and HPMC apoptosis showing the percentage of Annexin V+ HPMC (B). (C) The involvement of TRAIL apoptosis signaling was analyzed by adding the anti-TRAIL blocking antibody (10 μ g/ml) to the co-culture. (D) Loss-of-function analysis was conducted by applying neutralizing anti-TNF α and anti-IL-21 antibodies (each 10 μ g/ml) to the activated T cell CM (1 hour pre-incubation) for NK cell stimulation for 2 days. The induction of HPMC apoptosis after co-culture with these NK cells was again flow cytometrically analyzed. The horizontal bars and column heights indicate the mean. p-values were determined by two-sided, paired student's t-test: ns=non-significant with $p>0.05$, $*=p<0.05$, $**=p<0.01$, $***=p<0.001$.

3.10 HGSC-derived HPMC are susceptible to TRAIL-mediated killing, which is associated with high expression levels of TRAIL death receptors

To tackle the question whether HPMC are selectively targeted by TRAIL-dependent NK cell-mediated cytotoxicity within the malignant TME, we analyzed death and decoy receptor expressions on HGSC patient omentum-derived HPMC and ascites-derived tumor cells in the next step. Previously obtained RNA-sequencing data (Sommerfeld et al. 2021) of *ex vivo* HPMC and tumor cells were exploited to determine the expression levels of the activating receptors TNFRSF10A (DR4, TRAIL R1) and TNFRSF10B (DR5, TRAIL R2), as well as decoy receptors TNFRSF10C (DcR1, TRAIL R3) and TNFRSF10C (DcR2, TRAIL R4) on mRNA level. These results are depicted as transcripts per million (TPM), clearly exhibiting that the TRAIL activating receptor DR5 is selectively expressed on HPMC compared to tumor cells (figure 20A). DR4 and DcR1 are expressed at very low levels in both HPMC and tumor cells. DcR2, on the other hand, is expressed at higher levels on the HPMC (figure 20A). The RNA-sequencing results were confirmed on protein level by flow cytometry, depicted as the geometric MFI (figure 20B). The results on protein level were compared to control HPMC derived from the peritoneal lavage of patients with benign gynecological diseases (Ctrl). This comparison was performed to determine specific TRAIL-sensitizing effects the malignant TME may have on the HPMC. Importantly, opposing the RNA-sequencing data, the activating receptor DR4 was expressed significantly higher on HGSC-derived HPMC compared to tumor cells on protein level. Moreover, these expression levels were also higher in comparison to the control HPMC. The high DR5 expression on HPMC was

endorsed with similar levels between control and HGSC-derived HPMC. Both decoy receptors were expressed at slightly higher levels on the HPMC types compared to the tumor cells. Of note, in contrast to the RNA-sequencing data, DcR1 was expressed at high protein levels on the HPMC. Taken together, as depicted in figure 20B, all 4 receptors were expressed at higher levels on both HPMC types compared to the tumor cells, most strikingly DR5. Furthermore, a trend towards a higher expression of DR4 and DcR1 on HGSC-derived HPMC compared to the control HPMC could be seen (figure 20B). Exemplary histograms of the flow cytometric measurements representing the tumor cells and HGSC-derived HPMC are depicted in figure 21C as staged blots. These results demonstrate that in agreement with the TRAIL-dependent killing of HGSC-derived HPMC by NK cells, they strongly express the required TRAIL receptors DR4 and DR5, enabling TRAIL apoptosis signaling.

Seeing as the HPMC had to be cultured in order to apply them for functional analysis *in vitro*, we made sure that the death cell receptor expression did not vary too strongly compared to *ex vivo* HPMC due to culture effects. Therefore RNA-sequencing data determining the death receptor expression on mRNA level (TPM) for OCMI/5% FCS and OCMI/50% ascites pool cultured HPMC compared to *ex vivo* HPMC was analyzed. As shown in figure 20D, a general decline of all 4 receptors upon cultivation of the HPMC in OCMI/5% FCS or OCMI/50% ascites pool was observed, while the general expression pattern was maintained (highest expression level of DR5). No specific ascites effects could be seen. Consequently, we were able to rule out an artificial susceptibility of cultured HPMC to TRAIL-mediated cell death and concluded that the HPMC had already been sensitized toward TRAIL-induced killing in the *in vivo* TME.

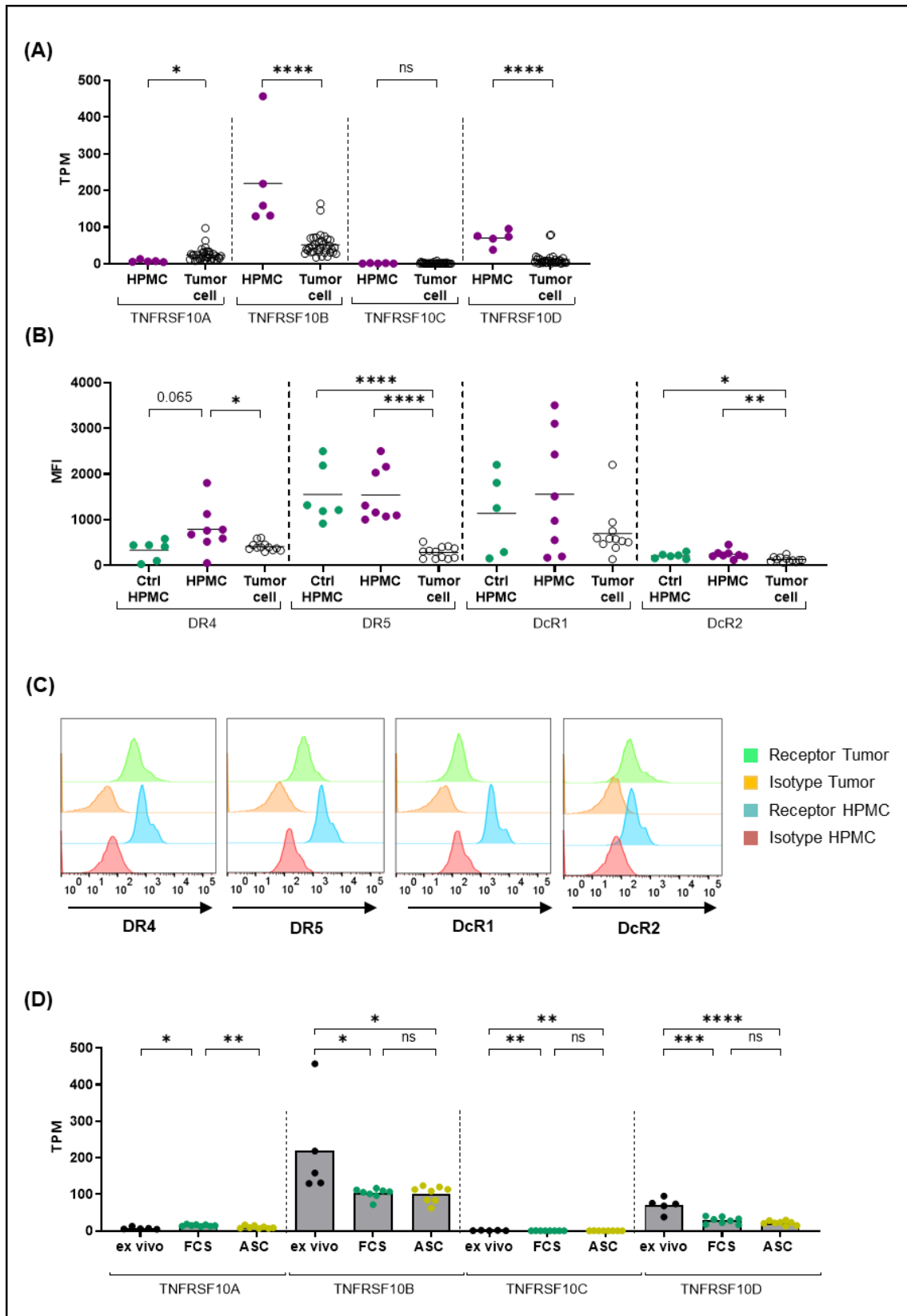


Figure 20. High expression levels of the activating death receptors on HGSC-derived HPMC render them liable toward TRAIL-induced apoptosis conducted by NK cells. (A) RNA-sequencing analysis of *ex vivo* omentum-derived HPMC (n=5 patients) and tumor cells (n=34 patients) derived from HGSC patient ascites for the expression of the TRAIL receptors

TNFRSF10A (DR4, TRAIL R1), TNFRSF10B (DR5, TRAIL R2), TNFRSF10C (DcR1, TRAIL R3) and TNFRSF10C (DcR2, TRAIL R4). The corresponding TPM values are depicted. (B, C) Flow cytometric analysis of TRAIL receptor expression on protein level comparing HGSC-derived HPMC (n=8), control HPMC (Ctrl) derived from patients with benign gynecological diseases (n=6) and *ex vivo* tumor cells (n=11). The geometric MFI is depicted (B). Representative staged blots of measured HGSC-derived HPMC and tumor cells are depicted for the expression of all four receptors (C). (D) RNA-sequencing data showing the TPM values of TRAIL receptor expression comparing *ex vivo* HPMC (n=5 patients) and cultured HPMC (OCMI/5% FCS and OCMI/50% ascites pool) (n=8 patients). The horizontal bars and column heights indicate the mean. p-values were determined by two-sided, unpaired student's t-test: ns=non-significant with $p>0.05$, $*=p<0.05$, $**=p<0.01$, $***=p<0.001$, $****=p<0.0001$.

3.11 HGSC tumor cells are resistant against TRAIL-mediated killing by TAL

Tumor cells are deprived of both activating TRAIL receptors DR4 and DR5, meaning that the prerequisite for TRAIL-induced apoptosis is not given and implies that they are resistant against TRAIL signaling. We evaluated this hypothesis by performing co-culture experiments between ascites-cultivated TAL and *ex vivo* tumor cells. Subsequent apoptosis detection by Annexin V/PI staining was performed as described previously for HPMC-TAL co-cultures. It was important to apply malignant ascites to resemble and maintain the *in vivo* situation in the best possible way *in vitro*. The results revealed that the tumor cells were generally less sensitive toward TAL-mediated killing (mean increase over background = 25,62% Annexin V+ (figure 21) compared to mean = 51% Annexin V+ HPMC (Figure 11A)), seeing as the background apoptosis of untreated tumor cells was slightly higher (figure 21) compared to HGSC-derived HPMC. Furthermore, adding a neutralizing anti-TRAIL antibody did not significantly decrease the amount of apoptotic tumor cells. Based on these data, we concluded that in accordance with the deprivation of DR4 and DR5 on tumor cells, they are resistant against TRAIL-mediated apoptosis signaling in the TME. Whether this slight, TRAIL-independent induction of tumor cell apoptosis was NK or T cell-facilitated was not of our interest in this case and therefore not further analyzed.

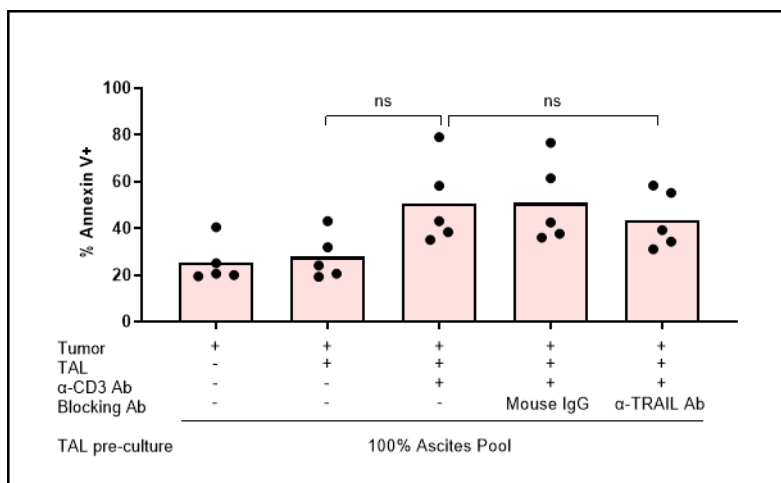


Figure 21. Tumor cells are insensitive against TRAIL-dependent apoptosis. Co-culture experiments between ex vivo tumor cells after an over night resting period in OCMI/50% ascites pool and 100% ascites pool-derived anti-CD3 antibody stimulated and unstimulated TAL were conducted. Apoptosis-induction in tumor cells was flow cytometrically determined after Annexin V/PI staining (n=5 independent experiments). The column heights indicate the mean. p-values were determined by two-sided, paired student's t-test: ns=non-significant with $p > 0.05$.

3.12 The HGSC TME sensitizes HPMC to TRAIL-mediated killing by NK cells

Another important question we wanted to tackle is how mesothelial cells in the TME become sensitized toward NK cell-induced apoptosis by TRAIL. To address this, we applied control HPMC derived from patients with benign gynecological diseases not only for the analysis of the TRAIL receptor expression (figure 20B) but also for functional experiments. Co-culture experiments between the control HPMC and TAL pre-cultured in ascites with or without anti-CD3 antibody stimulation were performed following our standard protocol. The results, depicting the amount of Annexin V+ control HPMC, are shown in figure 22. We hereby observed that activated TAL were generally able to induce apoptosis in these control HPMC, with an increased mean of 23.6% (figure 22), which was far lower compared to HGSC-derived HPMC with a mean of 51% (figure 11A). Importantly, it could be shown that the control HPMC, in striking contrast to HPMC derived from the HGSC TME, were resistant toward TRAIL-mediated killing since the anti-TRAIL blocking antibody did not inhibit the apoptosis induction. The TRAIL resistance of the control HPMC correlated with a reduced DR4 expression, while DR5 expression was comparably high in both HPMC types (figure 20B). Therefore, it could be assumed that the expression of both death cell receptors, DR4 and DR5, is necessary for TRAIL-induced apoptosis of HPMC. Similar to the

analysis of apoptosis induction in tumor cells (section 3.11), we were again not interested in deciphering the TAL subpopulation promoting slight, TRAIL-independent apoptosis levels in these control HPMC. Thus, no further experiments were performed.

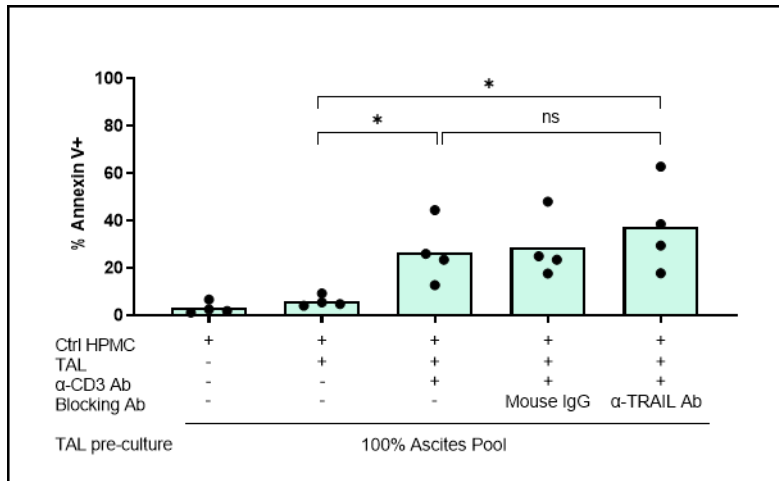


Figure 22. Control HPMC derived from lavage of patients with benign gynecological diseases were insensitive to TRAIL-mediated killing. Co-culture experiments between control HPMC and TAL derived from 100% ascites pool with or without anti-CD3 antibody stimulation were performed. Apoptosis-induction was determined by flow cytometry after Annexin V/PI staining (n=4 biological replicates). The column heights indicate the mean. p-values were determined by two-sided, paired student's t-test: ns=non-significant with $p>0.05$, $*=p<0.05$.

3.13 HPMC – NK cell crosstalk: Additional mechanisms rendering NK cell activation

Further analyses concerning the predisposition of HGSC omentum-derived HPMC towards NK cell-mediated killing were performed by analyzing the expression of MHC class I (HLA-A, -B and -C) molecules on HPMC, which determines the “immunological self” recognition (reviewed in Abel et al. 2018). Interestingly, the mRNA expression of HLA-A, -B and -C, shown by RNA-sequencing data, declined significantly compared to immune cells, such as TAT (figure 23A). The expression level on HPMC was similarly low compared to tumor cells, making them both potentially vulnerable to NK cell attack.

In the following, we examined the role of the stress-induced ligands MICA/B in rendering the HPMC sensitive to NK cell-induced killing. MICA and MICB interact with the activating NKG2D receptor expressed on NK cells important for activation of their cytotoxic potential upon ligand binding (Bauer et al. 1999).

RNA-sequencing data revealed that only MICA is expressed on HPMC at high levels, depicted as TPM values in figure 23B. This could be confirmed on protein level by flow cytometry detection using a MICA/B-specific antibody (figure 23C and D). Of note, the expression was only slightly decreased upon cultivation in the presence of ascites, indicating the persistence of the expression in the TME. On the other hand, RNA-sequencing data also revealed a strong expression of MICA and MICB in tumor cells and TAT which could make them a target for NKG2D-expressing NK cells (figure 23B).

Indeed, the activating receptor NKG2D on NK cells was stably expressed, even in the presence of ascites, as demonstrated by flow cytometry (figure 23E). To address whether HPMC are attacked by NK cells in a MICA/B – NKG2D driven interaction, we applied a neutralizing anti-NKG2D antibody to the co-culture between HPMC and activated TAL. However, blocking NKG2D only slightly decreased the amount of apoptotic HPMC, even though this was statistically significant (figure 23F). Based on our findings, we assume that the MICA/B – NKG2D interaction plays a subordinate role in contributing to HPMC apoptosis and the TRAIL signaling pathway is the main axis leading to mesothelial clearance in the HGSC TME. Apart from this, further relevant mechanisms concerning HPMC – NK cell crosstalk are yet to be determined.

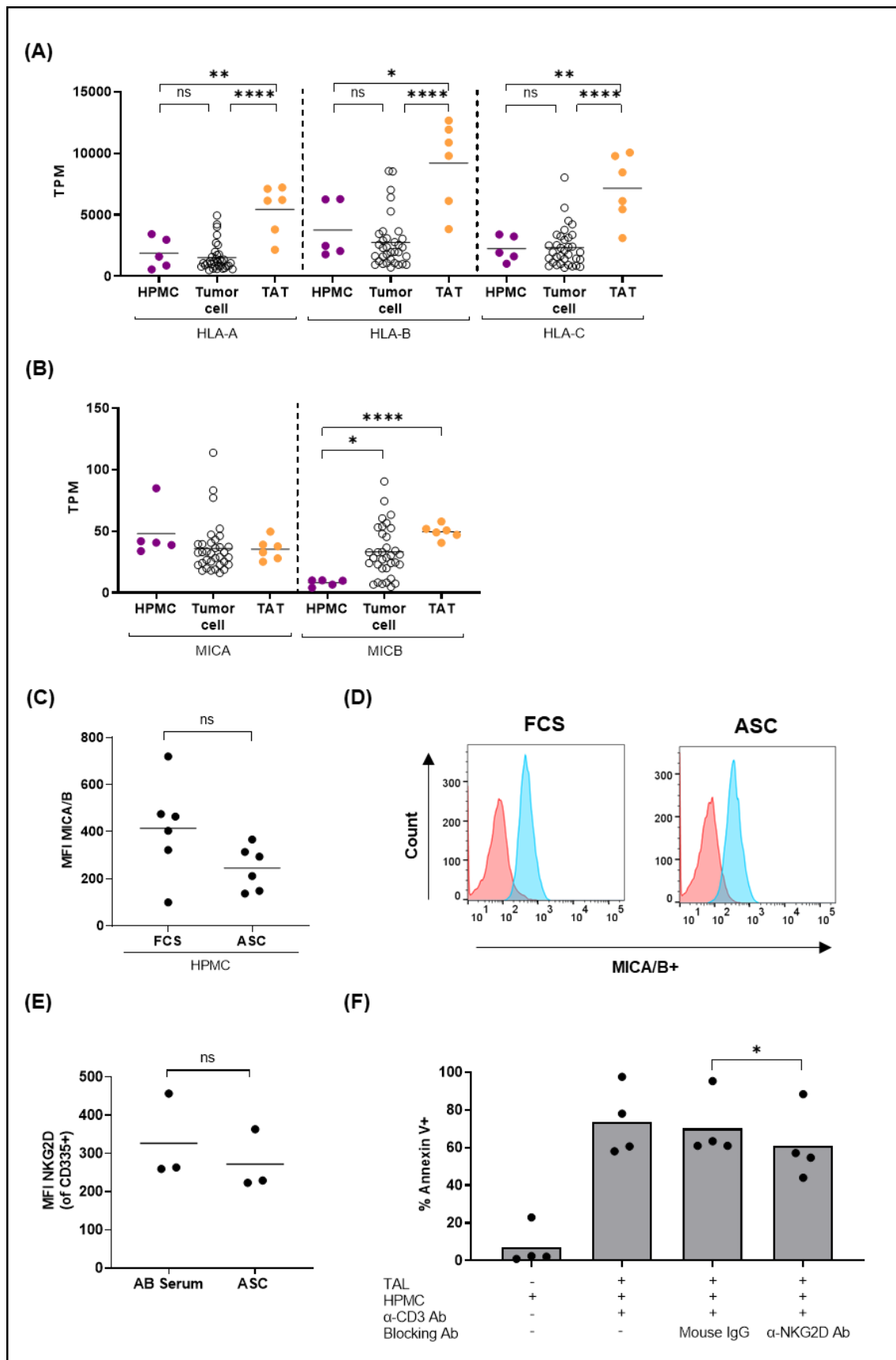


Figure 23. Low MHC I and high MICA/B expression levels on HPMC possibly further contribute to NK cell attack. (A, B) mRNA expression levels of MHC I genes (HLA-A, HLA-B

and HLA-C) (A) and MICA/B (B) in *ex vivo* omentum-derived HPMC (n=5), as well as tumor cells (n=34) and TAT (n=6) derived from ascites (RNA-sequencing Data) depicting TPM values. (C, D) MICA/B expression on protein level on HGSC-derived HPMC cultivated in OCMI/5% FCS or OCMI/50% ascites pool shown by geometric MFI determined by flow cytometry (n=6 individual experiments). Representative FACS histograms are shown (D). (E) Flow cytometric analysis of NKG2D expression levels (geometric MFI depicted) on NK cells derived from a pre-culture in RPMI/5% AB serum/1% sodium pyruvate or 100% ascites pool (n=3 biological replicates). (F) Application of an anti-NKG2D blocking antibody (TAL pre-cultured with 10 µg/ml antibody for 1 hour) to the co-culture. The percentage of Annexin V+ HPMC is depicted (n=4 individual experiments). The horizontal bars and column heights indicate the mean. p-values were determined by two-sided, unpaired (A, B) or paired (C, E, F) student's t-test: ns=non-significant with $p>0.05$, $*=p<0.05$, $**=p<0.01$, $****=p<0.0001$.

3.14 Apoptosis of the protective mesothelial barrier promotes HGSC tumor cell invasion

To prove our fundamental hypothesis that TAL-induced apoptosis of mesothelial cells leads to clearance and wounding of the protective peritoneal barrier enabling extensive tumor spreading into the submesothelial ECM, we established a three-dimensional *in vitro* trans-mesothelial invasion assay. In a first step, we analyzed a direct contribution of TRAIL-mediated killing of HPMC by applying rh-TRAIL. As visualized in figure 24A, this led to an extensive disruption of the HPMC monolayer on the collagen I gel compared to the untreated HPMC demonstrated by light microscopic pictures and fluorescence microscopy of the CT-orange stained HPMC. Big holes exposing the collagen I gel were introduced by TRAIL-mediated apoptosis of the HPMC, which was in agreement with our previous findings (section 3.6).

As depicted in figure 24B and C, invasion of the primary HGSC tumor cell line OC_58 towards an FCS-chemoattractant was indeed strongly increased upon disruption of the HPMC monolayer by rh-TRAIL treatment. This was validated by quantification of n=6 experiments of OC_58 tumor invasion. As expected, the background invasion without FCS chemoattractant was significantly lower compared to the corresponding approach with FCS chemoattractant. These results could be confirmed by applying a second HGSC primary tumor cell line (patient OC_37), as demonstrated in figure 24D. Of note, this HGSC cell line seemed much more invasive than the OC_58 cell line, seeing as the background

invasion through the HPMC monolayer pre-treated with rh-TRAIL already yielded increased tumor cell invasion without a chemoattractant.

To provide evidence that TRAIL-mediated killing of HPMC by ascites-derived TAL promote tumor invasion, HPMC monolayer, built on collagen I-coated transwell inserts, were pre-treated with TAL with or without anti-CD3 antibody stimulation prior to tumor cell invasion. Substantial clearance of the HPMC monolayer was conducted by the anti-CD3 antibody-stimulated TAL, which was not the case for the unstimulated TAL (figure 24E). These findings are in accordance with our previous results, where in particular anti-CD3 antibody-stimulated TAL promoted HPMC apoptosis (figure 11). By contrast, a strong promotion of tumor cell invasion was observed upon co-cultivation of the HPMC monolayer with anti-CD3 antibody-stimulated TAL (figure 24F). This could be demonstrated for primary tumor cell lines of two different patients (invaded OC_58 are depicted as blue dots, pink squares represent invaded OC_37, figure 24F). Due to the high variances caused by applying primary patient material, the increased invasion through the injured mesothelial layer did not reach statistical significance compared to the intact HPMC monolayer. Nevertheless, by applying primary patient material for all functional experiments and analysis, as was the case throughout this work, the advantage is that inter-patient variations are included *in vitro* and can be considered when drawing conclusions.

To sum up, the effects observed indicate that excessive tumor cell invasion is favored by selective TRAIL-dependent killing of HPMC introduced by T cell-activated NK cells in the unique TME of ovarian carcinoma.

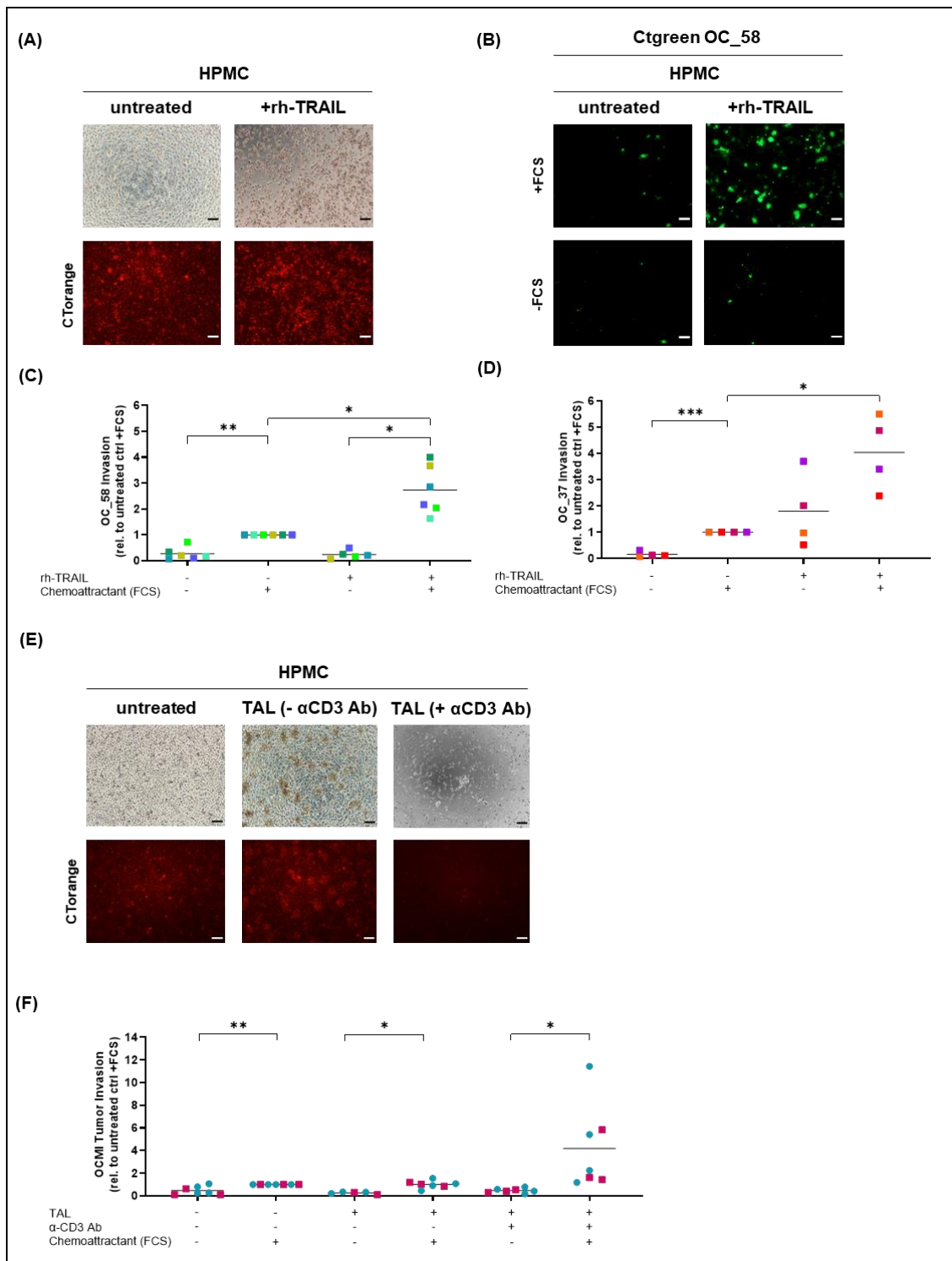


Figure 24. Clearance of the mesothelial barrier favors extensive tumor cell invasion. (A) Visualization of TRAIL-mediated HPMC clearance: Light and fluorescence microscopic pictures of CT-orange stained HPMC monolayer with or without rh-TRAIL treatment for 18 hours. (B) Fluorescence pictures visualizing OC_58 tumor cell (CT-green stained) invasion (2 hours) after treatment of the HPMC monolayer with rh-TRAIL (100 ng/ml) for 18 hours, with or without FCS chemoattractant. (C, D) Quantification of OC_58 (C) and OC_37 (D) tumor cell invasion in response to rh-TRAIL treatment of the HPMC monolayer and FCS chemoattractant. The mean of

6 visual fields per Insert was calculated for each preparation. The invasion is depicted relative to the untreated control with FCS chemoattractant. (E) Microscopic pictures representing the destroyed HPMC monolayer upon co-cultivation with anti-CD3 antibody-activated TAL under the light microscope and fluorescence microscope detecting the CT-orange stained HPMC. (F) Quantification of invaded OC_58 (blue dots) and OC_37 (pink squares) tumor cells relative to the untreated control with FCS chemoattractant. The horizontal bars indicate the mean. p-values were determined by two-sided, paired student's t-test: *= $p < 0.05$, **= $p < 0.01$, ***= $p < 0.001$.

3.15 In the clinical context: Immunohistological identification of apoptotic mesothelial cells *in vivo*

In order to determine whether our novel findings were of clinical relevance, matched omentum and ascites samples from $n=8$ HGSC patients were immunohistologically analyzed. One of these analyzed clinical omentum specimen was of high interest since it showed an early micrometastatic area, where, according to our hypothesis, NK cell-mediated apoptosis induction of HPMC could have taken place.

In figure 25, slides of paraffin-embedded omentum tissue samples derived from this particular patient (OC_67 patient) are visualized by general HE staining (A). Importantly, via caspase-3 staining (B), a lot of apoptotic cells could be detected located in stromal regions (asterisks), which were not of mesothelial origin since calretinin staining (C) did not detect any cells. By contrast, further evaluation of this specimen revealed the total absence of an intact mesothelial lining in close proximity to micrometastasis, the latter identified by cytokeratin (CKMNF 116) staining (D). Via alpha-smooth muscle actin (α -SMA) staining, the apoptotic caspase 3+ cells were detected as fibroblasts surrounding the micrometastasis, which indicates that apoptosis induction is probably not limited to the mesothelial cells and that these possibly also transdifferentiate into cancer-associated fibroblasts (CAF). In conclusion, these results demonstrate that the protective mesothelial barrier was completely lost at the site of the early micrometastasis, explaining why the detection of apoptotic mesothelial cells was not possible in tissue samples. Due to issues concerning the timing and process of apoptosis, it is difficult to catch the right moment for identifying apoptotic mesothelial cells in the omental tissue context before they are desquamated.

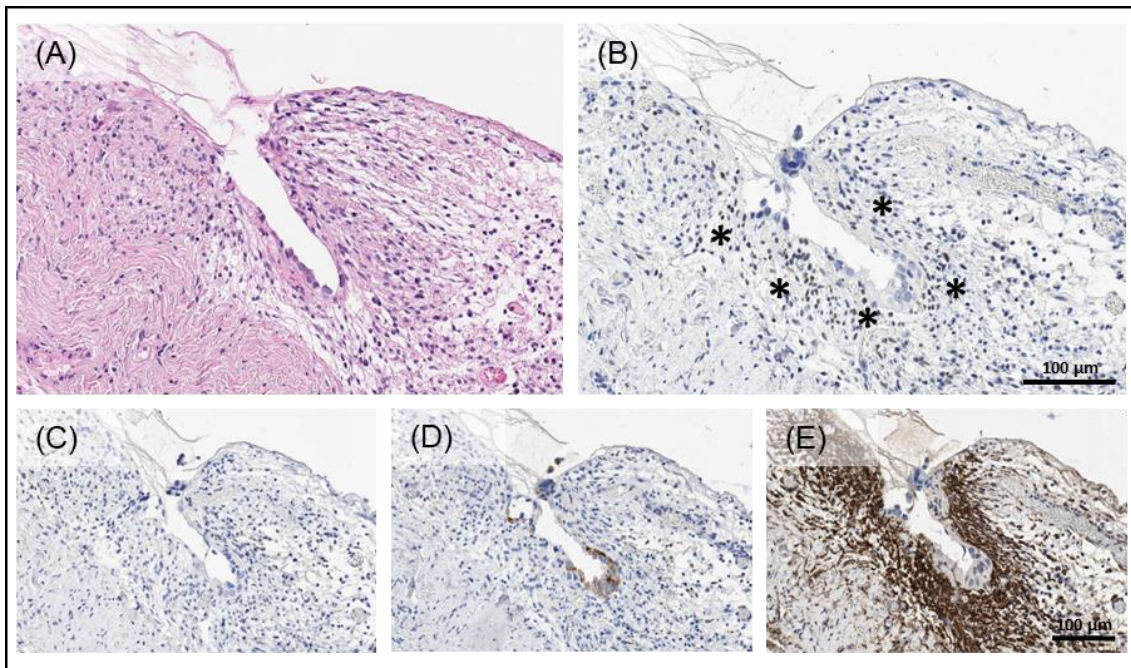


Figure 25. Immunohistological analysis of HGSC specimen: mesothelium is lost in regions of omental micrometastasis. Metastatic omentum tissue derived from a HGSC patient (OC_67) during operation was embedded in paraffin. Sections were subject to HE staining (A), caspase 3 staining for detection of apoptotic cells indicated by asterisks (B), calretinin staining to detect mesothelial cells, which were not present here (C), CKMNF 116 to mark tumor cells depicting the micrometastasis (D) and α SMA detecting apoptotic fibroblasts (E). Scale bars indicate 100 μ m.

Thus, we postulated that apoptotic mesothelial cells could have been shedded into the ascites fluid. Therefore, immunohistological analysis of ascites-derived peritoneal cells of the same patient (OC_67) was performed in the following, as depicted in figure 26. Interestingly, upon caspase 3 (F, H, J) and calretinin (G, I, K) staining, as well as close observation of the typical mesothelial morphology, we were able to verify the presence of apoptotic mesothelial cells in the ascites. These caspase 3+ mesothelial cells were present as single cells (figure 26 F and G) or within cell aggregates (figure 26 H-K). Finally, these striking findings support our concept that the induction of mesothelial apoptosis followed by a disruption of the protective peritoneal barrier may be of great importance in enabling early metastatic spread.

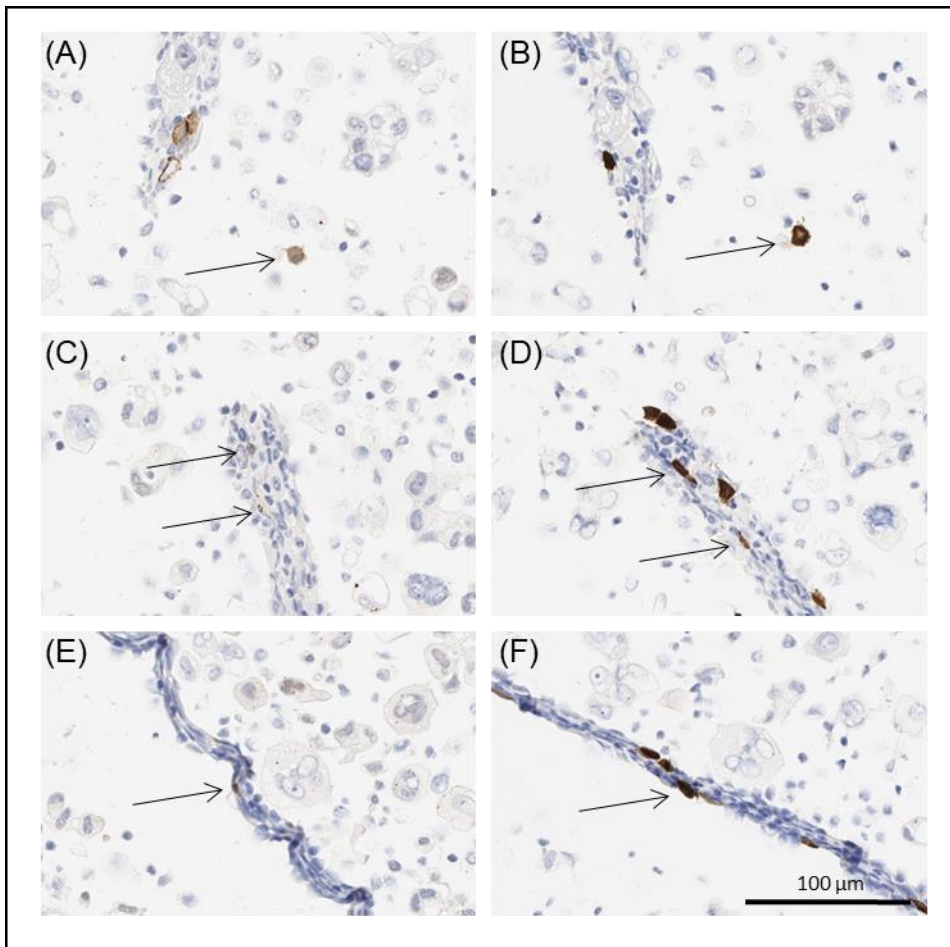


Figure 26. Detached floating apoptotic mesothelial cells are found in the ascites. Peritoneal cells in the ascites of the same (OC_67) HGSC patient were embedded in agarose and paraffin blocks. Sections were stained for caspase 3 (A, C, E) and calretinin (B, D, F) to detect apoptotic mesothelial cells indicated by arrows, showing the typical mesothelial morphology (A, B).

4. Discussion

4.1 HPMC lose their protective function in the HGSC TME

Intraperitoneal dissemination, particularly to the omentum, favored by tumor exfoliation into the largely accumulated ascites fluid, is an important hallmark of HGSC. Upon initiation, metastatic outspread within the peritoneum is strongly promoted in a feed-forward fashion causing poor prognosis (reviewed in Sodek et al. 2012). While the hematological metastatic route is quite strenuous for the tumor cells since it involves the penetration of multiple barriers and tumor outgrowth in an unfavorable surrounding, peritoneal dissemination is strikingly more effective. Here, effortless locoregional spread following interstitial transport by peritoneal fluid circulation is possible (reviewed in Sodek et al. 2012; Finger and Giaccia 2010; Lu et al. 2010). To avoid anoikis and lymphatic eviction, the tumor cells form spheroids and subsequently attach and overcome the non-adhesive protective peritoneal mesothelial barrier (reviewed in Dhaliwal and Shepherd 2022; Li, Junliang and Guo, Tiankang 2022). We and others (Kenny et al. 2007) have demonstrated this protective function of the intact mesothelial monolayer inhibiting invasion of HGSC cells into the sub-mesothelial ECM *in vitro* (figure 24 B, C, D and F). However, in the context of the TME, the protective mesothelial barrier is disrupted and re-educated into enabling tumor cell invasion (reviewed in Zheng et al. 2022). To this date, the exact underlying mechanism leading to mesothelial clearance in the HGSC TME is poorly understood. A number of aspects concerning the interaction between tumor and host cells in the TME to overcome the mesothelium have been described (figure 27):

- I. Mesothelial-mesenchymal transition (MMT) into myofibroblasts induced by soluble factors present in the malignant ascites, as well as secreted by immune cells and tumor cells, leads to architectural reorganization introducing gaps exposing the ECM and enabling tumor attachment (Sandoval et al. 2013; Mutsaers et al. 2015; Zheng et al. 2022)
- II. Age-related mesothelial senescence stimulating ovarian cancer proliferation, migration and invasion by direct physical contact, as well as secreted mediators (Mikuła-Pietrasik et al. 2016)

- III. Activation of myosin and traction forces exerted by tumor spheroids in an integrin and talin-dependent manner (Iwanicki et al. 2011; Kenny et al. 2011)
- IV. Introduction of mesothelial apoptosis by tumor cells in a Fas/FasL dependent manner (Heath et al. 2004)

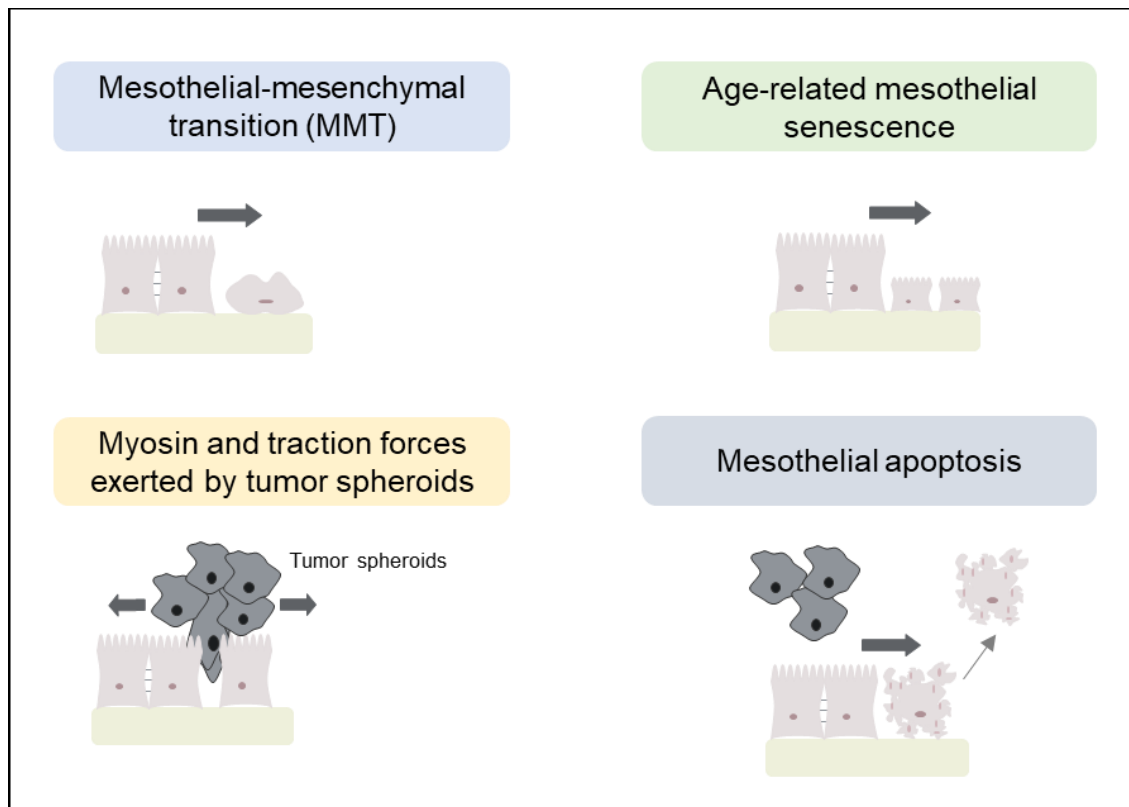


Figure 27. Schematic illustration of mechanisms leading to mesothelial rearrangement or clearance promoting tumor invasion. Mesothelial rearrangement occurs via MMT and senescence. Furthermore, tumor cells can overcome the protective barrier by exerting myosin and traction forces or inducing mesothelial apoptosis.

Importantly, introduced mesothelial lesions have been reported at metastatic sites in experimental settings *in vitro* (Niedbala et al. 1985), as well as *in vivo* by immunohistological analysis of HGSC metastasized omentum tissue (Kenny et al. 2011). We were able to confirm these findings by performing histological examination of HGSC omental and matched ascites specimens. Our findings revealed the loss of the omental mesothelium in close proximity to early metastatic lesions, indicating clinical relevance (Figure 25C, D). Since the mesothelium plays a pivotal role in the TME contributing to tumor metastatic outspread (reviewed in Zheng et al. 2022), we aimed at revealing further insights

into the dissemination process of HGCS defeating the protective peritoneal barrier.

4.2 Mechanisms of HPMC vulnerability introduced by lymphocyte-mediated apoptosis

Throughout this work, we could demonstrate that ascites-derived NK cells, in concert with T cells, are able to induce apoptosis in mesothelial cells isolated from the HGSC TME. This was linked to enhanced tumor invasion *in vitro*. Importantly, we are the first to assign this role of promoting tumorigenesis by selectively introducing mesothelial apoptosis, thereby clearing the protective barrier and exposing the sub-mesothelial ECM, to the TAL present within the metastatic TME. The clinical relevance of our findings was emphasized by the presence of detached, floating apoptotic mesothelial cells in the ascites of the patient with desquamated mesothelium near early omental metastasis (figure 25C, D and figure 26). These findings raised the question which mode of NK cell-mediated HPMC killing is active in the HGSC TME. As described in section 1.8.1-1.8.3, NK cells exert their cytotoxicity by release of cytolytic granules containing GrB and Perforin, secretion of cytotoxic cytokines such as TNF α and IFN γ or death receptor-mediated by FasL and TRAIL engagement with receptor counterparts on target cells, which has been analyzed throughout this work (reviewed in Prager and Watzl 2019; Castro et al. 2018; Sedger and McDermott 2014; Jorgovanovic et al. 2020).

4.2.1 Ineffective NK cell cytotoxicity in the TME: Fas/FasL and cytokine-independent HPMC killing

Heath et al. 2004 previously demonstrated that the induction of mesothelial apoptosis is promoted by gastrointestinal tumor cells via the Fas/FasL signaling pathway. Here, HPMC constitutively expressed the Fas receptor and were sensitive towards FasL-induced apoptosis (Heath et al. 2004). Moreover, mesothelial clearance due to Fas/FasL-mediated apoptosis has also been described during acute peritonitis after long-term peritoneal dialysis, probably due to the inflammation process. This was associated with a strong increase in infiltrating leukocytes over time. However, this study could not prove a direct causal relationship of cytolytically active leukocytes (Catalan et al. 2003; Chen et al. 2003). In a gastrointestinal tumor-induced ascites mouse model, it could be

shown that gastric dysfunction was induced by infiltrating T cells promoting Fas/FasL-dependent apoptosis in intestinal cells of cajal (Wang et al. 2018). Nonetheless, we demonstrated that the TAL-induced mesothelial apoptosis was Fas/FasL independent, despite the fact that HGSC-derived HPMC strongly expressed FasR (CD95) and TAL-subsets, including NK cells, expressed FasL (CD178) (figure 14A and D). As a possible explanation, we found that the HPMC were far less sensitive towards apoptosis induction by a crosslinked sFasL compared to the Jurkat cell line (figure 14B), known to be susceptible to FasL apoptosis (Dhein et al. 1995). Interestingly, Fas/FasL susceptibility of mesothelial cells was lost upon malignant transformation into mesothelioma, which under non-malignant conditions plays an important role in mesothelial homeostasis (Rippo et al. 2004). Even though the HGSC omentum-derived HPMC we used were non-malignant, they had been exposed to malignant ascites *in vivo* and *in vitro*, promoting changes in their cellular architecture and functionality (Mikula-Pietrasik et al. 2017), possibly reducing normal homeostasis by making them less sensitive towards FasL. However, it remains possible that HPMC derived from a benign background are more sensitive to Fas/FasL-mediated killing. This was not further investigated in the present study.

It is known that activated NK cells secrete pro-inflammatory cytokines and chemokines, including TNF α and IFN γ , promoting the activation of the innate and adaptive immune system, such as dendritic cell maturation followed by T cell activation (reviewed in Vivier et al. 2011; Vitale et al. 2005) or exhibit cytotoxic effects (reviewed in Ikeda et al. 2002). It has been reported that IFN γ , together with the STAT1 signaling pathway, can induce tumor cell apoptosis by inducing the expression of intracellular caspase-1 or membrane Fas/FasL (reviewed in Ikeda et al. 2002). Recent reports demonstrated that TNF α and IFN γ synergize in killing intestinal epithelial cells in a non-canonical way, which may play an important role in autoimmune diseases (i.e. Crohn's disease). Here, the caspase-8-JAK1/2-STAT1 signaling module was required (Woznicki et al. 2021). Moreover, these lethal cytokines render HPMC sensitive towards Fas/FasL mediated apoptosis by up-regulating Fas, introduced during inflammation processes (Chen et al. 2003; Catalan et al. 2003). We therefore analyzed the relevance of these cytokines in our system. After treatment of HPMC with rh-

TNF α and rh-IFN γ alone or in combination, apoptosis induction was analyzed, identifying that these cytokines themselves were insufficient in promoting mesothelial apoptosis (figure 15).

4.2.2 Inhibitory effects of ascites on NK cell cytotoxicity

In the presence of T cells, NK cells strongly degranulate in response to HGSC omentum-derived HPMC, indicating a GrB/Perforin apoptosis signaling (Betts et al. 2003; Alter et al. 2004). However, this was completely blocked in the presence of ascites, indicating that GrB/Perforin signaling does not play a pivotal role in our study (figure 13A). In agreement with our results, Fraser et al. 2022 also demonstrated a significant reduction of NK cell degranulation and reduced ability to kill ovarian cancer cells in the presence of ascites. This could be partly reasoned by the high CA125 levels in ascites leading to transcriptional suppression of genes involved in NK cell activation and cytotoxicity (Fraser et al. 2022). Furthermore, Vyas et al. 2017 reported a CD16 down-regulation on NK cells upon cultivation in ascites, which correlated with a decreased CD16-dependent degranulation. Based on these results, it could be postulated that ascites compounds inhibit NK cell degranulation and, by this, the GrB/Perforin signaling pathway.

4.2.3 Effective NK cell cytotoxicity in the TME: TRAIL-dependent HPMC killing

It has been reported that TRAIL apoptosis signaling does not play a role in the non-malignant inflammatory context (Catalan et al. 2003) or in tumor cell-induced mesothelial apoptosis in the malignant context (Heath et al. 2004). In contrast, we identified that HGSC-derived HPMC were susceptible towards TRAIL-induced apoptosis mediated by ascites-associated NK cells (section 3.6). This was supported by several independent observations: (i) Elevated expression levels of the cell death receptors DR4 and DR5 on HGSC-derived HPMC (figure 20A, B), (ii) increased TRAIL expression on NK cells after encounter with activated T cells (figure 17C), (iii) susceptibility of HGSC-derived HPMC to apoptosis induction by rh-TRAIL (figure 16A, B) and finally, (iv) reduced NK cell cytotoxicity against HPMC by addition of an anti-TRAIL neutralizing antibody (figure 16D). Importantly, ascites did not block TRAIL-mediated HPMC apoptosis by T cell-activated NK cells (figure 16E).

In addition to our findings, others have also demonstrated DR4 and DR5 expression in non-malignant (Catalan et al. 2003; Rippo et al. 2004), as well as malignant peritoneal mesothelial cells (Rippo et al. 2004). Moreover, we demonstrated that HPMC derived from non-malignant peritoneal lavage of patients with benign gynecological diseases were generally less sensitive towards TAL-induced apoptosis, which above all, was independent of TRAIL (figure 22). Since DR5 expression remained high in the control HPMC, TRAIL resistance was likely due to decreased DR4 expression, indicating that both death receptors are important for full TRAIL-mediated cytotoxicity (figure 20B). Thus, this indicates an ascites-induced transformation of the mesothelial characteristics regarding TRAIL sensitivity, which probably increases during cancer progression and metastasis and turns them susceptible to NK cell-mediated attack.

Notably, our results underline why the therapeutic application of soluble TRAIL or agonistic DR4/DR5 antibodies, which has been tested in the past (reviewed in Khaider et al. 2012), is not beneficial. Due to TRAIL sensitivity of some ovarian cancer cell lines, targeting TRAIL apoptosis signaling was originally considered for ovarian carcinoma treatment (Lane et al. 2004). However, one should keep in mind that upon cultivation of primary ovarian carcinoma cells, the expression pattern of multiple receptors and further proteins could change. Therefore, we applied *ex vivo* HGSC cells after an overnight resting period for all functional analyses (figure 21). Moreover, immortalized cell lines highly differ from the original primary cells they derived from, which should be considered to avoid drawing hasty conclusions. Importantly, ovarian epithelial cells and further untransformed cell types also responded to TRAIL-induced cell death (reviewed in Khaider et al. 2012) since they expressed the TRAIL death receptors, making them TRAIL-sensitive. As described above, this is also the case for the TME-derived HPMC.

4.3 Mechanisms of HPMC-NK cell crosstalk in the ovarian cancer TME

Since the balance between inhibitory and activating receptors is important for NK cell activation, we sought to elucidate which factors favor mesothelial recognition by NK cells and subsequent TRAIL-dependent killing. In general, a “non-self” reactivity of the NK cells could be excluded in an autologous system applying

matching TAL and HPMC from the same patient (see section 3.1) (reviewed in Abel et al. 2018). We found that MHC I was strongly down-regulated on mRNA level in mesothelial cells, similar to tumor cells (figure 23A), therefore an inhibitory signal for the NK cells via KIR binding was absent. Additionally, the NKG2D activating receptor was expressed on ascites-derived NK cells, seemingly unaffected by the presence of ascites (figure 23E). Our findings are in agreement with previous data of the research group, published in Vyas et al. 2017. The corresponding NKG2D-ligand MICA/B was found to be expressed on both, mesothelial and tumor cells, offering another explanation for HPMC-sensitivity to NK cell-induced killing. Generally, this also indicates a sensitivity of tumor cells towards NK cell-mediated apoptosis. It has been reported that tumor cells gain the ability to shed their MICA/B ligands by proteolysis following posttranslational modifications (reviewed in Xing and Ferrari de Andrade 2020). This is associated with increased soluble NKG2D ligands in the ascites of HGSC patients, leading to poor relapse-free survival (Vyas et al. 2017). Furthermore, Vyas et al. 2017 could show that these soluble ligands inhibited NKG2D-dependent target cell lysis. Therefore, it is feasible that the soluble NKG2D ligands block the receptor on the NK cells, leading to reduced ligand binding on target cells. This could support our hypothesis that the MICA/B – NKG2D interaction axis plays a less prominent role in contributing to HPMC recognition by NK cells since NKG2D neutralization did not show drastic effects concerning mesothelial apoptosis (figure 23F). Nevertheless, this may support TRAIL-mediated killing by shifting the balance towards NK cell-activating signaling. The involvement of further receptor-ligand interaction remains a prospect for future analysis.

4.4 HPMC themselves recruit and possibly activate leukocytes *in vivo*

HGSC patient-derived malignant ascites is rich in immune cells, including TAM, T and NK cells, which are actively attracted by HPMC (Negus et al. 1997; Worzfeld et al. 2017). Hence, mesothelial cells possibly attract their own “killers” within the metastatic TME. The HPMC also play a key role in inflammatory response upon mesothelial injury, bacterial infections or malignancies by promoting leukocyte infiltration through secretion of chemokines (i.e. MCP-1, CCL2) and cytokines (i.e. IL-1, IL-6, IL-8). Previously published transcriptome and secretome data of tumor and host cells in the HGSC TME verified the HPMC

as main providers of leukocyte-attracting cytokines, including IL-6 and CCL2 (Sommerfeld et al. 2021). Furthermore, cell surface adhesion molecules (ICAM-1, V-CAM-1) are up-regulated, enabling immune cell attachment and activation (reviewed in Sodek et al. 2012; Topley et al. 1993; Jonjić et al. 1992; Sommerfeld et al. 2021). It has been demonstrated that the omental blood flow increases under inflammatory conditions leading to an expansion of milky spots, possibly supporting immune cell recruitment (reviewed in Liu et al. 2016). Intriguingly, besides ICAM-1 (as accessory molecule), peritoneal mesothelial cells expressed MHC class II molecules upon IFN γ stimulation by which they were able to present antigens and facilitate T cell activation (Hausmann et al. 2000; Valle et al. 1995). The activated T cells in turn secreted IL-2 and IFN γ (Hausmann et al. 2000), with the potential to activate NK cells (reviewed in Wu et al. 2017).

Recently, tumor-infiltrating lymphocytes of metastasized omentum specimens have been described (Zhang et al. 2021; Gertych et al. 2022). Multi-omics analysis of several HGSC sites hereby revealed a regional heterogeneity of T cells (Yang et al. 2022). Two distinct immune patterns were identified, including the primary tumor site at ovarian lesions with low infiltration of mostly exhausted CD8 $^+$ T cells (immunosuppressive) and the metastatic omental lesions with higher infiltration of tumor unspecific T cells. Here, bystander NK-like and effector T cells were found, which were not tumor antigen-specific (Yang et al. 2022). Furthermore, increasing amounts of CD8 $^+$ T cells in the stroma, unable to reach the metastatic tumor, have been identified (Gertych et al. 2022). This might hint towards a suppression of tumor-specific responses while supporting immune cell subsets with cytolytic activity against stromal cells, which would be an important subject of future studies. While increased T cell infiltration has been described to prolong patient survival in many studies on ovarian carcinoma analyzing the primary tumors (Zhang et al. 2003; Gertych et al. 2022), we demonstrated that this may differ in the metastatic environment, promoting tumor metastatic outspread.

4.5 Pro-tumorigenic effects of ascites – specific NK cell cytotoxicity against HPMC

One of our important findings is a selective susceptibility of HGSC TME-derived HPMC against NK cell-mediated apoptosis in a TRAIL-dependent manner, while

tumor cells are resistant (figure 20A, B). This leads to inefficient tumor cell killing (figure 21), while the HPMC lining the omentum are successfully killed (figure 11A), enabling extensive tumor invasion (figure 24F). A reason for reduced DR4/DR5 death receptor expression on HGSC cells was recently elucidated by Ding et al. 2020. They reported an overexpression of the transcriptional co-regulator C-terminal binding protein -1 and -2 (CtBP1/2) binding to the promoter regions of DR4 and DR5, leading to suppressed transcription. By RNAi depletion of CtBP1/2, tumor cells were sensitized to TRAIL-mediated apoptosis, harboring prospective therapeutic options (Ding et al. 2020). Due to constitutive receptor endocytosis, a reduced DR4 and DR5 expression has also been described for breast cancer (Zhang and Zhang 2008). Furthermore, malignant ascites activates focal adhesion kinase (FAK) and Akt signaling to protect ovarian cancer cells from TRAIL-induced apoptosis (Lane et al. 2010). Additionally, by down-regulating the protease-deficient caspase-8 homolog c-Flip via RNAi in TRAIL-resistant tumor cells, the induction of cell death was significantly enhanced (Lane et al. 2004). It has been reported that ascites contains high levels of the soluble TRAIL decoy receptor OPG, which however, does not seem to be involved in tumor resistance against TRAIL-mediated apoptosis (Emery et al. 1998; Lane et al. 2012; Finkernagel et al. 2019). Further evaluation of ascites compounds on TRAIL-blocking or sensitizing effects are still pending.

Importantly, while demonstrating that ascites-derived NK cells were generally less cytotoxic without further stimulation (figure 11C) and showed significantly decreased TRAIL expression levels (figure 16F), we and others were able to evidence that they were generally functional and able to be reactivated upon stimulation (figure 11C) (Hoogstad-van Evert et al. 2018; Tonetti et al. 2021), also in the presence of ascites (figure 13B). The reactivated NK cells then direct their cytotoxicity selectively against HGSC omentum-derived mesothelial cells (see section 3.10) while being unable to kill primary tumor cells. Furthermore, ascites fluid seemed to sensitize HPMC towards TRAIL-induced apoptosis compared to FCS, as demonstrated upon treatment with rh-TRAIL (figure 16A, B). Therefore, tumor metastatic spread is promoted in *in vitro* functional experiments (figure 24F) and the tumor cells seem to escape immune response (figure 21).

4.6 Mechanisms of T-NK cell crosstalk promoting TRAIL-dependent HPMC killing

Soluble factors secreted by activated CD4⁺ and CD8⁺ T cell subfractions were sufficient to induce TRAIL up-regulation on ascites-derived NK cells (figure 17C). These findings prompted the rationale for deciphering the secretomes of activated versus inactive T cells. In our experimental setting, we mimicked T cell activation by anti-CD3 antibody stimulation, which was sufficient in triggering responsive cytokine release leading to NK cell cytotoxic activation directed against TME-derived HPMC.

Olink analysis of CD3⁺ T cell secretomes revealed the secretion of 45 proteins linked to NK cell activation and TRAIL signaling pathway upon anti-CD3 antibody stimulation, which was in agreement with previously published T cell transcriptome data (Sousa et al. 2019). Thus, we were able to confirm the secretion of IFN γ , IL-17A, TNF, IL-32, IL-2, CTLA4, PDCD1, GZMB, TNFRSF4, TNFRSF9, Fas, FasL, IL-2RA, IL-18R1, associated with NK cell activation upon anti-CD3 antibody stimulation (figure 18A) (Sousa et al. 2019). Intriguingly, TNF α , IFN γ and IL-2 could also be found in the ascites of HGSC patients, as previously demonstrated by SOMAscan analysis (Finkernagel et al. 2019). Based on these data and reports from the literature, we concentrated on the effects of TNF α , IFN γ and IL-2 on NK cell cytolytic activation (section 3.9). Interestingly, Ostensen et al. 1987 reported an increased NK cell cytolytic potential upon treatment with recombinant TNF α alone or combined with IL-2. Treatment of NK cells with rh-IL-2 on its own in gain-of-function analysis did not result in TRAIL up-regulation or increased cytotoxicity directed against HPMC (figure 19A, B). Both TNF α receptors (TNFR1 and TNFR2) were found to be expressed on NK cells (Almishri et al. 2016). TNF α has also been described to positively induce NK cell differentiation and maturation while promoting IFN γ production in the presence of IL-2 and IL-12 (Almishri et al. 2016) or IL-15 (Lee et al. 2009). At the same time, IL-2 has been described to up-regulate the TNFR2 receptor on NK cells, which is essential for the cytotoxic activation by TNF α (Mason et al. 1995). In agreement with our results, this indicates a crucial role of TNF α in NK cell activation while interacting with further cytokines to elicit the NK cells' full potential. This supports the hypothesis of a cytokine network functioning together. Importantly, we are the

first to demonstrate that T cell-secreted TNF α regulates TRAIL expression on NK cells. Upon treatment of NK cells with rh-TNF α combined with rh-IL-2, TRAIL was significantly up-regulated on their outer membrane (figure 19A). This was concomitant with TRAIL-mediated NK cell cytotoxicity directed against HPMC (figure 19B, C). In contrast, performing loss-of-function analysis by neutralizing TNF α in the activated T cell secretome during NK cell treatment, the critical role of T cell-secreted TNF α was emphasized (figure 19D). Subsequently, this led to a significant impairment of the NK cell cytolytic activity against HPMC. Besides this, only little has been reported about TRAIL-regulation in response to TNF α . Kamohara et al. 2004 demonstrated that TNF α stimulation of neutrophils induced TRAIL down-regulation, while IFN γ promoted its up-regulation. Both cytokines contributed to increased TRAIL expression in human fibroblasts. In addition, IFN γ protected uninfected fibroblasts against apoptosis by down-regulating death receptors. At the same time, IFN γ reduced survival signaling in target cells via NF κ B (Sedger et al. 1999). Therefore, IFN γ is able to sensitize target cells (i.e. virus infected) towards TRAIL apoptosis signaling (Sedger et al. 1999), which could also describe the importance of IFN γ secretion by NK cells. Since IFN γ and TNF α are present in ascites, as described above (Finkernagel et al. 2019), this could explain why HPMC cultured in ascites were more sensitive to rh-TRAIL-mediated apoptosis (figure 16B), since an IFN γ -dependent TRAIL-sensitization has also been reported for multiple cell lines (Park et al. 2004). A specific TRAIL-regulation in NK cells by T cell-secreted IFN γ has not been described so far. Interestingly, in liver NK cells, IFN γ acts as an autocrine regulator of TRAIL expression (Takeda et al. 2001), contributing to its constitutive expression (Takeda et al. 2001; Tang et al. 2016). This supports the liver's important function as an innate immune organ (reviewed in Peng et al. 2016). Furthermore, Smyth et al. 2001 demonstrated an autologous IFN γ effect upon IL12 stimulation on TRAIL-induced NK cell cytolytic activity. However, we measured only slight effects of rh-IFN γ combined with rh-IL-2 on TRAIL up-regulation and activation of NK cell cytotoxicity against mesothelial cells (figure 19A, B), indicating a subordinate role of IFN γ . Since IL-2 represents the cytokine generally released upon T cell activation by T helper and cytotoxic T cells (reviewed in Mitra and Leonard 2018), the other cytokines were combined with IL-2 for NK cell stimulation.

The effects of rh-IL-2 and rh-TNF α on NK cell cytolytic activation were potentiated by adding IL-21 (figure 19A, B). IL-21 was not part of the Olink panel, but its increased expression upon anti-CD3 antibody stimulation of T cells has been reported on a transcriptional level (Sousa et al. 2019). We confirmed the IL-21 expression on mRNA level by qPCR, which was significantly increased in activated T cells (figure 18C). Furthermore, the presence of IL-21 in ascites was identified by a cytokine bead array (Chen et al. 2015), indicating a possible role in our system. IL-21 has been described to play a key part in NK cell maturation (Parrish-Novak et al. 2000), cytotoxic activation and IFN γ production (Park et al. 2012). Moreover, Wagner et al. 2017 demonstrated the up-regulation of TRAIL on IL-15 treated NK cells after additive stimulation with IL-21, promoting an anti-rhabdomyosarcoma cytolytic NK cell potential with increased IFN γ and TNF α secretion. However, blocking T cell-secreted IL-21 alone did not influence the NK cell's lytic potential against HPMC (figure 19D). This indicates that IL-21 could be an ancillary contributor to NK cell cytolytic activation together with further cytokines (i.e. IL-2 and TNF α , as depicted in figure 19A, B, C). Based on RNA-sequencing data from our group, it was identified that IL-2, IL-21 and IFN γ are mainly delivered by ascites TAT, while TNF α is expressed by TAT, TAM and tumor cells (Sommerfeld et al. 2021). In conclusion, these data underline the relevance of these cytokines in the TME, albeit a strong CD3-dependent T cell activation was used for our experiments. Of note, we did not observe T cell exhaustion in the short-term stimulation (2 days): although we did not explicitly analyze the surface expression of inhibitory receptors, we could show that the T cells were functional in activating NK cells by secreting sufficient amounts of IL-2, TNF α , IFN γ and IL-21. Functionally impaired T cells lose their ability to secrete IL-2 at early stages, TNF α at intermediate stages and IFN γ at late stages of exhaustion (reviewed in Jiang et al. 2015; Wherry et al. 2003).

A multitude of further cytokines has been identified to induce TRAIL expression on NK cells, such as IL-15, IL-12 (reviewed in Prager and Watzl 2019; Smyth et al. 2001) and IFN α/β secreted by virally infected cells (Sato et al. 2001). Since these cytokines are not part of the ascites-derived T cell secretome, they are not important for the T-NK cell crosstalk in the HGSC TME. Further T cell-secreted cytokines and chemokines were found in the course of the Olink analysis, which

are not described to have a direct role on TRAIL-mediated apoptosis signaling by NK cells (figure 18A). We analyzed a possible effect of CD40 and CD27 on NK cell cytolytic activation by applying agonistic antibodies identifying that these interactions did not seem to be important (figure 18B).

4.7 Limitations of the study and outlook

By artificially activating the ascites-derived T cells applying an anti-CD3 antibody and imitating an activation by antigen presentation, an extensive cytokine release, comparable to the occurrence of a “cytokine storm” during *in vivo* therapy (Sousa et al. 2019; Chatenoud et al. 1990), is induced. Therefore, it is plausible that next to the secretion of key players in NK cell cytolytic activation (TNF α , IFN γ and IL-2) (section 3.9), the Olink analysis of the activated T cell secretomes additionally identified multiple cytokines not important for the crosstalk with NK cells (figure 18A). Examples of this are the secretion of CD40LG and CD70 (figure 18B), as well as GZMB (section 3.3), Fas and FasL (section 3.4). For future developments of this project, it is important to further approach how the T cells are activated *in vivo*, i.e. analyzing the involvement of APC, such as dendritic cells, or antigen-presenting functions of the mesothelial cells themselves. If the TME-derived mesothelial cells have antigen-presenting functions, it could be interesting to decipher exactly which antigens, i.e. tumor-specific or mesothelial-specific, they present. Consequently, a possible cytotoxic NK cell activation axis *in vivo* could exist: HPMC with lymphocyte recruiting- and antigen presenting-functions \rightarrow T cell activation and cytokine secretion \rightarrow cytotoxic NK cell activation \rightarrow TRAIL-dependent apoptosis of HPMC, clearing the protective barrier \rightarrow tumor progression. In this context, applying an omental mouse model could be interesting. Moreover, in the clinical context, it is important to approach further analysis concerning the presence of T cells and NK cells at early omental metastatic sites to demonstrate their relevance in tumor metastasis *in vivo*. Our so far conducted attempts at immunohistologically staining CD56+ NK cells in omental metastatic specimens failed. A reason for this could be the time point of metastasis initiation and whether omentum-resident NK cells or NK cells found in ascites are the responsible killers. To study this in more detail it could be useful to apply a multi-cellular 3D omentum model, as generated by Estermann et al. 2023, additionally including T and NK cells. Interestingly, next to the identification

of desquamated HPMC at the site of an early metastasis (figure 25), as well as apoptotic mesothelial cells in the ascites of this patient (figure 26), we found apoptotic cancer-associated fibroblasts (CAF) in the omentum surrounding the micrometastasis (figure 25B, E). This possibly indicates that next to mesothelial loss due to apoptosis, they could also have transdifferentiated into CAFs, promoting tumor implantation and progression (reviewed in Li, Junliang and Guo, Tiankang 2022; Zheng et al. 2022; Sandoval et al. 2013). Mesothelial transdifferentiation promoted by TGF β 1 present in the malignant ascites has been described by Lv et al. 2013 for gastric cancer. Furthermore, next to the induction of mesothelial apoptosis by NK cells, CAFs could also be affected. The exact reason and mechanism behind this remains elusive, bearing questions for future prospects.

In consideration of the current state-of-the-art research on ovarian carcinoma delineated in the literature and based on our findings, it has become more and more apparent that the TME of the metastatic site, differs strongly from the primary tumor, including the role of the local immune conditions, host cell compositions, extra cellular matrix dynamics (Dötzer et al. 2019; Gertych et al. 2022) and cancer cell properties (Brodsky et al. 2014). This should be considered for future research and drug developments since clinical trials on immunotherapy have so far not yielded the desired outcome (Siminiak et al. 2022). Our work has shown that HGSC cells are resistant against TRAIL-mediated NK cell attack (figure 21). Therefore, further enhancing the immune activity in line with immunotherapy could possibly increase a devastating outcome for the patients. Instead, a possible immune-suppression at the metastatic front could be necessary, for example by applying the TNF α inhibitor Infliximab to prevent/reduce NK cell cytotoxic activation by T cells. Infliximab has been tested in clinical trials for metastatic melanoma treatment in combination with immune checkpoint inhibitors to reduce immune-related adverse events concerning inflammatory diseases (reviewed in Montfort et al. 2019). Interestingly, Madhusudan and colleagues performed a clinical study demonstrating beneficial effects of the TNF α inhibitor Etanercept in recurrent ovarian cancer (Madhusudan et al. 2005). This was followed up by Charles and colleagues, showing that ovarian cancer patient treatment with Infliximab reduced IL-17 levels in plasma

concomitant with decreased tumor-promoting Th17 signaling (Charles et al. 2009). Kulbe et al. 2012 defined the “TNF network” as a crucial therapeutic target in ovarian carcinoma. Regarding the complexity of HGSC TME and the multiple ways of tumor immune escape and adaptation, further studies eliciting increased patient survival are of great importance, in which targeting TNF α could be beneficial but surely not exclusive.

Finally, the susceptibility of TME-derived HPMC towards TRAIL-mediated apoptosis by NK cells should be further proven by confirming the necessity of cell surface expressed activating death receptors, DR4 and DR5 (figure 20A, B), by applying neutralizing anti-DR4 and anti-DR5 antibodies to the co-culture of HPMC with TAL. Moreover, further insights into the HPMC-NK cell interaction concerning the expression of activating and inhibiting NK cell receptors and their counterparts on HPMC could be interesting.

4.8 Conclusion

In conclusion, we have demonstrated that T cell-secreted cytokines, with TNF α as a key player, activate the NK cell cytolytic potential selectively directed against HGSC omentum-derived mesothelial cells in a TRAIL-dependent manner. Consequently, the protective mesothelial barrier lining the omentum is disrupted, exposing the underlying ECM and enabling increased tumor cell invasion. While the HGSC patient-derived mesothelial cells express high levels of the activating death receptors DR4 and DR5, they are significantly down-regulated on tumor cells, demonstrating a line of immune evasion. The key findings of this study are summarized in figure 28. Thus, the tumor seems to utilize the functions of the immune system for its own advantage by enabling mesothelial clearance while suppressing anti-tumor immune responses and developing tumor escape mechanisms. Our findings could be contextualized with clinical data demonstrating abrogated mesothelium at metastatic omental sites with detached floating apoptotic HPMC in ascites. Moreover, our findings provide further explanation for the unbeneficial effects of TRAIL-based ovarian cancer clinical trials and rather suggest more intense research on the pro-inflammatory metastatic TME site with analysis of an immune-suppressive benefit.

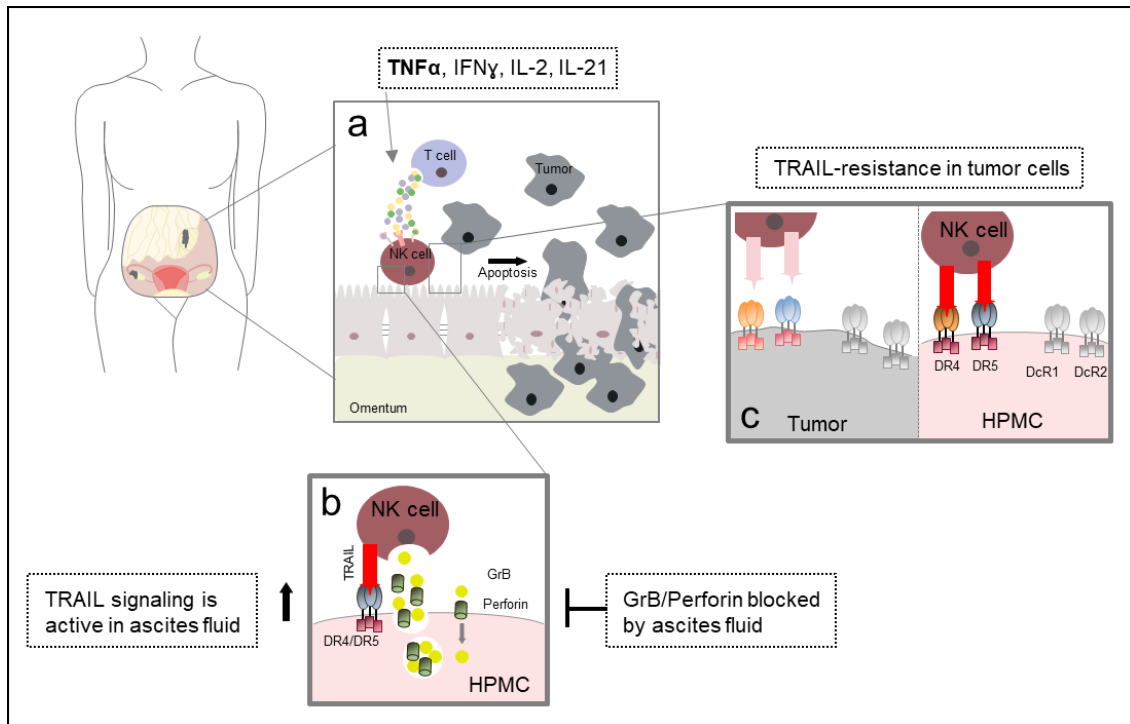


Figure 28. NK cell cytolysis induced by T cell-secreted cytokines (particularly TNF α) selectively directed against HPMC in a TRAIL-mediated fashion. (a, b, c) Schematic overview representing our findings: Upon activation of NK cells by T cell-secreted cytokines, including in particular TNF α , as well as IFN γ , IL-2 and IL-21 (a), TRAIL-mediated apoptosis is introduced selectively in death receptor expressing HPMC (a, b). NK cell degranulation, and by this, the GrB/Perforin signaling pathway, is blocked in ascites representing reduced relevance in ascites-bearing HPMC patients (b). Tumor cells do not express the death receptors and are resistant towards TRAIL-mediated apoptosis by activated NK cells favoring metastatic spread (a, c).

References

- Abel, Alex M.; Yang, Chao; Thakar, Monica S.; Malarkannan, Subramaniam (2018): Natural Killer Cells: Development, Maturation, and Clinical Utilization. In: *Frontiers in Immunology* 9, S. 1869. DOI: 10.3389/fimmu.2018.01869.
- Ai, Wenchao; Li, Haishan; Song, Naining; Li, Lei; Chen, Huiming (2013): Optimal Method to Stimulate Cytokine Production and Its Use in Immunotoxicity Assessment. In: *International Journal of Environmental Research and Public Health* (10), S. 3834–3842. DOI: 10.3390/ijerph10093834.
- Almishri, Wagdi; Santodomingo-Garzon, Tania; Le, Tyson; Stack, Danuta; Mody, Christopher H.; Swain, Mark G. (2016): TNF α Augments Cytokine-Induced NK Cell IFN γ Production through TNFR2. In: *Journal of innate immunity* 8 (6), S. 617–629. DOI: 10.1159/000448077.
- Alter, Galit; Malenfant, Jessica M.; Altfeld, Marcus (2004): CD107a as a functional marker for the identification of natural killer cell activity. In: *Journal of immunological methods* 294 (1-2), S. 15–22. DOI: 10.1016/j.jim.2004.08.008.
- Bauer, Stefan; Groh, Veronika; Wu, Jun; Steinle, Alexander; Phillips, Joseph H.; Lanier, Lewis L.; Spies, Thomas (1999): Activation of NK Cells and T Cells by NKG2D, a Receptor for Stress-Inducible MICA. In: *Science* 285, S. 727–729. DOI: 10.1126/science.285.5428.727.
- Berek, Jonathan S.; Renz, Malte; Kehoe, Sean; Kumar, Lalit; Friedlander, Michael (2021): Cancer of the ovary, fallopian tube, and peritoneum. 2021 update. In: *International journal of gynaecology and obstetrics: the official organ of the International Federation of Gynaecology and Obstetrics* 155 Suppl 1 (Suppl 1), S. 61–85. DOI: 10.1002/ijgo.13878.
- Betts, Michael R.; Brenchley, Jason M.; Price, David A.; Rosa, Stephen C. de; Douek, Daniel C.; Roederer, Mario; Koup, Richard A. (2003): Sensitive and viable identification of antigen-specific CD8 $^{+}$ T cells by a flow cytometric assay for degranulation. In: *Journal of immunological methods* 281 (1-2), S. 65–78. DOI: 10.1016/s0022-1759(03)00265-5.
- Brodsky, Alexander S.; Fischer, Andrew; Miller, Daniel H.; Vang, Souriya; MacLaughlan, Shannon; Wu, Hsin-Ta et al. (2014): Expression Profiling of Primary and Metastatic Ovarian Tumors Reveals Differences Indicative of Aggressive Disease. In: *PLOS one* 9 (4). DOI: 10.1371/journal.pone.0094476.
- Callahan, Michael J.; Crum, Christopher P.; Medeiros, Fabiola; Kindelberger, David W.; Elvin, Julia A.; Garber, Judy E. et al. (2007): Primary fallopian tube malignancies in BRCA-positive women undergoing surgery for ovarian cancer risk reduction. In: *Journal of clinical oncology : official journal of the American Society of Clinical Oncology* 25 (25), S. 3985–3990. DOI: 10.1200/JCO.2007.12.2622.
- Castro, Flávia; Cardoso, Ana Patrícia; Gonçalves, Raquel Madeira; Serre, Karine; Oliveira, Maria José (2018): Interferon-Gamma at the Crossroads of Tumor Immune Surveillance or Evasion. In: *Frontiers in Immunology* 9 (4). DOI: 10.3389/fimmu.2018.00847.

- Catalan, Marina Penélope; Subirá, Dolores; Reyero, Ana; Selgas, Rafael; Ortiz-Gonzalez, Arturo; Egido, Jesús; Ortiz, Alberto (2003): Regulation of apoptosis by lethal cytokines in human mesothelial cells. In: *Kidney international* 64 (1), S. 321–330. DOI: 10.1046/j.1523-1755.2003.00062.x.
- Charles, Kellie A.; Kulbe, Hagen; Soper, Robin; Escorcio-Correia, Monica; Lawrence, Toby; Schultheis, Anne et al. (2009): The tumor-promoting actions of TNF- α involve TNFR1 and IL-17 in ovarian cancer in mice and humans. In: *The Journal of clinical investigation* 119 (10), S. 3011–3023. DOI: 10.1172/JCI39065.
- Chatenoud, Lucienne; Ferran, Christiane; Legendre, Christophe; Thouard, Isabelle; Merite, Sylvie; Reuter, Aimée et al. (1990): In vivo cell activation following OKT3 administration. Systemic cytokine release and modulation by corticosteroids. In: *Transplantation* 49 (4), S. 697–702. DOI: 10.1097/00007890-199004000-00009.
- Chatila, T.; Silverman, L.; Miller, R.; Geha, R. (1989): Mechanisms of T cell activation by the calcium ionophore ionomycin. In: *The Journal of Immunology* 143 (4), S. 1283–1289. DOI: 10.4049/jimmunol.143.4.1283.
- Chen, Jinn-Yang; Chi, Chin-Wen; Chen, Hui-Ling; Wan, Chiung-Pei; Yang, Wu-Chang; Yang, An-Hang (2003): TNF-alpha renders human peritoneal mesothelial cells sensitive to anti-Fas antibody-induced apoptosis. In: *Nephrology Dialysis Transplantation* 18 (9), S. 1741–1747. DOI: 10.1093/ndt/gfg275.
- Chen, Yu-Li; Chou, Cheng-Yang; Chang, Ming-Cheng; Lin, Han-Wei; Huang, Ching-Ting; Hsieh, Shu-Feng et al. (2015): IL17a and IL21 combined with surgical status predict the outcome of ovarian cancer patients. In: *Endocrine-related cancer* 22 (5), S. 703–711. DOI: 10.1530/ERC-15-0145.
- Dhaliwal, Dolly; Shepherd, Trevor G. (2022): Molecular and cellular mechanisms controlling integrin-mediated cell adhesion and tumor progression in ovarian cancer metastasis: a review. In: *Clinical & Experimental Metastasis* 39, S. 291–301. DOI: 10.1007/s10585-021-10136-5.
- Dhein, Jens; Walczak, Henning; Bäumlér, Caroline; Debatin, Klaus-Michael; Krammer, Peter H. (1995): Autocrine T-cell suicide mediated by APO-1/(Fas/CD95). In: *Letters to Nature* (373), S. 438–441. DOI: 10.1038/373438a0.
- Ding, Boxiao; Yuan, Fang; Damle, Priyadarshan K.; Litovchick, Larisa; Drapkin, Ronny; Grossman, Steven R. (2020): CtBP determines ovarian cancer cell fate through repression of death receptors. In: *Cell death & disease* 286 (11). DOI: 10.1038/s41419-020-2455-7.
- Dötzer, Katharina; Schlüter, Friederike; Schoenberg, Markus Bo; Bazhin, Alexandr V.; Edler von Koch, Franz; Schnelzer, Andreas et al. (2019): Immune Heterogeneity Between Primary Tumors and Corresponding Metastatic Lesions and Response to Platinum Therapy in Primary Ovarian Cancer. In: *Cancers* 11 (9). DOI: 10.3390/cancers11091250.
- Emery, J. G.; McDonnell, P.; Burke, M. B.; Deen, K. C.; Lyn, S.; Silverman, C. et al. (1998): Osteoprotegerin is a receptor for the cytotoxic ligand TRAIL. In: *The*

Journal of biological chemistry 273 (23), S. 14363–14367. DOI: 10.1074/jbc.273.23.14363.

Estermann, Manuela; Coelho, Ricardo; Jacob, Francis; Huang, Yen-Lin; Liang, Ching-Yeu; Faia-Torres, Ana Bela et al. (2023): A 3D multi-cellular tissue model of the human omentum to study the formation of ovarian cancer metastasis. In: *Biomaterials* 294, S. 121996. DOI: 10.1016/j.biomaterials.2023.121996.

Fidler, Isaiah J. (2003): The pathogenesis of cancer metastasis: the 'seed and soil' hypothesis revisited. In: *Nature reviews. Cancer* 3 (6), S. 453–458. DOI: 10.1038/nrc1098.

Finger, Elizabeth C.; Giaccia, Amato J. (2010): Hypoxia, inflammation, and the tumor microenvironment in metastatic disease. In: *Cancer metastasis reviews* 29 (2), S. 285–293. DOI: 10.1007/s10555-010-9224-5.

Finkernagel, Florian; Reinartz, Silke; Lieber, Sonja; Adhikary, Till; Wortmann, Annika; Hoffmann, Nathalie et al. (2016): The transcriptional signature of human ovarian carcinoma macrophages is associated with extracellular matrix reorganization. In: *Oncotarget* 7 (46), S. 75339–75352. DOI: 10.18632/oncotarget.12180.

Finkernagel, Florian; Reinartz, Silke; Schuldner, Maximiliane; Malz, Alexandra; Jansen, Julia M.; Wagner, Uwe et al. (2019): Dual-platform affinity proteomics identifies links between the recurrence of ovarian carcinoma and proteins released into the tumor microenvironment. In: *Theranostics* 9 (22), S. 6601–6617. DOI: 10.7150/thno.37549.

Ford, Caroline Elizabeth; Werner, Bonnita; Hacker, Neville Frederick; Warton, Kristina (2020): The untapped potential of ascites in ovarian cancer research and treatment. In: *The British Journal of Cancer* 123, S. 9–16. DOI: 10.1038/s41416-020-0875-x.

Fraser, Christopher C.; Jia, Bin; Hu, Guangan; Al Johani, Lojain Ibrahim; Fritz-Klaus, Roberta; Ham, James Dongjoo et al. (2022): Ovarian Cancer Ascites Inhibits Transcriptional Activation of NK Cells Partly through CA125. In: *Journal of immunology (Baltimore, Md. : 1950)* 208 (9), S. 2227–2238. DOI: 10.4049/jimmunol.2001095.

Fucikova, Jitka; an Coosemans; Orsulic, Sandra; Cibula, David; Vergote, Ignace; Galluzzi, Lorenzo; Spisek, Radek (2021): Immunological configuration of ovarian carcinoma: features and impact on disease outcome. In: *Journal for immunotherapy of cancer* 9 (10). DOI: 10.1136/jitc-2021-002873.

Gao, Qinglei; Yang, Zongyuan; Xu, Sen; Li, Xiaoting; Yang, Xin; Jin, Ping et al. (2019): Heterotypic CAF-tumor spheroids promote early peritoneal metastasis of ovarian cancer. In: *The Journal of Experimental Medicine* 216 (3), S. 688–703. DOI: 10.1084/jem.20180765.

Gao, Yi; Yang, Jianjian; Cai, Yixin; Fu, Shengling; Zhang, Ni; Fu, Xiangning; Li, Lequn (2018): IFN- γ -mediated inhibition of lung cancer correlates with PD-L1 expression and is regulated by PI3K-AKT signaling. In: *International journal of cancer* 143 (4), S. 931–943. DOI: 10.1002/ijc.31357.

- Gertych, Arkadiusz; Walts, Ann E.; Cheng, Keyi; Liu, Manyun; John, Joshi; Lester, Jenny et al. (2022): Dynamic Changes in the Extracellular Matrix in Primary, Metastatic, and Recurrent Ovarian Cancers. In: *Cells* 11 (23). DOI: 10.3390/cells11233769.
- Giuntoli, Robert L.; Webb, Tonya J.; Zoso, Alessia; Rogers, Ophelia; Diaz-Montes, Teresa P.; Bristow, Robert E.; Oelke, Mathias (2009): Ovarian cancer-associated ascites demonstrates altered immune environment: implications for antitumor immunity. In: *Anticancer Research* 29 (8), S. 2875–2884.
- Golubovskaya, Vita; Wu, Lijun (2016): Different Subsets of T Cells, Memory, Effector Functions, and CAR-T Immunotherapy. In: *Cancers* 8 (3). DOI: 10.3390/cancers8030036.
- Guescini, Michele; Sisti, Davide; Rocchi, Marco B. L.; Stocchi, Laura; Stocchi, Vilberto (2008): A new real-time PCR method to overcome significant quantitative inaccuracy due to slight amplification inhibition. In: *BMC Bioinformatics* 9. DOI: 10.1186/1471-2105-9-326.
- Hamann, D.; Baars, P. A.; Rep, M. H.; Hooibrink, B.; Kerkhof-Garde, S. R.; Klein, M. R.; van Lier, R. A. (1997): Phenotypic and functional separation of memory and effector human CD8+ T cells. In: *The Journal of Experimental Medicine* 186 (9), S. 1407–1418. DOI: 10.1084/jem.186.9.1407.
- Haslehurst, Alexandria M.; Koti, Madhuri; Dharsee, Moyez; Nuin, Paulo; Evans, Ken; Geraci, Joseph et al. (2012): EMT transcription factors snail and slug directly contribute to cisplatin resistance in ovarian cancer. In: *BMC cancer* 12, S. 91. DOI: 10.1186/1471-2407-12-91.
- Hausmann, M. J.; Rogachev, B.; Weiler, M.; Chaimovitz, C.; Douvdevani, A. (2000): Accessory role of human peritoneal mesothelial cells in antigen presentation and T-cell growth. In: *Kidney international* 57 (2), S. 476–486. DOI: 10.1046/j.1523-1755.2000.00867.x.
- Heath, R. M.; Jayne, D. G.; O'Leary, R.; Morrison, E. E.; Guillou, P. J. (2004): Tumour-induced apoptosis in human mesothelial cells: a mechanism of peritoneal invasion by Fas Ligand/Fas interaction. In: *British journal of cancer* 90 (7), S. 1437–1442. DOI: 10.1038/sj.bjc.6601635.
- Hoogstad-van Evert, Janneke S.; Maas, Ralph J.; van der Meer, Jolien; Cany, Jeannette; van der Steen, Sophieke; Jansen, Joop H. et al. (2018): Peritoneal NK cells are responsive to IL-15 and percentages are correlated with outcome in advanced ovarian cancer patients. In: *Oncotarget* 9 (78), S. 34810–34820. DOI: 10.18632/oncotarget.26199.
- Horiuchi, Takahiko; Mitoma, Hiroki; Harashima, Shin-ichi; Tsukamoto, Hiroshi; Shimoda, Terufumi (2010): Transmembrane TNF-alpha. Structure, function and interaction with anti-TNF agents. In: *Rheumatology (Oxford, England)* 49 (7), S. 1215–1228. DOI: 10.1093/rheumatology/keq031.
- Huang, Junjie; Chan, Wing Chung; Ngai, Chun Ho; Lok, Veeleah; Zhang, Lin; Lucero-Prisno III, Don Eliseo et al. (2022): Worldwide Burden, Risk Factors, and

- Temporal Trends of Ovarian Cancer: A Global Study. In: *Cancers* 9. DOI: 10.3390/cancers14092230.
- Ikeda, Hiroaki; Old, Lloyd J.; Schreiber, Robert D. (2002): The roles of IFN gamma in protection against tumor development and cancer immunoediting. In: *Cytokine & growth factor reviews* 13 (2), S. 95–109. DOI: 10.1016/s1359-6101(01)00038-7.
- Ince, Tan A.; Sousa, Aurea D.; Jones, Michelle A.; Harrell, J. Chuck; Agoston, Elin S.; Krohn, Marit et al. (2015): Characterization of twenty-five ovarian tumour cell lines that phenocopy primary tumours. In: *Nature communications* 6, S. 7419. DOI: 10.1038/ncomms8419.
- Iwanicki, Marcin P.; Davidowitz, Rachel A.; Ng, Mei Rosa; Besser, Achim; Muranen, Taru; Merritt, Melissa et al. (2011): Ovarian cancer spheroids use myosin-generated force to clear the mesothelium. In: *Cancer discovery* 1 (2), S. 144–157. DOI: 10.1158/2159-8274.CD-11-0010.
- Jiang, Y.; Li, Y.; Zhu, B. (2015): T-cell exhaustion in the tumor microenvironment. In: *Cell death & disease* 6 (6), e1792. DOI: 10.1038/cddis.2015.162.
- Johnsen, Ann-Charlotte; Haux, Johan; Steinkjer, Bjørg; Nonstad, Unni; Egeberg, Kjartan; Sundan, Anders et al. (1999): Regulation of APO-2 Ligand/TRAIL expression in NK cells-involvement in NK cell-mediated cytotoxicity. In: *Cytokine* (11), S. 664–672. DOI: 10.1006/cyto.1999.0489.
- Jonjić, Nives; Peri, Giuseppe; Bernasconi, Sergio; Sciacca, Francesca Luisa; Colotta, Francesco; Pelicci, Pier Guisepe et al. (1992): Expression of Adhesion Molecules and Chemotactic Cytokines in Cultured Human Mesothelial Cells. In: *Journal of Experimental Medicine* 176 (4), S. 1165–1174. DOI: 10.1084/jem.176.4.1165.
- Jorgovanovic, Dragica; Song, Mengjia; Wang, Liping; Zhang, Yi (2020): Roles of IFN- γ in tumor progression and regression: a review. In: *Biomarker research* 8, S. 49. DOI: 10.1186/s40364-020-00228-x.
- Kamohara, Hidenobu; Matsuyama, Wataru; Shimozato, Osamu; Abe, Koichiro; Galligan, Carole; Hashimoto, Shin-Ichi et al. (2004): Regulation of tumour necrosis factor-related apoptosis-inducing ligand (TRAIL) and TRAIL receptor expression in human neutrophils. In: *Immunology* 111 (2), S. 1186–1194. DOI: 10.1111/j.0019-2805.2003.01794.x.
- Kenny, Hilary A.; Krausz, Thomas; Yamada, Seiko D.; Lengyel, Ernst (2007): Use of a novel 3D culture model to elucidate the role of mesothelial cells, fibroblasts and extra-cellular matrices on adhesion and invasion of ovarian cancer cells to the omentum. In: *International journal of cancer* 121 (7), S. 1463–1472. DOI: 10.1002/ijc.22874.
- Kenny, Hilary A.; Nieman, Kristin M.; Mitra, Anirban K.; Lengyel, Ernst (2011): The First Line of Intra-abdominal Metastatic Attack: Breaching the Mesothelial Cell Layer. In: *Cancer discovery* 1 (2), S. 100–102. DOI: 10.1158/2159-8290.CD-11-0117.

- Khaider, Nadzeya Goncharenko; Lane, Denis; Matte, Isabelle; Rancourt, Claudine; Piché, Alain (2012): Targeted ovarian cancer treatment: the TRAILs of resistance. In: *American Journal of Cancer Research* 2 (1), S. 75–92.
- Kim, Soochi; Kim, Boyun; Song, Yong Sang (2016): Ascites modulates cancer cell behavior, contributing to tumor heterogeneity in ovarian cancer. In: *Cancer science* 107 (9), S. 1173–1178. DOI: 10.1111/cas.12987.
- Kotredes, Kevin P.; Gamero, Ana M. (2013): Interferons as inducers of apoptosis in malignant cells. In: *Journal of interferon & cytokine research : the official journal of the International Society for Interferon and Cytokine Research* 33 (4), S. 162–170. DOI: 10.1089/jir.2012.0110.
- Krishnan, Venkatesh; Tallapragada, Supreeti; Schaar, Bruce; Kamat, Kalika; Chanana, Anita M.; Zhang, Yue et al. (2020): Omental macrophages secrete chemokine ligands that promote ovarian cancer colonization of the omentum via CCR1. In: *Communications biology* 3 (1), S. 524. DOI: 10.1038/s42003-020-01246-z.
- Krockenberger, Mathias; Dombrowski, Yvonne; Weidler, Claudia; Ossadnik, Monika; Hönig, Arnd; Häusler, Sebastian et al. (2008): Macrophage migration inhibitory factor contributes to the immune escape of ovarian cancer by down-regulating NKG2D. In: *The Journal of Immunology* 180 (11), S. 7338–7348. DOI: 10.4049/jimmunol.180.11.7338.
- Ksiazek, Krzysztof; Mikula-Pietrasik, Justyna; Korybalska, Katarzyna; Dworacki, Grzegorz; Jörres, Achim; Witowski, Janusz (2009): Senescent peritoneal mesothelial cells promote ovarian cancer cell adhesion: the role of oxidative stress-induced fibronectin. In: *The American journal of pathology* 174 (4), S. 1230–1240. DOI: 10.2353/ajpath.2009.080613.
- Kulbe, Hagen; Chakravarty, Probir; Leinster, D. Andrew; Charles, Kellie A.; Kwong, Joseph; Thompson, Richard G. et al. (2012): A dynamic inflammatory cytokine network in the human ovarian cancer microenvironment. In: *Cancer research* 72 (1), S. 66–75. DOI: 10.1158/0008-5472.CAN-11-2178.
- Kumar, Brahma V.; Connors, Thomas J.; Farber, Donna L. (2018): Human T Cell Development, Localization, and Function throughout Life. In: *Immunity* 48 (2), S. 202–213. DOI: 10.1016/j.immuni.2018.01.007.
- Lane, D.; Goncharenko-Khaider, N.; Rancourt, C.; Piché, A. (2010): Ovarian cancer ascites protects from TRAIL-induced cell death through α 5 β 1 integrin-mediated focal adhesion kinase and Akt activation. In: *Oncogene* 29 (24), S. 3519–3531. DOI: 10.1038/onc.2010.107.
- Lane, Denis; Cartier, Andréanne; L'Espérance, Sylvain; Côté, Marceline; Rancourt, Claudine; Piché, Alain (2004): Differential induction of apoptosis by tumor necrosis factor-related apoptosis-inducing ligand in human ovarian carcinoma cells. In: *Gynecologic oncology* 93 (3), S. 594–604. DOI: 10.1016/j.ygyno.2004.03.029.
- Lane, Denis; Matte, Isabelle; Rancourt, Claudine; Piché, Alain (2012): Osteoprotegerin (OPG) protects ovarian cancer cells from TRAIL-induced

apoptosis but does not contribute to malignant ascites-mediated attenuation of TRAIL-induced apoptosis. In: *Journal of Ovarian Research* 34 (5). DOI: 10.1186/1757-2215-5-34.

Ledermann, J. A. (2017): Front-line therapy of advanced ovarian cancer. New approaches. In: *Annals of oncology : official journal of the European Society for Medical Oncology* 28 (suppl_8), viii46-viii50. DOI: 10.1093/annonc/mdx452.

Lee, Jiwon; Lee, Suk Hyung; Shin, Nara; Jeong, Mira; Kim, Mi Sun; Kim, Mi Jeong et al. (2009): Tumor necrosis factor-alpha enhances IL-15-induced natural killer cell differentiation. In: *Biochemical and biophysical research communications* 386 (4), S. 718–723. DOI: 10.1016/j.bbrc.2009.06.120.

Lee, WonJae; Ko, Song Yi; Mohamed, Muhaned S.; Kenny, Hilary A.; Lengyel, Ernst; Naora, Honami (2019): Neutrophils facilitate ovarian cancer premetastatic niche formation in the omentum. In: *The Journal of Experimental Medicine* 216 (1), S. 176–194. DOI: 10.1084/jem.20181170.

Lengyel, Ernst (2010): Ovarian cancer development and metastasis. In: *The American journal of pathology* 177 (3), S. 1053–1064. DOI: 10.2353/ajpath.2010.100105.

Levi, Inbar; Amsalem, Hagai; Nissan, Aviram; Darash-Yahana, Merav; Peretz, Tamar; Mandelboim, Ofer; Rachmilewitz, Jacob (2015): Characterization of tumor infiltrating Natural Killer cell subset. In: *Oncotarget* 6 (15), S. 13835–13843. DOI: 10.18632/oncotarget.3453.

Li, Junliang and Guo, Tiankang (2022): Role of Peritoneal Mesothelial Cells in the Progression of Peritoneal Metastases. In: *Cancers* 14 (12). DOI: 10.3390/cancers14122856.

Lieber, Sonja; Reinartz, Silke; Raifer, Hartmann; Finkernagel, Florian; Dreyer, Tobias; Bronger, Holger et al. (2018): Prognosis of ovarian cancer is associated with effector memory CD8+ T cell accumulation in ascites, CXCL9 levels and activation-triggered signal transduction in T cells. In: *Oncoimmunology* 7 (5), e1424672. DOI: 10.1080/2162402X.2018.1424672.

Liu, Jiuyang; Geng, Xiafei; Li, Yan (2016): Milky spots: omental functional units and hotbeds for peritoneal cancer metastasis. In: *Springer* 37 (5), S. 5715–5726. DOI: 10.1007/s13277-016-4887-3.

Lu, Ze; Wang, Jie; Wientjes, M. Guillaume; Au, Jessie L-S (2010): Intraperitoneal therapy for peritoneal cancer. In: *Future oncology (London, England)* 6 (10), S. 1625–1641. DOI: 10.2217/fon.10.100.

Luckheeram, Rishi Vishal; Zhou, Rui; Verma, Asha Devi; Xia, Bing (2012): CD4+T cells: differentiation and functions. In: *Clinical & developmental immunology* 2012, S. 925135. DOI: 10.1155/2012/925135.

Lv, Zhi-Dong; Wang, Hai-Bo; Dong, Qian; Kong, Bin; Li, Jian-guo; Yang, Zhao-Chuan et al. (2013): Mesothelial cells differentiate into fibroblast-like cells under the scirrhous gastric cancer microenvironment and promote peritoneal

carcinomatosis in vitro and in vivo. In: *Molecular and cellular biochemistry* 377 (1-2), S. 177–185. DOI: 10.1007/s11010-013-1583-0.

Madhusudan, Srinivasan; Muthuramalingam, Sethupathi R.; Braybrooke, Jeremy P.; Wilner, Susan; Kaur, Kulwinder; Han, Cheng et al. (2005): Study of etanercept, a tumor necrosis factor-alpha inhibitor, in recurrent ovarian cancer. In: *Journal of clinical oncology : official journal of the American Society of Clinical Oncology* 23 (25), S. 5950–5959. DOI: 10.1200/JCO.2005.04.127.

Mason, Anna T.; McVicar, Daniel W.; Smith, Craig A.; Young, Howard A.; Ware, Carl F.; Ortaldo, John R. (1995): Regulation of NK cells through the 80-kDa TNFR (CD120b). In: *Journal of Leukocyte Biology* 58 (2), S. 249–255. DOI: 10.1002/jlb.58.2.249.

Mei, Shuangshuang; Chen, Xing; Wang, Kai; Chen, Yuxin (2023): Tumor microenvironment in ovarian cancer peritoneal metastasis. In: *Cancer cell international* 23 (1), S. 11. DOI: 10.1186/s12935-023-02854-5.

Mikuła-Pietrasik, Justyna; Uruski, Paweł; Sosińska, Patrycja; Maksin, Konstantin; Piotrowska-Kempisty, Hanna; Kucińska, Małgorzata et al. (2016): Senescent peritoneal mesothelium creates a niche for ovarian cancer metastases. In: *Cell death & disease* 7 (12). DOI: 10.1038/cddis.2016.417.

Mikuła-Pietrasik, Justyna; Uruski, Paweł; Szubert, Sebastian; Szperek, Dariusz; Sajdak, Stefan; Tykarski, Andrzej; Książek, Krzysztof (2017): Malignant ascites determine the transmesothelial invasion of ovarian cancer cells. In: *The international journal of biochemistry & cell biology* 92, S. 6–13. DOI: 10.1016/j.biocel.2017.09.002.

Mirza, M. R.; Coleman, R. L.; González-Martín, A.; Moore, K. N.; Colombo, N.; Ray-Coquard, I.; Pignata, S. (2020): The forefront of ovarian cancer therapy. Update on PARP inhibitors. In: *Annals of oncology : official journal of the European Society for Medical Oncology* 31 (9), S. 1148–1159. DOI: 10.1016/j.annonc.2020.06.004.

Mitra, Suman; Leonard, Warren J. (2018): Biology of IL-2 and its therapeutic modulation. Mechanisms and strategies. In: *Journal of Leukocyte Biology* 103 (4), S. 643–655. DOI: 10.1002/JLB.2RI0717-278R.

Momenimovahed, Zohre; Tiznobaik, Azita; Taheri, Safoura; Salehiniya, Hamid (2019): Ovarian cancer in the world: epidemiology and risk factors. In: *International Journal of Women's Health* 11, S. 287–299. DOI: 10.2147/IJWH.S197604.

Montfort, Anne; Colacios, Céline; Levade, Thierry; Andrieu-Abadie, Nathalie; Meyer, Nicolas; Ségui, Bruno (2019): The TNF Paradox in Cancer Progression and Immunotherapy. In: *Frontiers in Immunology* 10. DOI: 10.3389/fimmu.2019.01818.

Moser, Tammy L.; Pizzo, Salvatore V.; Bafetti, Lisa M.; Fishman, David A.; Stack, M. Sharon (1996): Evidence for preferential adhesion of ovarian epithelial carcinoma cells to type I collagen mediated by the $\alpha 2\beta 1$ integrin. In: *Int. J.*

Cancer 67 (5), S. 695–701. DOI: 10.1002/(SICI)1097-0215(19960904)67:5<695::AID-IJC18>3.0.CO;2-4.

Moss, Natalie M.; Barbolina, Maria V.; Liu, Yueying; Sun, Limin; Munshi, Hidayatullah G.; Stack, M. Sharon (2009): Ovarian cancer cell detachment and multicellular aggregate formation are regulated by membrane type 1 matrix metalloproteinase: a potential role in l.p. metastatic dissemination. In: *Cancer research* 69 (17), S. 7121–7129. DOI: 10.1158/0008-5472.CAN-08-4151.

Motohara, Takeshi; Masuda, Kenta; Morotti, Matteo; Zheng, Yiyang; El-Sahhar, Salma; Chong, Kay Yi et al. (2019): An evolving story of the metastatic voyage of ovarian cancer cells: cellular and molecular orchestration of the adipose-rich metastatic microenvironment. In: *Oncogene* 38, S. 2885–2898. DOI: 10.1038/s41388-018-0637-x.

Mutsaers, Steven E.; Birnie, Kimberly; Lansley, Sally; Herrick, Sarah E.; Lim, Chuan-Bian; Prêlle, Cecilia M. (2015): Mesothelial cells in tissue repair and fibrosis. In: *Frontiers in Pharmacology* 113 (6). DOI: 10.3389/fphar.2015.00113.

Negus, Rupert P. M.; Stamp, Gordon W. H.; Hadley, Joanna; Balkwill, Frances R. (1997): Quantitative Assessment of the Leukocyte Infiltrate in Ovarian Cancer and Its Relationship to the Expression of C-C Chemokines. In: *American Journal of Pathology* 150 (5), S. 1723–1734.

Niedbala, Michael J.; Crickard, Kent; Bernacki, Ralph J. (1985): Interactions of Human Ovarian Tumor Cells with Human Mesothelial Cells Grown on Extracellular Matrix. An In Vitro Model System for Studying Tumor Cell Adhesion and Invasion. In: *Experimental Cell Research* 160 (2), S. 499–513. DOI: 10.1016/0014-4827(85)90197-1.

Nielsen, Julie S.; Sahota, Rob A.; Milne, Katy; Kost, Sara E.; Nesslinger, Nancy J.; Watson, Peter H.; Nelson, Brad H. (2012): CD20+ tumor-infiltrating lymphocytes have an atypical CD27- memory phenotype and together with CD8+ T cells promote favorable prognosis in ovarian cancer. In: *Clinical cancer research : an official journal of the American Association for Cancer Research* 18 (12), S. 3281–3292. DOI: 10.1158/1078-0432.CCR-12-0234.

Ostensen, M. E.; Thiele, D. L.; Lipsky, P. E. (1987): Tumor necrosis factor-alpha enhances cytolytic activity of human natural killer cells. In: *The Journal of Immunology* 138 (12), S. 4185–4191. DOI: 10.4049/jimmunol.138.12.4185.

Pakuła, Martyna; Witucka, Anna; Uruski, Paweł; Radziemski, Artur; Moszyński, Rafał; Szpurek, Dariusz et al. (2019): Senescence-related deterioration of intercellular junctions in the peritoneal mesothelium promotes the transmesothelial invasion of ovarian cancer cells. In: *Scientific reports* 9 (1), S. 7587. DOI: 10.1038/s41598-019-44123-4.

Park, Sang-Youel; Seol, Jae-Won; Lee, You-Jin; Cho, Jong-Hoo; Kang, Hyung-Sub; Kim, In-Shik et al. (2004): IFN-gamma enhances TRAIL-induced apoptosis through IRF-1. In: *European journal of biochemistry* 271 (21), S. 4222–4228. DOI: 10.1111/j.1432-1033.2004.04362.x.

- Park, Young-Ki; Shin, Dong-Jun; Cho, Duck; Kim, Sang-Ki; Lee, Je-Jung; Shin, Myung-Geun et al. (2012): Interleukin-21 Increases Direct Cytotoxicity and IFN- γ Production of Ex Vivo Expanded NK Cells towards Breast Cancer Cells. In: *Anticancer Research* 32 (3), S. 839–846.
- Parrish-Novak, Julia; Dillon, Stacey R.; Nelson, Andrew; Hammond, Angie; Sprecher, Cindy; Gross, Jane A. et al. (2000): Interleukin 21 and its receptor are involved in NK cell expansion and regulation of lymphocyte function. In: *Nature* 408, S. 57–63. DOI: 10.1038/35040504.
- Patankar, Manish S.; Jing, Yu; Morrison, Jamie C.; Belisle, Jennifer A.; Lattanzio, Frank A.; Deng, Yuping et al. (2005): Potent suppression of natural killer cell response mediated by the ovarian tumor marker CA125. In: *Gynecologic oncology* 99 (3), S. 704–713. DOI: 10.1016/j.ygyno.2005.07.030.
- Pearce, Oliver M. T.; Delaine-Smith, Robin M.; Maniati, Eleni; Nichols, Sam; Wang, Jun; Böhm, Steffen et al. (2018): Deconstruction of a Metastatic Tumor Microenvironment Reveals a Common Matrix Response in Human Cancers. In: *Cancer discovery* 8 (3), S. 304–319. DOI: 10.1158/2159-8290.CD-17-0284.
- Peng, Hui; Wisse, Eddie; Tian, Zhigang (2016): Liver natural killer cells. Subsets and roles in liver immunity. In: *Cellular & molecular immunology* 13 (3), S. 328–336. DOI: 10.1038/cmi.2015.96.
- Pesce, Silvia; Greppi, Marco; Tabellini, Giovanna; Rampinelli, Fabio; Parolini, Silvia; Olive, Daniel et al. (2016): Identification of a subset of human natural killer cells expressing high levels of programmed death 1: A phenotypic and functional characterization. In: *The Journal of allergy and clinical immunology* 139 (1), 335–346.e3. DOI: 10.1016/j.jaci.2016.04.025.
- Pesce, Silvia; Tabellini, Giovanna; Cantoni, Claudia; Patrizi, Ornella; Coltrini, Daniela; Rampinelli, Fabio et al. (2015): B7-H6-mediated downregulation of NKp30 in NK cells contributes to ovarian carcinoma immune escape. In: *Oncoimmunology* 4 (4), e1001224. DOI: 10.1080/2162402X.2014.1001224.
- Peter, Peter J.; Borst, Jannie; Oorschot, Viola; Fukuda, Minoru; Krähenbühl, Olivier; Tschopp, Jürg et al. (1991): Cytotoxic T Lymphocyte Granules Are Secretory Lysosomes, Containing Both Perforin and Granzymes. In: *Journal of Experimental Medicine* 173, S. 1099–1109. DOI: 10.1084/jem.173.5.1099.
- Pickup, Michael W.; Mouw, Janna K.; Weaver, Valerie M. (2014): The extracellular matrix modulates the hallmarks of cancer. In: *EMBO reports* 15 (12), S. 1243–1253. DOI: 10.15252/embr.201439246.
- Pogge von Strandmann, Elke; Reinartz, Silke; Wager, Uwe; Müller, Rolf (2017): Tumor-Host Cell Interactions in Ovarian Cancer. Pathways to Therapy Failure. In: *Trends in cancer* 3 (2), S. 137–148. DOI: 10.1016/j.trecan.2016.12.005.
- Prager, Isabel; Watzl, Carsten (2019): Mechanisms of natural killer cell-mediated cellular cytotoxicity. In: *Journal of Leukocyte Biology* 105 (6), S. 1319–1329. DOI: 10.1002/JLB.MR0718-269R.

- Qi, Qian; Liu, Yi; Cheng, Yong; Glanville, Jacob; Zhang, David; Lee, Ji-Yeun et al. (2014): Diversity and clonal selection in the human T-cell repertoire. In: *Proceedings of the National Academy of Sciences of the United States of America* 111 (36), S. 13139–13144. DOI: 10.1073/pnas.1409155111.
- Ramírez-Labrada, Ariel; Pesini, Cecilia; Santiago, Llipsis; Hidalgo, Sandra; Calvo-Pérez, Adanays; Oñate, Carmen et al. (2022): All About (NK Cell-Mediated) Death in Two Acts and an Unexpected Encore: Initiation, Execution and Activation of Adaptive Immunity. In: *Frontiers in Immunology* 13, S. 896228. DOI: 10.3389/fimmu.2022.896228.
- Rangel-Moreno, Javier; Moyron-Quiroz, Juan E.; Carragher, Damian M.; Kusser, Kim; Hartson, Louise; Moquin, Amy; Randall, Troy D. (2009): Omental milky spots develop in the absence of lymphoid tissue-inducer cells and support B and T cell responses to peritoneal antigens. In: *Immunity* 30 (5), S. 731–743. DOI: 10.1016/j.immuni.2009.03.014.
- Raskov, Hans; Orhan, Adile; Christensen, Jan Pravsgaard; Gögenur, Ismail (2021): Cytotoxic CD8+ T cells in cancer and cancer immunotherapy. In: *British journal of cancer* 124 (2), S. 359–367. DOI: 10.1038/s41416-020-01048-4.
- Reinartz, Silke; Finkernagel, Florian; Adhikary, Till; Rohnalter, Verena; Schumann, Tim; Schober, Yvonne et al. (2016): A transcriptome-based global map of signaling pathways in the ovarian cancer microenvironment associated with clinical outcome. In: *Genome Biology* 17 (1). DOI: 10.1186/s13059-016-0956-6.
- Reinartz, Silke; Lieber, Sonja; Pesek, Jelena; Brandt, Dominique T.; Asafova, Alina; Finkernagel, Florian et al. (2019): Cell type-selective pathways and clinical associations of lysophosphatidic acid biosynthesis and signaling in the ovarian cancer microenvironment. In: *Molecular oncology* 13 (2), S. 185–201. DOI: 10.1002/1878-0261.12396.
- Reinartz, Silke; Schumann, Tim; Finkernagel, Florian; Wortmann, Annika; Jansen, Julia M.; Meissner, Wolfgang et al. (2014): Mixed-polarization phenotype of ascites-associated macrophages in human ovarian carcinoma: correlation of CD163 expression, cytokine levels and early relapse. In: *International journal of cancer* 134 (1), S. 32–42. DOI: 10.1002/ijc.28335.
- Rippo, Maria Rita; Moretti, Simona; Vescovi, Silvia; Tomasetti, Marco; Orecchia, Sara; Amici, Giuseppe et al. (2004): FLIP overexpression inhibits death receptor-induced apoptosis in malignant mesothelial cells. In: *Oncogene* 23 (47), S. 7753–7760. DOI: 10.1038/sj.onc.1208051.
- Ritch, Sabrina J.; Telleria, Carlos M. (2022): The Transcoelomic Ecosystem and Epithelial Ovarian Cancer Dissemination. In: *Frontiers in Endocrinology* 13. DOI: 10.3389/fendo.2022.886533.
- Roederer, M.; Bowser, R.; Murphy, R. F. (1987): Kinetics and temperature dependence of exposure of endocytosed material to proteolytic enzymes and low pH. Evidence for a maturation model for the formation of lysosomes. In: *Journal of cellular physiology* 131 (2), S. 200–209. DOI: 10.1002/jcp.1041310209.

- Sandoval, Pilar; Jiménez-Heffernan, Jose Antonio; Rynne-Vidal, Ángela; Pérez-Lozano, María Luisa; Gilsanz, Álvaro; Ruiz-Carpio, Vicente et al. (2013): Carcinoma-associated fibroblasts derive from mesothelial cells via mesothelial-to-mesenchymal transition in peritoneal metastasis. In: *The Journal of pathology* 231 (4), S. 517–531. DOI: 10.1002/path.4281.
- Sato, Kojiro; Hida, Shigeaki; Takayanagi, Hiroshi; Yokochi, Taeko; Kayagaki, Nobuhiko; Takeda, Kazuyoshi et al. (2001): Antiviral response by natural killer cells through TRAIL gene induction by IFN- α/β . In: *Eur. J. Immunol.* 31 (11), S. 3138–3146. DOI: 10.1002/1521-4141(200111)31:11<3138::AID-IMMU3138>3.0.CO;2-B.
- Schoutrop, Esther; Moyano-Galceran, Lidia; Lheureux, Stephanie; Mattsson, Jonas; Lehti, Kaisa; Dahlstrand, Hanna; Magalhaes, Isabelle (2022): Molecular, cellular and systemic aspects of epithelial ovarian cancer and its tumor microenvironment. In: *Seminars in cancer biology* 86 (Pt 3), S. 207–223. DOI: 10.1016/j.semcancer.2022.03.027.
- Sedger, Lisa M.; McDermott, Michael F. (2014): TNF and TNF-receptors: From mediators of cell death and inflammation to therapeutic giants - past, present and future. In: *Cytokine & growth factor reviews* 25 (4), S. 453–472. DOI: 10.1016/j.cytogfr.2014.07.016.
- Sedger, Lisa M.; Shows, Donna M.; Blanton, Rebecca A.; Peschon, Jacques J.; Goodwin, Ray G.; Cosman, David; Wiley, Steven R. (1999): IFN- γ Mediates a Novel Antiviral Activity Through Dynamic Modulation of TRAIL and TRAIL Receptor Expression. In: *The Journal of Immunology* 163 (2), S. 920–926.
- Shankar, Keerthana; Capitini, Christian M.; Saha, Krishanu (2020): Genome engineering of induced pluripotent stem cells to manufacture natural killer cell therapies. In: *Stem cell research & therapy* 11 (1), S. 234. DOI: 10.1186/s13287-020-01741-4.
- Shield, Kristy; Riley, Clyde; Quinn, Michael A.; Rice, Gregory E.; Ackland, Margaret L.; Ahmed, Nuzhat (2007): Alpha2beta1 integrin affects metastatic potential of ovarian carcinoma spheroids by supporting disaggregation and proteolysis. In: *Journal of carcinogenesis* 6, S. 11. DOI: 10.1186/1477-3163-6-11.
- Siminiak, Natalia; Czepczyński, Rafał; Zaborowski, Mikołaj Piotr; Iżycki, Dariusz (2022): Immunotherapy in Ovarian Cancer. In: *Archivum Immunologiae et Therapiae Experimentalis* 70 (1), S. 19. DOI: 10.1007/s00005-022-00655-8.
- Sivori, Simona; Vacca, Paola; Del Zotto, Genny; Munari, Enrico; Mingari, Maria Cristina; Moretta, Lorenzo (2019): Human NK cells: surface receptors, inhibitory checkpoints, and translational applications. In: *Cellular & molecular immunology* 16 (5), S. 430–441. DOI: 10.1038/s41423-019-0206-4.
- Smyth, Mark J.; Cretney, Erika; Takeda, Kazuyoshi; Wiltrot, Robert H.; Sedger, Lisa M.; Kayagaki, Nobuhiko et al. (2001): Tumor Necrosis Factor-related Apoptosis-inducing Ligand (TRAIL) Contributes to Interferone γ -dependent

- Natural Killer Cell Protection from Tumor Metastasis. In: *The Journal of Experimental Medicine* 193 (6), S. 661–670. DOI: 10.1084/jem.193.6.661.
- Sodek, Katharine L.; Murphy, K. Joan; Brown, Theodore J.; Ringuette, Maurice J. (2012): Cell-cell and cell-matrix dynamics in intraperitoneal cancer metastasis. In: *Cancer metastasis reviews* 31 (1-2), S. 397–414. DOI: 10.1007/s10555-012-9351-2.
- Sommerfeld, Leah; Finkernagel, Florian; Jansen, Julia M.; Wagner, Uwe; Nist, Andrea; Stiewe, Thorsten et al. (2021): The multicellular signalling network of ovarian cancer metastases. In: *Clinical and Translational Medicine* (11). DOI: 10.1002/ctm2.633.
- Sousa, Isabel Garcia; Simi, Kelly Cristina Rodrigues; do Almo, Manuela Maragno; Bezerra, Maryani Andressa Gomes; Doose, Gero; Raiol, Tainá et al. (2019): Gene expression profile of human T cells following a single stimulation of peripheral blood mononuclear cells with anti-CD3 antibodies. In: *BMC genomics* 20 (1), S. 593. DOI: 10.1186/s12864-019-5967-8.
- Stadlmann, Sylvia; Raffener, Ruth; Amberger, Albert; Margreiter, Raimund; Zeimet, Alain Gustave; Abendstein, Burkhardt et al. (2003): Disruption of the integrity of human peritoneal mesothelium by interleukin-1beta and tumor necrosis factor-alpha. In: *Virchows Archiv : an international journal of pathology* 443 (5), S. 678–685. DOI: 10.1007/s00428-003-0867-2.
- Steitz, Anna Mary; Steffes, Alina; Finkernagel, Florian; Unger, Annika; Sommerfeld, Leah; Jansen, Julia M. et al. (2020): Tumor-associated macrophages promote ovarian cancer cell migration by secreting transforming growth factor beta induced (TGFB1) and tenascin C. In: *Cell death & disease* 11 (4), S. 249. DOI: 10.1038/s41419-020-2438-8.
- Sung, Hyuna; Ferlay, Jacques; Siegel, Rebecca L.; Laversanne, Mathieu; Soerjomataram, Isabelle; Jemal, Ahmedin; Bray, Freddie (2021): Global Cancer Statistics 2020. GLOBOCAN Estimates of Incidence and Mortality Worldwide for 36 Cancers in 185 Countries. In: *CA: a cancer journal for clinicians* 71 (3), S. 209–249. DOI: 10.3322/caac.21660.
- Takeda, Kazuyoshi; Hayakawa, Yoshihiro; Smyth, Mark J.; Kayagaki, Nobuhiko; Yamaguchi, Noriko; Kakuta, Shigeru et al. (2001): Involvement of tumor necrosis factor-related apoptosis-inducing ligand in surveillance of tumor metastasis by liver natural killer cells. In: *Nature* (7), S. 94–100. DOI: 10.1038/83416.
- Tang, Ling; Peng, Hui; Zhou, Jing; Chen, Yongyan; Wei, Haiming; Sun, Rui et al. (2016): Differential phenotypic and functional properties of liver-resident NK cells and mucosal ILC1s. In: *Journal of autoimmunity* 67, S. 29–35. DOI: 10.1016/j.jaut.2015.09.004.
- Tesone, Amelia J.; Rutkowski, Melanie R.; Brencicova, Eva; Svoronos, Nikolaos; Perales-Puchalt, Alfredo; Stephen, Tom L. et al. (2016): Satb1 Overexpression Drives Tumor-Promoting Activities in Cancer-Associated Dendritic Cells. In: *Cell reports* 14 (7), S. 1774–1786. DOI: 10.1016/j.celrep.2016.01.056.

- Tonetti, Cláudia Rodrigues; Souza-Araújo, Caroline Natânia de; Yoshida, Adriana; da Silva, Rodrigo Fernandes; Alves, Paulo César Martins; Mazzola, Taís Nitsch et al. (2021): Ovarian Cancer-Associated Ascites Have High Proportions of Cytokine-Responsive CD56bright NK Cells. In: *Cells* 10 (7). DOI: 10.3390/cells10071702.
- Topley, Nicholas; Brown, Zarin; Jörres, Achim; Westwick, John; Davies, Malcolm; Coles, Gerald A.; Williams, John D. (1993): Human Peritoneal Mesothelial Cells Synthesize Interleukin-8. Synergistic Induction by Interleukin-1beta and Tumor Necrosis Factor-alpha. In: *American Journal of Pathology* 142 (6), S. 1876–1886.
- Valle, M. T.; Degl' Innocenti, M. L.; Bertelli, R.; Facchetti, P.; Perfumo, F.; Fenoglio, D. et al. (1995): Antigen-presenting function of human peritoneal mesothelial cells. In: *Clinical & Experimental Immunology* 101 (1), S. 172–176. DOI: 10.1111/j.1365-2249.1995.tb02294.x.
- Vitale, M.; Castriconi, R.; Parolini, S.; Pende, D.; Hsu, M. L.; Moretta, L. et al. (1999): The leukocyte Ig-like receptor (LIR)-1 for the cytomegalovirus UL18 protein displays a broad specificity for different HLA class I alleles: analysis of LIR-1 + NK cell clones. In: *International immunology* 11 (1), S. 29–35. DOI: 10.1093/intimm/11.1.29.
- Vitale, Massimo; Della Chiesa, Mariella; Carlomagno, Simona; Pende, Daniela; Aricò, Maurizio; Moretta, Lorenzo; Moretta, Alessandro (2005): NK-dependent DC maturation is mediated by TNFalpha and IFNgamma released upon engagement of the NKp30 triggering receptor. In: *Blood* 106 (2), S. 566–571. DOI: 10.1182/blood-2004-10-4035.
- Vivier, Eric; Raulet, David H.; Moretta, Alessandro; Caligiuri, Michael A.; Zitvogel, Laurence; Lanier, Lewis L. et al. (2011): Innate or adaptive immunity? The example of natural killer cells. In: *Science* 331 (6013), S. 44–49. DOI: 10.1126/science.1198687.
- Vyas, Maulik; Reinartz, Silke; Hoffmann, Nathalie; Reiners, Katrin S.; Lieber, Sonja; Jansen, Julia M. et al. (2017): Soluble NKG2D ligands in the ovarian cancer microenvironment are associated with an adverse clinical outcome and decreased memory effector T cells independent of NKG2D downregulation. In: *Oncoimmunology* 6 (9). DOI: 10.1080/2162402X.2017.1339854.
- Wagner, Juliane; Pfannenstiel, Viktoria; Waldmann, Anja; Bergs, Judith W. J.; Brill, Boris; Huenecke, Sabine et al. (2017): A Two-Phase Expansion Protocol Combining Interleukin (IL)-15 and IL-21 Improves Natural Killer Cell Proliferation and Cytotoxicity against Rhabdomyosarcoma. In: *Frontiers in Immunology* 8, S. 676. DOI: 10.3389/fimmu.2017.00676.
- Wang, Xiuli; Li, Jing; Liu, Duanyang; Zhang, Lei; Zhao, Baoshan; Tang, Jing et al. (2018): Relationship between infiltrating lymphocytes in cancerous ascites and dysfunction of Cajal mesenchymal cells in the small intestine. In: *International Journal of Clinical and Experimental Pathology* 11 (4), S. 2201–2213.
- Webb, John R.; Milne, Katy; Watson, Peter; Deleeuw, Ronald J.; Nelson, Brad H. (2014): Tumor-infiltrating lymphocytes expressing the tissue resident memory

marker CD103 are associated with increased survival in high-grade serous ovarian cancer. In: *Clinical cancer research : an official journal of the American Association for Cancer Research* 20 (2), S. 434–444. DOI: 10.1158/1078-0432.CCR-13-1877.

Weidle, Ulrich H.; Birzele, Fabian; Kollmorgen, Gwendlyn; Rueger, Rüdiger (2016): Mechanisms and Targets Involved in Dissemination of Ovarian Cancer. In: *Cancer genomics & proteomics* 13 (6), S. 407–423. DOI: 10.21873/cgp.20004.

Wherry, E. John; Blattman, Joseph N.; Murali-Krishna, Kaja; van der Most, Robbert; Ahmed, Rafi (2003): Viral persistence alters CD8 T-cell immunodominance and tissue distribution and results in distinct stages of functional impairment. In: *Journal of virology* 77 (8), S. 4911–4927. DOI: 10.1128/jvi.77.8.4911-4927.2003.

Worzfeld, Thomas; Finkernagel, Florian; Reinartz, Silke; Konzer, Anne; Adhikary, Till; Nist, Andrea et al. (2018): Proteotranscriptomics Reveal Signaling Networks in the Ovarian Cancer Microenvironment. In: *Molecular & cellular proteomics : MCP* 17 (2), S. 270–289. DOI: 10.1074/mcp.RA117.000400.

Worzfeld, Thomas; Pogge von Strandmann, Elke; Huber, Magdalena; Adhikary, Till; Wagner, Uwe; Reinartz, Silke; Müller, Rolf (2017): The Unique Molecular and Cellular Microenvironment of Ovarian Cancer. In: *Frontiers in Oncology* (7). DOI: 10.3389/fonc.2017.00024.

Woznicki, Jerzy A.; Saini, Nisha; Flood, Peter; Rajaram, Subhasree; Lee, Ciaran M.; Stamou, Panagiota et al. (2021): TNF- α synergises with IFN- γ to induce caspase-8-JAK1/2-STAT1-dependent death of intestinal epithelial cells. In: *Cell death & disease* 12 (10), S. 864. DOI: 10.1038/s41419-021-04151-3.

Wu, Yang; Tian, Zhigang; Wei, Haiming (2017): Developmental and Functional Control of Natural Killer Cells by Cytokines. In: *Frontiers in Immunology* (8). DOI: 10.3389/fimmu.2017.00930.

Xing, Samantha; Ferrari de Andrade, Lucas (2020): NKG2D and MICA/B shedding. A 'tag game' between NK cells and malignant cells. In: *Clinical & translational immunology* 9 (12), e1230. DOI: 10.1002/cti2.1230.

Yang, Bin; Li, Xiong; Zhang, Wei; Fan, Junpeng; Zhou, Yong; Li, Wenting et al. (2022): Spatial heterogeneity of infiltrating T cells in high-grade serous ovarian cancer revealed by multi-omics analysis. In: *Cell Reports Medicine* 12 (3). DOI: 10.1016/j.xcrm.2022.100856.

Yin, Mingzhu; Li, Xia; Tan, Shu; Zhou, Huanjiao Jenny; Ji, Weidong; Bellone, Stefania et al. (2016): Tumor-associated macrophages drive spheroid formation during early transcoelomic metastasis of ovarian cancer. In: *The Journal of clinical investigation* 126 (11), S. 4157–4173. DOI: 10.1172/JCI87252.

Zhang, Lin; Conejo-Garcia, Jose R.; Katsaros, Dionyssios; Gimotty, Phyllis A.; Massobrio, Marco; Regnani, Giorgia et al. (2003): Intratumoral T Cells, Recurrence, and Survival in Epithelial Ovarian Cancer. In: *The New England Journal of Medicine* 348 (3), S. 203–213. DOI: 10.1056/NEJMoa020177.

Zhang, Tao; Liu, Qin; Zhu, Yingfan; Huang, Yizhou; Qin, Jiale; Wu, Xiaodong; Zhang, Songfa (2021): Lymphocyte and macrophage infiltration in omental metastases indicates poor prognosis in advance stage epithelial ovarian cancer. In: *The Journal of international medical research* 49 (12), 3000605211066245. DOI: 10.1177/03000605211066245.

Zhang, Yaqin; Zhang, Baolin (2008): TRAIL resistance of breast cancer cells is associated with constitutive endocytosis of death receptors 4 and 5. In: *Molecular cancer research : MCR* 6 (12), S. 1861–1871. DOI: 10.1158/1541-7786.MCR-08-0313.

Zheng, Aiping; Wei, Yuhao; Zhao, Yunuo; Zhang, Tao; Ma, Xuelei (2022): The role of cancer-associated mesothelial cells in the progression and therapy of ovarian cancer. In: *Frontiers in Immunology* (13). DOI: 10.3389/fimmu.2022.1013506.

Appendix

Supplementary data

Supplementary table S1. Primary ovarian carcinoma patient data and samples

Patient ID	Diagnosis	FIGO	Cell type	Application
OC_26	HGSC	IIIB	ascTU	IHC
OC_27	HGSC	IIIC	ascTU	IHC, Seq
OC_31	HGSC	IIIC	ascTAT	Seq
OC_37	HGSC	IIIC	ascTU	Inv
OC_50	HGSC	IIIC	ascTAT	Seq
OC_54	HGSC	IIIC	ascTU	IHC
OC_51	HGSC	IIIC	ascTAT	Seq
OC_58	HGSC	IIIB	ascTU	Inv
OC_65	HGSC	IIIC	ascTU	Co, Seq
OC_66	HGSC	IIIC	ascTU	IHC, Seq
OC_67	peritoneal, G2		ascTU	IHC
OC_70	HGSC	IIIC	ascTU	Seq
OC_87	HGSC	IIIC	ascTU	Seq
OC_92	HGSC	IIIC	ascTU	Seq
OC_101	HGSC	IIIC	ascTAT	Seq
OC_105	HGSC	IIIC	ascTU	Seq
OC_106	HGSC	IIIC	ascTAT	Seq
OC_107	HGSC	IIB	HPMC	Co, FC
OC_108	HGSC	IIIC	ascTU	Co, Seq
OC_111	LGSC	IIIC	HPMC	Co

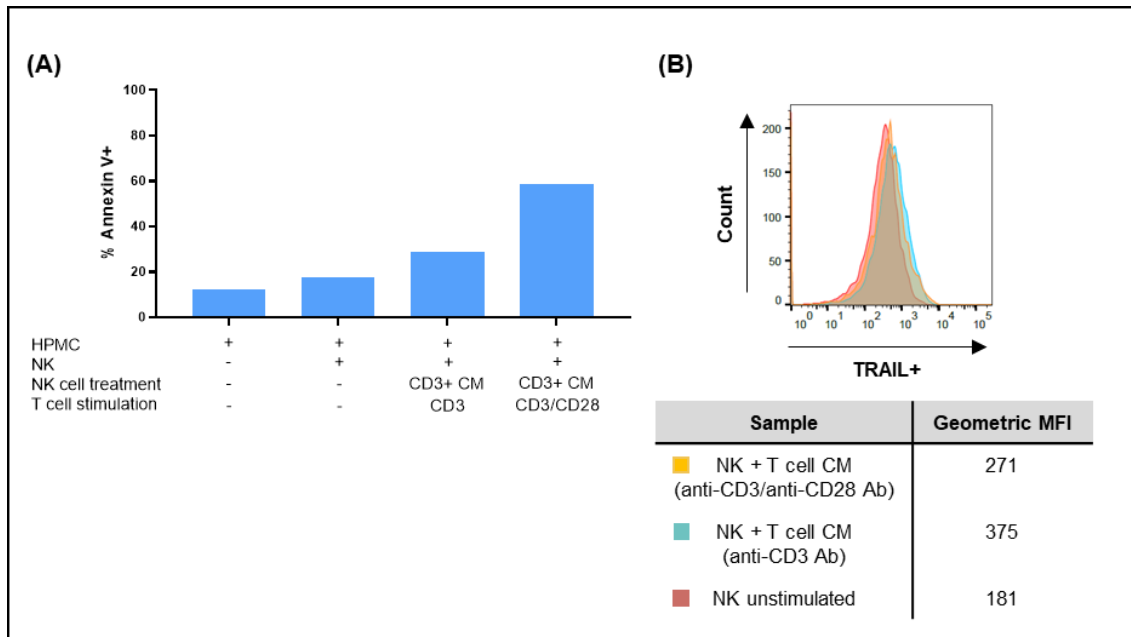
OC_112	HGSC	IIIC	ascTU	Seq
OC_114	HGSC	IIIC	ascTU	Co, Seq
OC_116	HGSC	IIIC	ascTU	Seq
OC_117	HGSC	IIIC	ascTU	Seq
			ascTAT	Seq
OC_119	HGSC	IIIC	ascTU	Co, FC
OC_122	HGSC	IIIC	ascTU	Co, IHC
OC_125	HGSC	IIIC	ascTAL	Co, Olink, qPCR
OC_127	HGSC	IIIC	ascTAL	Olink, qPCR
OC_128	HGSC	IIIC	ascTU	Seq
OC_133	HGSC	IIIC	ascTU	Seq
OC_140	LGSC	IIIB	HPMC	Co
OC_145	HGSC	IIIC	HPMC	Co
OC_150	endometrioid, G1	IC	HPMC	Co, FC
OC_151	HGSC	IIIC	HPMC	Co
OC_153	HGSC	IIIC	ascTAL	Co
OC_166	HGSC	IIIC	ascTAL	Co
OC_186	HGSC	IIIC	HPMC	Seq
OC_188	HGSC	IIIC	ascTAL	Co, FC, Inv
OC_193	HGSC	IIIC	ascTU	Seq
OC_194	HGSC	IIIC	ascTU	Seq
OC_195	HGSC	IIIB	ascTU	Seq
OC_196	HGSC	IIIC	ascTAL	Co, FC, Inv

			ascTU	Seq
OC_197	endometrioid, G1	IA	ascTAL	Co
OC_202	HGSC	IIIC	HPMC	Seq
OC_204	peritoneal, G3	IIIC	ascTAL	Co, FC, Olink
OC_208	HGSC	IIIC	ascTAL	Co
OC_211	HGSC	IIIC	ascTAL	FC
OC_213	HGSC	IIIC	ascTAL	Co
OC_217	HGSC	IIIC	HPMC	Seq
			ascTU	Seq
OC_218	HGSC	IIIC	HPMC	Seq
			ascTU	Seq
OC_220	HGSC	IIIB	HPMC	Seq
OC_221	HGSC	IIIC	HPMC	Seq
			ascTU	Seq
OC_222	HGSC	IIIC	HPMC	Seq
OC_224	HGSC	IIIC	ascTAL	Co
OC_226	HGSC	IIIC	HPMC	Co, FC, Inv
OC_227	HGSC	IIIC	HPMC	Seq
OC_229	HGSC	IIIC	ascTAL	Co, FC, Seq
OC_231	Carcinomatosis, G3	IIB	HPMC	Seq
OC_242	HGSC	IIIC	HPMC	Co, Seq
OC_245	HGSC	IIIC	ascTAL	FC
OC_254	HGSC	IIA	ascTAL	Co

			HPMC	Seq
OC_258	HGSC	IIIC	ascTAL	Co
			HPMC	Co
OC_259	HGSC	IIIC	ascTAL	Co
OC_261	HGSC	IIIB	ascTU	Co, FC, Inv
OC_262	HGSC	IIIC	ascTAL	Co
			HPMC	Co, FC, Inv
OC_272	HGSC	IIIC	HPMC	Co, FC, Inv
OC_280	HGSC	IIIC	HPMC	Co, FC
			ascTU	Co, FC
OC_281	HGSC	IIIC	ascTU	Co
OC_287	HGSC	IIIC	HPMC	Co
OC_288	HGSC	IIB	HPMC	Co, FC
OC_289	HGSC	IIIC	HPMC	Co, Inv
OC_291	HGSC	IIIC	ascTAL	Co
			HPMC	Co
OC_295	HGSC	IIIC	ascTAL	Co, FC, Olink
			HPMC	Co
OC_292	HGSC	IIIC	ascTU	FC
OC_298	HGSC	IIIC	ascTAL	Co, FC, Olink
OC_299	HGSC	IIIC	HPMC	Co, FC, Inv
OC_301	HGSC	IIIC	HPMC	Co, FC, Inv
OC_312	ovarian sarcoma		ascTAL	Co, FC, Inv


OC_314	HGSC	IIIC	ascTAL	Co, FC, Inv, qPCR
			ascTU	FC
OC_315	HGSC	IIIC	ascTAL	Co, FC, Inv, qPCR
			ascTU	FC
OC_316	HGSC	IIIC	ascTU	FC
OC_318	HGSC	IIIC	ascTU	FC
MpH_35	benign (Cystadenofibroma)	N/A	HPMC	Co, FC
MpH_39	benign (inflammatory)	N/A	HPMC	Co, FC
MpH_29	benign (Uterus myomatosus)	N/A	HPMC	Co, FC

Co = Co-culture; FC = Flow Cytometry; IHC = Immunohistochemistry; Inv = Invasion; Seq = RNA sequencing



Supplementary figure S1. NK cell treatment with the secretome of T cells activated by anti-CD3/anti-CD28 antibody stimulation did not increase TRAIL-mediated cytotoxicity directed against HPMC. (A, B) Treatment of NK cells with the CM derived from T cells treated with anti-CD3 antibody (0.5 $\mu\text{g/ml}$) alone or simultaneously with additional anti-CD28 (2 $\mu\text{g/ml}$) antibody was compared. (A) Subsequent co-culture with HPMC was performed to flow cytometrically measure the induction of HPMC apoptosis by determining the amount of Annexin V+ HPMC. The column heights indicate the mean (n=2 biological replicates). (B) Furthermore, the up-regulation of the TRAIL expression on the outer membrane of NK cells was determined in one experiment. Overlapping histograms illustrating the TRAIL expression on NK cells and a table indicating the geometric MFI is shown for untreated NK cells (red), NK cells treated with the CM of anti-CD3 antibody stimulated T cells (yellow), as well as NK cells treated with the anti-CD3/anti-CD28 antibody stimulated T cell CM are shown.

Ethics vote



Philipps **Universität**
Marburg

Philipps-Universität - 35032 Marburg

Frau
Dr. Silke Reinartz
Zentrum für Tumor- u. Immunbiologie (ZTI)
Forschungslabor der Klinik für Gynäkologie,
gynäkologische Endokrinologie und Onkologie
Philipps-Universität Marburg
Hans-Meerwein-Str. 3
35037 Marburg

Fachbereich Medizin
Dekanat/Ethikkommission
Prof. Dr. med. Gerd Richter (Vors.)

Tel.: 06421 586 6487
Fax: 06421 586 6585
Sek.: D. Raiss/S. Hausmann
E-Mail: ethikkom@post.med.uni-marburg.de
Anschrift: Baldingerstrasse/Postfach 2360
35032 Marburg
Web: www.med.uni-marburg.de/ethikkomm
Az.: 205/10

Marburg, den 19.02.2019

— **Studie:** „Rolle von Peroxisome-Proliferator-activated Receptors β/δ (PPAR β/δ) in der Aktivierung tumor-assoziiertes Makrophagen (TAM) von Patientinnen mit fortgeschrittenem Ovarialkarzinom“.

- Amendment 1 vom 07.11.2012: „Rolle des Peroxisome-Proliferator-activated Receptors β/δ (PPAR β/δ) in der Aktivierung tumor-assoziiertes Makrophagen (TAM) von Patientinnen mit Aszites-bildenden Platin-resistenten Rezidiven für fortgeschrittene Ovarialkarzinome“.
- Amendment 2 vom 27.05.2015: „Lysophosphatidsäure-vermittelte Therapieresistenz beim Ovarialkarzinom“.
- Amendment 3 vom 01.12.2016: „Therapieresistenz beim Ovarialkarzinom – Globale Analyse des interzellulären Signalnetzwerks in der Mikroumgebung des Ovarialkarzinoms“.
- Amendment 4 vom 06.02.2019: „Therapieresistenz beim Ovarialkarzinom – Globale Analyse des interzellulären Signalnetzwerks in der Mikroumgebung des Ovarialkarzinoms“.

Eingereichte Unterlagen:

1. Anschreiben vom 08.02.2019
2. Amendment Nr. 4 vom 06.02.2019
3. Anlage der projektbezogenen Kooperationspartner
4. Patienteninformation und Einwilligungserklärung Version 04 vom 06.02.2019
5. Patienteninformation-Kontrollkollektiv und Einwilligungserklärung Version 04 vom 06.02.2019
- 6.

Sehr geehrte Frau Dr. Reinartz,

mit Schreiben vom 08.02.2019 (eingegangen am 11.02.2019) reichen Sie einen Antrag auf Aufnahme des Amendments 4 „Therapieresistenz beim Ovarialkarzinom – Globale Analyse des interzellulären Signalnetzwerks in der Mikroumgebung des Ovarialkarzinoms“ in das positive Ethikkommissionsvotum vom 21.12.2010 ein.

Nach kritischer Durchsicht der oben aufgeführten und eingereichten Unterlagen ergeben sich keine berufsethischen und berufsrechtlichen Bedenken, sodass wir das Amendment 4 in das positive Ethikkommissionsvotum vom 21.12.2010 mit aufnehmen.

Sekretariat: Frau Raiss Montag – Donnerstag 8.00 – 12.00 Uhr, Freitag 8.00 – 11.00 Uhr
Frau Hausmann Montag – Freitag 12.00 – 14.00 Uhr

Kommissionsmitglieder: Prof. Dr. Czubyko, Prof. Dr. N. Donner-Banzhoff, Dr. B. Greene, Frau Prof. Dr. H. Korbmacher-Steiner, Prof. Dr. J.-C. Krieg, Prof. Dr. R. Maier (stellvertr. Vorsitzender), Prof. Dr. A. Neubauer, Dr. T. Neubert, Frau B. Nieth, Prof. Dr. J. Puschke, PD Dr. J.-P. Reese, Prof. Dr. G. Richter (Vorsitzender), Frau S. Riedemann, Frau PD Dr. C. Selfart, Prof. Dr. med. Uwe Wagner, Frau Prof. Dr. S. Weber, PD Dr. B. Tackenberg.

- 2 -

Hinweise zu den datenschutzrechtlichen Aspekten:

Details zu Ihren Informationspflichten gegenüber Studienteilnehmern entnehmen Sie bitte insbesondere Art. 13 ff DS-GVO. Die Ethikkommission prüft die Angaben zu den zuständigen Datenschutzbeauftragten und Aufsichtsbehörden nicht auf Richtigkeit.

Datenschutzrechtliche Aspekte von Forschungsvorhaben werden durch die Ethikkommission grundsätzlich nur kursorisch geprüft. Dieses Votum / diese Bewertung ersetzt mithin nicht die Konsultation des zuständigen Datenschutzbeauftragten.

Mit freundlichen kollegialen Grüßen
für die Ethik-Kommission des
Fachbereichs Humanmedizin
der Philipps-Universität Marburg

Prof. Dr. med. G. Richter
(Vorsitzender Ethikkommission)

Philipps-Universität - 35032 Marburg

Frau Dr. Silke Reinartz
Klinik für Gynäkologie und Gynäkologische
Endokrinologie und Onkologie
Universitätsklinikum Giessen und Marburg,
Standort Marburg
Baldingerstrasse
35043 Marburg

Fachbereich Medizin

Dekanat/Ethikkommission

PD Dr. med. Carola Seifart (Vors.)

Tel.: 06421 586 6487
Fax: 06421 586 6585
Sek.: D. Raiss/S. Hausmann
E-Mail: ethikkom@post.med.uni-marburg.de
Anschrift: Baldingerstrasse/Postfach 2360
35032 Marburg
Web: www.med.uni-marburg.de/ethikkomm
Az: Studie 205/10

Marburg, den 31.05.2021

Studie: „Rolle von Peroxisome-Proliferator-activated Receptors β/δ (PPAR β/δ) in der Aktivierung tumor-assoziiertes Makrophagen (TAM) von Patientinnen mit fortgeschrittenem Ovarialkarzinom“. Amendment 6 vom 28.05.2021: „Isolierung von Zellpopulationen aus der Peritoneallavage von Patientinnen mit benignen gynäkologischen Erkrankungen (Referenzkollektiv) für wissenschaftliche Untersuchungen im Rahmen der o.g. Studie

Eingereichte Unterlagen:


1. Anschreiben vom 18.05.2021
2. Aktualisierte Patienteninformation - Kontrollkollektiv

Sehr geehrte Frau Dr. Reinartz,

vielen Dank für die Einreichung des Amendment 6 zur o.g. Studie. Sie möchten in Ihrem Kontrollkollektiv (Patientinnen mit benignen gynäkologischen Erkrankungen) aus der Peritoneallavage nicht nur Immunzellen sondern auch weitere Zellpopulationen, wie Fibroblasten oder Mesothelzellen isolieren. Die Informationsschrift haben Sie dahingehend modifiziert („Zellpopulationen“ statt „Immunzellpopulationen“). Nach kritischer Durchsicht bestehen keine berufsrechtlichen oder berufsethischen Bedenken, sodass wir das Amendment 6 in das positive Ethikkommissionsvotum vom 21.12.2010 aufnehmen.

Mit freundlichen kollegialen Grüßen
für die Ethik-Kommission des
Fachbereichs Humanmedizin
der Philipps-Universität Marburg


PD Dr. med. Carola Seifart
(Vorsitzende Ethikkommission)


Dr. med. Irene Portig
(Geschäftsstelle Ethikkommission)

Sekretariat: Frau Raiss Dienstag/Donnerstag 8:00-12:00Uhr, Mittwoch 8:00-16:00Uhr, Freitag 8:00-11:00Uhr
Frau Dietrich Montag u. Dienstag 8:00-16:00Uhr, Donnerstag 11:00-15:00Uhr

Kommissionsmitglieder: Prof. Dr. med. K. Becker, J.W. Chae, Prof. Dr. F. Czubyko, Prof. Dr. med. N. Donner-Banzhoff, Prof. Dr. M. Geraedts, Prof. Dr. A. Jansen, Prof. Dr. med. A. Kirschbaum, Prof. Dr. jur. M. Kling, Prof. Dr. med. H. Korbmacher-Steiner, Prof. Dr. med. R. Maier (stellv. Vorsitzender), Prof. Dr. med. A. Neubauer, Prof. Dr. H. Schäfer, Prof. Dr. M. Hirsch (kooptiert), Dr. rer.nat. T. Neubert, Pfarrerin M. Kohl-Eckhardt, B. Nieth, Dr. med. I. Portig, Prof. Dr. jur. J. Puschke, cand. med. S. Riedemann, PD Dr. med. C. Seifart (Vorsitzende), cand. med. H. Traupe, Prof. Dr. med. S. Weber.



Philipps-Universität - 35032 Marburg

Herrn Prof. Dr. Rolf Müller
 Frau Prof. Dr. Elke Pogge von Strandmann
 Zentrum für Tumor- und Immunbiologie (ZTI)
 Philipps-Universität Marburg
 Hans-Meerwein-Str. 3
 35043 Marburg

Fachbereich Medizin

Dekanat/Ethikkommission

PD Dr. med. Carola Seifart (Vors.)

Tel.: 06421 588 6487
 Fax: 06421 588 6585
 Sek.: D. Raiss/S. Hausmann
 E-Mail: ethikkom@post.med.uni-marburg.de
 Anschrift: Baldingerstrasse/Postfach 2360
 35032 Marburg
 Web: www.med.uni-marburg.de/ethikkomm
 Az.: Studie 205/10

Marburg, den 29.03.2021

— **Studie:** „Rolle von Peroxisome-Proliferator-activated Receptors β/δ (PPAR β/δ) in der Aktivierung tumor-assoziiertes Makrophagen (TAM) von Patientinnen mit fortgeschrittenem Ovarialkarzinom“. Amendment 5 vom 19.03.2021: Verwendung von Abfallprodukten aus Blutspenden der Blutbank des UKGM Marburg / Giessen für wissenschaftliche Untersuchungen an gesunden peripheren Blutzellen im Rahmen der o.g. Studie

Eingereichte Unterlagen:

1. Anschreiben vom 19.03.2021
2. Aufnahmebogen für Blutspender mit Erklärung der Probenverwendung
3. Ethikvotum 05/00 Blutreste_Blutspende

— Sehr geehrter Herr Prof. Müller,
 sehr geehrte Frau Prof. Pogge von Strandmann,

Vielen Dank für die Einreichung des Amendment 5 zur o.g. Studie. Sie möchten die im Rahmen ihrer Studie gewonnenen Ergebnisse zu potentiellen Mediatoren, die Immunzellen aktivieren oder supprimieren können und damit die Tumorprogression und Metastasierung begünstigen könnten, an Immunzellen aus dem peripheren Blut gesunder Spender durchführen. Diese Zellen erhalten Sie aus Restmengen der Blutbank des UKGM Giessen, die ansonsten verworfen würden. Die Spender sind über die anonymisierte Verwendung von Restmengen für die Forschung aufgeklärt und haben dem zugestimmt. Dieses Vorgehen war mit der Ethikkommission der Justus-Liebig-Universität Giessen abgesprochen und die Informationsschrift mit Einwilligungserklärung wurde am 30.11.2000 zustimmend bewertet.

Nach kritischer Durchsicht bestehen keine berufsrechtlichen oder berufsethischen Bedenken, sodass wir das Amendment 5 in das positive Ethikkommissionsvotum vom 21.12.2010 aufnehmen.

Mit freundlichen kollegialen Grüßen
 für die Ethik-Kommission des
 Fachbereichs Humanmedizin
 der Philipps-Universität Marburg

PD Dr. med. Carola Seifart
 (Vorsitzende Ethikkommission)

Dr. med. Irene Portig
 (Geschäftsstelle Ethikkommission)

Sekretariat: Frau Raiss Dienstag/Donnerstag 8:00-12:00Uhr, Mittwoch 8:00-16:00Uhr, Freitag 8:00-11:00Uhr
 Frau Dietrich Montag u. Dienstag 8:00-16:00Uhr, Donnerstag 11:00-15:00Uhr

Kommissionsmitglieder: Prof. Dr. med. K. Becker, J.W. Chae, Prof. Dr. F. Czubyko, Prof. Dr. med. N. Donner-Banzhoff, Prof. Dr. M. Geraedts, Prof. Dr. A. Jansen, Prof. Dr. med. A. Kirschbaum, Prof. Dr. jur. M. Kling, Prof. Dr. med. H. Korbmacher-Steiner, Prof. Dr. med. R. Maier (stellv. Vorsitzender), Prof. Dr. med. A. Neubauer, Prof. Dr. H. Schäfer, Prof. Dr. M. Hirsch (kooptiert), Dr. rer.nat. T. Neubert, Pfarrerin M. Kohl-Eckhardt, B. Nieth, Dr. med. I. Portig, Prof. Dr. jur. J. Puschke, cand. med. S. Riedemann, PD Dr. med. C. Seifart (Vorsitzende), cand. med. H. Traupe, Prof. Dr. med. S. Weber.

List of abbreviations, figures and graphs**Supplementary table S2. List of abbreviations applied throughout this work**

Abbreviation	Translation
-RT	“Minus reverse transcriptase”
α -SMA	Alpha-Smooth Muscle Aktin
Ab	Antibody
ADCC	Antibody-dependent cell-mediated cytotoxicity
APC	Antigen-presenting cell
ApE	“A plasmid Editor”
Asc	Ascites
BAX	B-cell lymphoma-2 associated X protein
B cell	B lymphocyte
Bcl-2	B-cell lymphoma-2
Bim	B-cell lymphoma-2 interacting mediator
BRCA1/2	Breast cancer gene 1/2
BTLA	B- and T-Leukocyte attenuator
CAA	Cancer-associated adipocyte
CAD	Caspase-activated DNase
CAF	Cancer-associated fibroblast
CCL	Chemokine ligand
CD	Cluster of differentiation
cDC	Conventional dendritic cells
cDNA	Copy DNA
cFLIP	Cellular FADD-like IL-1 β -converting enzyme inhibitory protein
CLP	Common lymphoid progenitors
CM	Conditioned media
CMV	Cytomegalovirus
CRD	Cysteine-rich domain

CSF2	Colony-stimulating factor 2
CT	Computer tomography
CTLA4	Cytotoxic T-lymphocyte antigen 4
Ctrl	Control
CXCL	C-X-C motif cytokine ligand
DAP12	DNAX-activating protein of 12 kDa
DC	Dendritic cell
DcR1/2	Decoy receptor 1/2
DD	Death domain
DED	Death-effector domain
DISC	death-inducing signaling complex
DNA	Deoxyribonucleic acid
DNAM-1	DNAX accessory molecule-1
DMSO	Dimethyl sulfoxide
DR4/5	Death receptor 4/5
ECM	Extra cellular matrix
EDTA	Ethylenediaminetetraacetic acid
EGF	Epidermal growth factor
EGFR	Epidermal growth factor receptor
EMT	Epithelial-mesenchymal transition
Eomes	Eomesodermin
EpCAM	Epithelial cell adhesion molecule
EtOH	Ethanol
FACS	Fluorescence-activated cell sorting
FADD	Fas-associated protein with death domain
FAK	Focal adhesion kinase
FasL	Fas-ligand
FC	Fold change

FCS	Fetal calf serum
FIGO	International Federation of Gynaecology and Obstetrics
GAS	IFN γ -activated site
G-CSF	Granulocyte colony-stimulating factor
GEO	Gene expression Omnibus
GM-CSF	Granulocyte macrophage colony-stimulating factor
GrA/B	Granzyme A/B
GRO α	Growth-regulated protein alpha
GRO β	Growth-regulated protein beta
GZMA	Granzyme A
GZMB	Granzyme B
HE	Hematoxylin and eosin
HGF	Hepatocyte growth factor
HGSC	High-grade serous ovarian carcinoma
HLA-I	Human leukocyte antigen I
HPMC	Human peritoneal mesothelial cells
HSC	Hematopoietic stem cells
IAP	Inhibitor of apoptosis proteins
ICAM-1	Intercellular adhesion molecule
ICR	immune checkpoint receptors
IFN γ	Interferon gamma
IFNGR1/2	Interferon gamma receptor 1/2
IL	Interleukin
ILC	Innate lymphoid cell
IS	Immunological synapse
ITAM	Immunoreceptor tyrosine-based activation motifs
ITIM	Immunoreceptor-based tyrosine inhibitory motif
JAK	Janus Kinase

KARAP	Killer cell activating receptor-associated protein
KIR	Killer immunoglobulin-like receptors
LAG-3	Lymphocyte activation gene-3
LAMP-1	Lysosomal-associated membrane protein-1
LFA-1	Lymphocyte function-associated antigen 1
LG	Ligand
LIR-1	Leukocyte Ig-like receptor-1
LMPP	Lymphoid-primed multipotential progenitors
LRS	Leukocyte-reduction system
LTA	Lymphotoxin- α
LTB	Lymphotoxin beta
M1	Pro-inflammatory type 1 macrophage
M2	Immunosuppressive type 2 macrophage
MACS	Magnetic-activated cell sorting
MAPK	Mitogen activated protein kinases
Mcl-1	Myeloid cell leukemia-1
MCP-1	Monocyte chemoattractant protein-1
MDSC	Myeloid-derived suppressor cell
MFI	Mean fluorescence intensity
MHC I	Major histocompatibility complex class I
MICA/B	Major histocompatibility complex class I chain-related protein A/B
MIF	Macrophage migration inhibitory factor
ml	Milliliter
MMP	Matrix-metalloproteinase
MMT	Mesothelial-mesenchymal transition
MTOC	Microtubule-organizing center
n	Amount
NCAM	Neutral cell adhesion molecule

NCP	NK cell precursors
NCR	Natural cytotoxic receptors
NET	Neutrophil extracellular traps
NFκB	Nuclear factor kappa B
ng	Nano gram
NGS	Next-Generation Sequencing
NK cells	Natural killer cells
NKG2A/C/D	Natural killer group 2A/C/D
NKT	Natural killer T cells
NPX	Normalized Protein eXpression
NTB-A	Signaling lymphocytic activation molecule family member 6
OC	Ovarian cancer
OCMI	Ovarian Carcinoma Modified Ince media
OPG	Osteoprotegerin
OSM	Oncostatin M
PARP	Poly adenosine diphosphate-ribose polymerase
PBMC	Peripheral blood mononuclear cells
PBS	Phosphate buffered saline
PD-1	Programmed cell death protein-1
PDCD1	Programmed cell death-1
PDGFA	Platelet-derived growth factor subunit A
PED	Proximity Extention Assay
PI	Propidium iodide
PI3K	Phosphatidylinositol 3-kinase
PIAS	Protein inhibitor of activated STATs
PKB/AKT	Protein kinase B
PKC	Protein kinase C
PLAD	Pre-ligand assembly domain

PMA	Phorbil 12-myristate 13-acetate
PRRT3	Proline Rich Transmembrane Protein 3
Rac	Ras-related C3 botulinum toxin substrate
RBC	Red blood cell
RELT	Tumor Necrosis Factor Receptor Superfamily Member 19-like
RFS	Relapse-free survival
rh	Recombinant human
RIP-1	Receptor Interacting Protein 1
RNA	Ribonucleic Acid
RohA	Ras homolog family member A
qPCR	Quantitative polymerase chain reaction
SERPINE2	Serine proteinase inhibitor clade E member 2
Shp2	src homology 2 domain-containing tyrosine phosphatase-2
SMAC	Second mitochondria-derived activator of caspase
SOCS	Suppressor of cytokine signaling
SODD	Silencer of death domain
STAT	signal transducer and activators of transcription
TACE	TNF α -converting enzyme
TAL	Tumor-associated lymphocytes
TAM	Tumor-associated macrophages
TAT	Tumor-associated T cells
t-Bid	Truncated BH3 interacting-domain death agonist
T cells	T lymphocytes
TCR	T cell receptor
Tfh	Follicular T helper
TGF β 1	Transforming growth factor β 1
Th	T helper

TIGIT	T cell Ig and immunoreceptor-based tyrosine inhibitory motif
TIL	Tumor-infiltrating lymphocytes
TLR	Toll-like receptor
TIM-3	T cell immunoglobulin, mucin domain-3
TME	Tumor-microenvironment
TNF α	Tumor necrosis factor alpha
TNF-R1/2	Tumor necrosis factor receptor 1/2
TNFRSF	Tumor necrosis factor receptor superfamily
TNFSF	Tumor necrosis factor superfamily
TP53	Tumor protein p53
TPM	Transcript per million
TRADD	TNF-R-associated death domain protein
TRAF-1	TNF-R-associated factor
TRAIL	Tumor necrosis factor -related apoptosis-inducing ligand
Treg	Regulatory T cell
U	Units
UKGM	Universitätsklinikum Gießen und Marburg
ULBP	UL16 binding protein 1
μ g	Microgram
μ l	Microliter
VCAM-1	Vascular cell adhesion molecule-1
VEGF	Vascular endothelial growth factor
Wnt	Wingless-related integration site
ZO-1	Zonula occludens-1
ZEB-1	Zinc finger E-box binding homeobox 1

Supplementary table S3. List of figures

Figure	Description
1	Mechanism of malignant ascites formation during HGSC cancer progression
2	Compartments of the unique HGSC TME
3	Main activating and inhibiting receptors expressed on NK cells and the corresponding ligands found on target cells
4	Target cell recognition following the “altered balance” mechanism of NK cell activation
5	Schematic illustration of apoptosis signaling pathways executed by NK cells
6	Flow chart illustrating the experimental procedure to determine the role of TAL and mesothelial cells on HGSC tumor progression
7	Isolation strategy of T and NK cells from HGSC patient ascites or healthy donor PBMC
8	Layers of blood phases after ficoll gradient centrifugation
9	Schematic chart illustrating the experimental procedure of the co-culture experiments
10	Schematic illustration of in vitro 3D trans-mesothelial invasion assays
11	Induction of mesothelial apoptosis upon co-culture with anti-CD3 antibody-activated TAL
12	Strong degranulation of NK cells in the presence of HPMC after activation by anti-CD3 antibody stimulated T cells
13	Ascites fluid blocks NK cell degranulation while the induction of mesothelial apoptosis is sustained
14	NK cell-mediated killing of HPMC was Fas/FasL independent despite the expression of Fas on HPMC and FasL on NK cells
15	The cytotoxic cytokines TNF α and IFN γ are not able to induce HPMC apoptosis
16	TRAIL-mediated apoptosis of HGSC-derived mesothelial cells

17	The secretome of anti-CD3 antibody-stimulated T cells promotes TRAIL-mediated NK cell cytotoxic activation directed against HPMC
18	IFN γ , IL-2, TNF α and IL-21 are important cytokines secreted/ expressed by anti-CD3 antibody stimulated T cells activating NK cells
19	T cell-secreted TNF α is an important effector cytokine activating NK cells in the TME
20	High expression levels of the activating death receptors on HGSC-derived HPMC render them liable toward TRAIL-induced apoptosis conducted by NK cells
21	Tumor cells are insensitive against TRAIL-dependent apoptosis
22	Control HPMC derived from lavage of patients with benign gynecological diseases were insensitive to TRAIL-mediated killing
23	Low MHC I and high MICA/B expression levels on HPMC possibly further contribute to NK cell attack
24	Clearance of the mesothelial barrier favors extensive tumor cell invasion
25	Immunohistological analysis of HGSC specimen: mesothelium is lost in regions of omental micrometastasis
26	Detached floating apoptotic mesothelial cells are found in the ascites
27	Schematic illustration of mechanisms leading to mesothelial rearrangement or clearance promoting tumor invasion
28	NK cell cytolytic activation induced by T cell-secreted cytokines (particularly TNF α) selectively directed against HPMC in a TRAIL-mediated fashion
Supplementary figure S1	NK cell treatment with the secretome of T cells activated by anti-CD3/anti-CD28 antibody stimulation did not increase TRAIL-mediated cytotoxicity directed against HPMC

Supplementary table S4. List of tables

Table	Description
1	List of equipment applied conducting experiments
2	List of chemicals and reagents applied for experimental procedures
3	List of antibodies applied for flow cytometry, MACS, neutralization and T cell activation
4	List of recombinant cytokines and proteins applied for cellular treatments
5	List of kits and microbeads applied for experimental procedures of this thesis
6	List of buffers and solutions applied throughout this thesis
7	Software and internet sites applied throughout this thesis
8	List of applied oligonucleotides and their sequences
9	List of cell culture media and media components
Supplementary table S1	Primary ovarian carcinoma patient data and samples
Supplementary table S2	List of abbreviations applied throughout this work
Supplementary table S3	List of figures

Publications of the author

Steitz, Anna Mary; Steffes, Alina; Finkernagel, Florian; Unger, Annika; Sommerfeld, Leah; Jansen, Julia M.; Wagner, Uwe; Graumann, Johannes; Müller, Rolf and Reinartz, Silke (2020): Tumor-associated macrophages promote ovarian cancer cell migration by secreting transforming growth factor beta induced (TGFB1) and tenascin C. In: Cell death & disease 11 (4), S. 249. DOI: 10.1038/s41419-020-2438-8

Currently under revision:

Steitz, Anna Mary; Schröder, Clarissa; Knuth, Isabel; Keber, Corinna; Sommerfeld, Leah; Finkernagel, Florian; Jansen, Julia M.; Wagner, Uwe; Müller-Brüsselbach, Sabine; Worzfeld, Thomas; Huber, Magdalena; Beutgen, Vanessa M.; Graumann, Johannes; Pogge von Strandmann, Elke; Müller, Rolf and Reinartz, Silke (2023): TRAIL-dependent apoptosis of peritoneal mesothelial cells by T cell-activated NK cells promotes ovarian cancer cell invasion. In: iScience

Submitted:

Simon, Clara; Brunke, Inka D.; Stielow, Bastian; Forné, Ignasi; Steitz, Anna Mary; Geller, Merle; Rhoner, Iris; Weber, Lisa M.; Fischer, Sabrina; Jeude, Lea Marie; Nist, Andrea; Stiewe, Thorsten; Huber, Magdalena; Buchholz, Malte; Liefke, Robert (2023): SAMD1 suppresses epithelial-mesenchymal transition (EMT) pathways in pancreatic ductal adenocarcinoma. In: EMBO

Curriculum Vitae

[Removed for final print]

Directory of academic teachers**My academic teachers at the Philipps University in Marburg were:**

Adamkiewicz, Jürgen; Adhikary, Till; Bartsch, Jörg Walter; Bauer, Miriam; Bauer, Uta Maria; Bauer, Steffan; Brandt, Dominique; Brehm, Alexander; Brendel, Cornelia; Buchholz, Malte; Burchert, Andreas; Conrad, Matthias; Decher, Niels; Elsässer, Hans Peter; Feuser, Beate; Frech, Miriam; Fritz, Barbara; Garn, Holger; Greene, Brandon; Grgic, Ivica; Hänze, Jörg; Hertl, Michael; Huber, Magdalena; Höbenreich, Sabine; Jacob, Ralf; Jakob, Peter; Jänsch, Heinz; Kinscherf, Ralf; Lauth, Matthias; Lill, Roland; Lohoff, Michael; Maisner, Andrea; Mandic, Robert; Milani, Wiebke; Müller, Rolf; Müller-Brüsselbach, Sabine; Mühlenhoff, Ulrich; Neubauer, Andreas; Oberwinkler, Johannes; Oliver, Dominik; Pankuweit, Sabine; Plant, Timothy David; Preisig Müller, Regina; Pogge von Strandmann, Elke; Reinartz, Silke; Schmeck, Bernd; Schmidt, Ansgar; Stehling, Oliver; Steinhoff, Ulrich; Stiewe, Thorsten; Strauer, Dorothea; Suske, Guntram; Timmesfeld, Nina; Timofeev, Oleg; Visekruna, Alexander; Wanzel, Michael; Westermann, Reiner; Worzfeld, Thomas; Wrocklage, Christian.

Acknowledgements

First and foremost, I want to thank Dr. Silke Reinartz for giving me the opportunity to perform my PhD thesis under her supervision and enabling me to work on this highly interesting and novel project. Thank you for your constant support and paving my way as a doctoral candidate within the Graduate School GRK2573/1. I am very grateful for all your valuable advice, time, communication and assistance, which have promoted such a great outcome of my thesis project. Thank you for encouraging me and enabling me to participate in conferences, during which I was able to gain a lot of experience.

My huge thanks go to Prof. Dr. Rolf Müller for providing me with my research assistant position in the first place and enabling me to continue my research on this project during a PostDoc position. Thank you for all your support, advice and excellent ideas concerning my project and for being a part of my thesis advisory committee. Thank you for sharing your expertise on biostatistics and performing the bioinformatic analysis of the Olink data.

I am highly grateful to Prof. Dr. Elke Pogge von Strandmann for initiating the Graduate School GRK 2573/1 and creating doctoral positions, enabling me to perform my thesis within the graduate school and granting me with start-up funding for my research project. I am thankful for all the additional experience I was able to gain, the networking, cooperations and support during my participation in the Graduate School and the opportunity to take part in national and international conferences, as well as additional courses. Thank you, Elke, for sharing your expertise and providing me with reagents for my experiments.

Many thanks to Prof. Dr. Thomas Worzfeld for the exchange of ideas and suggestions concerning my thesis project in line with my thesis advisory committee meetings.

Thank you, Prof. Dr. Magdalena Huber, for sharing your expertise and great ideas with me, which have helped me during the development of my project.

I particularly want to thank Traute Plaum-Allmeroth and Achim Allmeroth for their constant help and support during the experimental procedure. Thank you, Traute, for sharing your incredible expertise on cell culture and the handling of primary patient material. Thank you, Achim, for providing your immense knowledge in biochemical and molecular experimental procedures. I am extremely grateful to you both for all the preliminary preparations, organization and experimental procedures you performed, which made my work in the laboratory a lot easier. Thank you for performing the isolations of cells from the primary patient material. I am grateful to Leah and Sophie for the great teamwork, exchange of ideas and conversations! Thank you for all your work on isolating cell types from the omentum. I really appreciate the teamwork and the familiar atmosphere within AG Reinartz and always enjoyed our conversations, laughs and gatherings.

Without Prof. Dr. Uwe Wagner and Dr. Julia Malin Jansen, the research on my project would not have been possible, since they provided us with the primary patient material. Thank you very much!

Furthermore, I want to thank the whole research group of Prof. Dr. Müller for the helpful discussions and exchanges during the regular seminars and providing additional support. Thank you, Florian, for providing your expertise on bioinformatics, performing analyses and sharing ideas and advise on my project. I particularly want to thank Kaire for her help and organizational skills, which we all benefitted from. I also want to thank Margitta Alt, Klaus Weber and Bernhard Wilke for the coordination of orders and the preparations of donor peripheral blood by Margitta.

I am grateful to the proteomics corefacility, in particular Prof. Ph.D. Johannes Graumann and Dr. Vanessa Beutgen, for the Olink secretome analysis and to Dr. Corinna Keber from the pathology department, for immunohistological analysis of primary patient specimens.

Thank you, PD Dr. Till Adhikary, for sharing your expertise with me. Thank you, María, for your encouragement and the help you provided for applications. Thank you, Vivianne, for your help in providing antibodies and equipment. Thank you, Dr. Karen Schwabe, for the cooperation concerning the Graduate School and the organization of the retreat.

Last but not least I want to thank my friends and family for their love, unconditional support, always believing in me and my abilities and encouraging me in hard times.

I am thankful to Caro, Michelle, Lisa, Franzi, Michelle, Clara and Felix for the memories we share and the time we spent together during our studies and beyond. Thank you for making this time so special and creating lasting memories. Thank you, Michelle, Clara, Felix, and Manuel, for the great time during our PhD, all the memories we built together, the shared sufferings, as well as celebrations and all your support and help. Thank you, Michelle, for being the best flat mate one could wish for. Thank you, Leah, María, Reem, Kaire and Veronika, for the friendship we have developed beyond the laboratory.

I want to thank my parents for making my studies and this career possible. Special thanks go to my Mum for her unconditional love, support and faith in me. Thank you for everything you do for me!

Ehrenwörtliche Erklärung

[Removed for final print]